PB 294334

WEIDLINGER ASSOCIATES, CONSULTING ENGINEERS

110 EAST 59TH STREET
NEW YORK, NEW YORK 10022

and

SUITE 245, BUILDING 4
3000 SAND HILL ROAD
MENLO PARK, CALIFORNIA 94025

DYNAMIC SEISMIC ANALYSIS OF
LONG SEGMENTED LIFELINES

By

Ivan Nelson and Paul Weidlinger

Grant Report No. 10

Prepared for

National Science Foundation (ASRA Directorate)
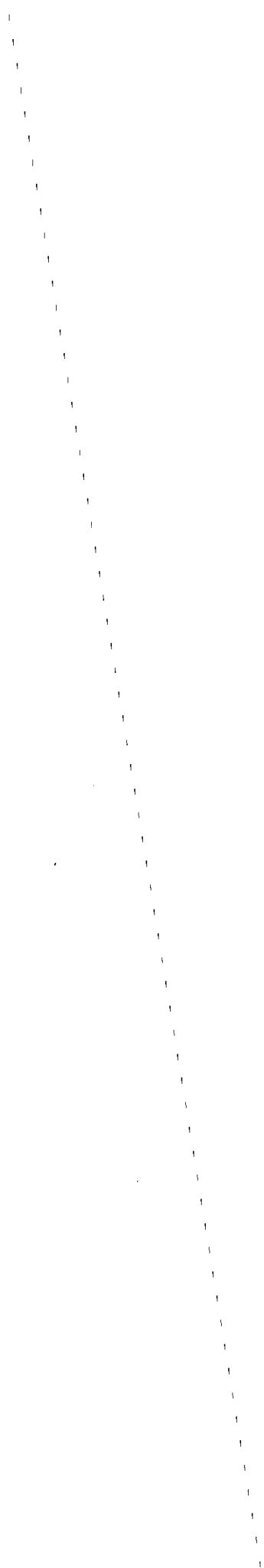1800 G Street
Washington, D.C. 20550

Grant No. PFR 78-15049

NOVEMBER 1978

50272-101

REPORT DOCUMENTATION PAGE	1. REPORT NO. NSF/RA-780465	2.	3. Recipient's Accession No. PB29 4334

4. Title and Subtitle	5. Report Date
Dynamic Seismic Analysis of Long Segmented Lifelines	November 1978
	6.

7. Author(s) I. Nelson, P. Weidlinger	8. Performing Organization Rept. No. Grant Report No. 10

9. Performing Organization Name and Address	10. Project/Task/Work Unit No.
Weidlinger Associates, Consulting Engineers * 110 East 59th Street New York, New York 10022	11. Contract(C) or Grant(G) No. (C) (G) PFR7815049

12. Sponsoring Organization Name and Address	13. Type of Report & Period Covered
Applied Science and Research Applications (ASRA) National Science Foundation 1800 G Street, N.W. Washington, D.C. 20550	14.

15. Supplementary Notes

* Also: Suite 245, Building 4
3000 Sand Hill Road
Menlo Park, California 94025

16. Abstract (Limit: 200 words)

The difference in ground motion along a lifeline, the incoherent motion, is an essential component of the input. A long, straight, segmented pipe, with each link attached to the ground via a spring and dashpot is subjected to incoherent ground motion caused by a phase delay. The equations governing the axial response of the system are developed. Modal decomposition is used and closed form expressions are given for the natural frequencies and mode shapes. Examples are given showing the center joint displacement time history when the lifeline is subjected to earthquake loading. Spectral techniques can be used to bound the motion with the Interference Response (IR) spectrum. This spectrum is the maximum difference in motion (response) of two adjacent points which are excited by a difference in ground input. It is seen that the IR spectrum is a useful tool in the dynamic analysis of lifeline over a broad range of parameters.

17. Document Analysis   a. Descriptors

Earthquakes
Dynamic structural analysis
Seismology

Earthquake resistant structures
Highways
Bridges (structures)

Pipelines
Tunnels

b. Identifiers/Open-Ended Terms

Long segmented lifelines

c. COSATI Field/Group

18. Availability Statement NTIS	19. Security Class (This Report)	21. No. of Pages 118
	20. Security Class (This Page)	22. Price A06 - A01

(See ANSI-Z39.18)   See Instructions on Reverse

OPTIONAL FORM 272 (4-77)
(Formerly NTIS-35)
Department of Commerce

WEIDLINGER ASSOCIATES, CONSULTING ENGINEERS

110 EAST 59TH STREET

NEW YORK, NEW YORK 10022

and

SUITE 245, BUILDING 4

3000 SAND HILL ROAD

MENLO PARK, CALIFORNIA 94025

DYNAMIC SEISMIC ANALYSIS OF

LONG SEGMENTED LIFELINES

By

Ivan Nelson and Paul Weidlinger

Grant Report No. 10

Prepared for

November 1978

i. a

TABLE OF CONTENTS

ABSTRACT

The difference in ground motion along a lifeline, the incoherent motion, is an essential component of the input. A long, straight, segmented pipe, with each link attached to the ground via a spring and dashpot is subjected to incoherent ground motion caused by a phase delay. The equations governing the axial response of the system are developed. Modal decomposition is used and closed form expressions are given for the natural frequencies and mode shapes.

Examples are given showing the center joint displacement time history when the lifeline is subjected to earthquake loading. Spectral techniques can be used to bound the motion with the Interference Response (IR) spectrum. This spectrum is the maximum difference in motion (response) of two adjacent points which are excited by a difference in ground input.

It is seen that the IR spectrum is a useful tool in the dynamic analysis of lifelines over a broad range of parameters.

LIST OF SYMBOLS

A = cross-sectional area of pipe; also constant

B = constant

c_B = boundary damping coefficient

c_g = ground damping coefficient

c_p = pipe-joint damping coefficient

D_m^k = influence coefficient for center joint displacement in mode k, for input at joint m, see Eq. (51)

E = Young's modulus

f_k = natural frequency of kth mode, Hz.

J_k = joint modal participation factor, see Eq. (38)

k = integer, mode number

k_B = boundary stiffness

k_g = ground stiffness

k_p = pipe-joint stiffness

L = total length of pipe

ℓ = length of pipe segment; also, integer (mode number)

m = mass of pipe segment and attached soil; also, integer (joint number)

N = number of segments

P_k = modal participation factor, see Eq. (31)

q_k = k^{th} generalized coordinate

r_{km} = response in k^{th} mode due to input at joint m, see Eq. (49)

S_I, $\bar{S}_I$ = interference response spectrum, cm, see Eq. (22)

$[T]$, $[T_c]$ = tridiagonal matrices, diagonal terms (except corners) = 2, off diagonal terms = - 1

t = time, sec

t_{11}, t_{NN} = corner terms of $[T]$ given by Eq. (5)

x_i = absolute displacement of ith segment, cm

$[z_B]$ = matrix (1 x N) of boundary displacements, see Eq. (4)

z_i = free field ground displacement at i^{th} segment, cm

$\bar{z}$ = coherent ground displacement, cm

Δx = difference in displacement between successive segments, center joint displacement, cm

$\Delta y = \Delta x - \Delta z$

Δz = difference in free field ground displacement between successive successive segments, cm

$\delta_{k\ell}$ = Kroneker delta

η_k = relative generalized coordinate in k^{th} mode, see Eqs. (28) and (39)

θ = angle, radians

λ_k = k^{th} eigenvalue of [T]

ξ = fraction of critical damping

τ = phase delay time between successive segments, sec

τ_L = phase delay time between ends of pipe, sec

$[\phi^k]$ = k^{th} eigenvector of [T]

ϕ_j^k = j^{th} element of $[\phi^k]$

Ω = circular frequency of (component of) the input

$\omega_g = \sqrt{k_g/m}$ = circular frequency, sec^{-1}

ω_k = circular natural frequency of kth mode of undamped system, sec^{-1}

Subscripts

i, j, m = segment or joint number

k, ℓ = mode number

g = ground

p = pipe-joint

Superscripts

k, ℓ = mode number

I   INTRODUCTION

Highways, bridges, tunnels and pipelines are called lifelines. A characteristic that distinguishes a lifeline from other structures is that it extends (essentially parallel to the ground surface) over a distance which is long compared to its other dimensions. The foundations, therefore, are either at widely separated points (e.g., bridges) or they extend continuously over long distances (pipes, tunnels). For this reason, in considering the effects of ground shaking, we cannot assume a priori that the motion at all points of ground contact is identical (i.e., that the ground motion is coherent). The significance of this has been recognized by other researchers concerned with lifelines, e.g., Newmark (Ref. [1]), Christian (Ref. [2]) and Matsushima (Ref. [3]).

When the motion is no longer the same at all points, i.e., when it is not coherent, the relative displacement of the points of contact produces stresses in the structure, whereas identical (i.e., coherent) excitation at continuous or closely spaced foundation points may result in primarily rigid body displacement, with no significant strain. The analysis and design of lifelines subjected to earthquake induced motion is, therefore, different from that of buildings, where we customarily assume that the ground motion over the entire foundation plane is coherent and that the relevant response is the displacement relative to the ground. The seismic analysis of buildings is well developed, e.g. Refs. [4] and [5]. When the structure may be considered linear, modal analysis and the use of response spectra is the most common procedure.

The important component of the ground input for lifelines is the incoherent motion. The various sources of incoherent ground motion are discussed by Weidlinger and Nelson (Refs. [6] and [7]). In the present paper, the difference caused by a phase delay between adjacent foundation

points will be the only source of non-coherent motion considered.

Failures of buried pipes subjected to ground shaking have been observed in both the United States and Japan. Many of the failures occurred at joints and involved pull out or crushing, Refs. [8] and [9]. In the present paper, a long, straight, segmented pipe, with each link attached to the ground through a ground spring and dashpot is subjected to a ground motion which advances along the axis of the pipe at a constant velocity. The input and the response are both restricted to the axial direction. The equations which govern the motion of the system are developed. Modal decomposition is used, and for specific boundary conditions, closed form expressions are given for the natrual frequencies and mode shapes. While the present analysis is for a discrete system, it obvously may be viewed as an approximate solution for a continuous system as well.

Examples are given showing the center joint displacement time history when the lifeline is subjected to earthquake type loading. Spectral techniques can be used to bound the motion if the standard shock spectrum is replaced by the Interference Response spectrum. This spectrum is the maximum difference in motion (response) of two adjacent points which are excited by a difference in ground input $\Delta z(t)$. It is described more fully and its properties are given by Weidlinger and Nelson (Refs. [6] and [7]).

II   EQUATIONS OF MOTION

It is convenient to represent a lifeline as a multi-degree of freedom discrete system. Consider the long, segmented pipe shown in Fig. 1, where the rigid (or elastic) links are interconnected by elastic springs and viscous dashpots. In addition, each segment is joined to the ground by another spring dashpot combination. It is assumed that the properties are uniform along the length of the pipe. A typical joint with two attached pipe segments of length ℓ is shown in Fig. 2. The stiffness k_p represents the effective stiffness of the weak elastomeric (or other caulking material) joint plus any contribution of the stiff pipe segment, while c_p is used to approximate the hysteresis in the joint. In the case of a continuous pipe, ℓ is the finite difference interval and k_p is the axial stiffness of the element (i.e., $k_p = EA/\ell$). The mass m includes the mass of the pipe segment plus possible contributions from the surrounding soil and the enclosed fluid. The soil stiffness k_g and damping c_g, as well as m, may only be found by solving the soil structure interaction problem. This will not be done here, but it will be assumed that the values are known and are constant, i.e., independent of frequency in the range of interest. It is noted that in general c_g includes both radiation and material damping.

The equation of motion of the typical i^{th} link is given by

$$m\ddot{x}_i + c_g \dot{x}_i - c_p(\dot{x}_{i-1} - 2\dot{x}_i + \dot{x}_{i+1}) + k_g x_i - k_p(x_{i-1} - 2x_i + x_{i+1})$$

$$= c_g \dot{z}_i + k_g z_i \tag{1}$$

where x_i is the absolute motion of the ith link, and z_i is the free field ground motion at the center of the ith link. The two ends of the pipe require special attention. The first link, Fig. 3, is assumed to be

directly attached to the ground via boundary spring and dashpot k_B and c_B. If axial motion along the pipe is considered, and if the pipe is attached to a transverse pipe, then the transverse pipe moves with the ground so that z_o is the motion of the ground at the pipe end. the equation of motion of the first link is thus

$$m\ddot{x}_1 + (c_B + c_p + c_g)\dot{x}_1 - c_p \dot{x}_2 + (k_B + k_p + k_g)x_1 - k_p x_2$$

$$= c_B \dot{z}_o + c_g \dot{z}_1 + k_B z_o + k_g z_1 \tag{2}$$

A similar expression may be written at the other end by letting $x_1 \to x_N$, $x_2 \to x_{N-1}$, and $z_o \to z_{N+1}$, where N is the total number segments.

The system defined by Eqs. (1) and (2) is tridiagonal. It may be written in matrix form as

$$m\{\ddot{x}\} + \{c_g[I] + c_p[T_c]\}\{\dot{x}\} + \{k_g[I] + k_p[T]\}[x]$$

$$= c_g[\dot{z}] + k_g[z] + c_B[\dot{z}_B] + k_B[z_B] \tag{3}$$

where [I] is the identity matrix, and where $[T_c]$ and [T] are tridiagonal matrices whose elements (except for the corners) are -1, 2 and -1. The boundary matrix $[z_B]$ is a 1 x N matrix defined by

$$[z_B]^T = [z_o, 0, 0 \ldots 0, z_{N+1}] \tag{4}$$

The two corner terms of [T] are

$$t_{11} = t_{NN} = 1 + {}^{k}B/k_p \tag{5}$$

The two matrices $[T_c]$ and [T] are identical, except ${}^{c}B/c_p$ replaces ${}^{k}B/k_p$ in the two corner terms.

We note that the only off-diagonal terms in the system, Eq. (3), result from [T] and $[T_c]$. Consequently, the natural frequencies of free vibration
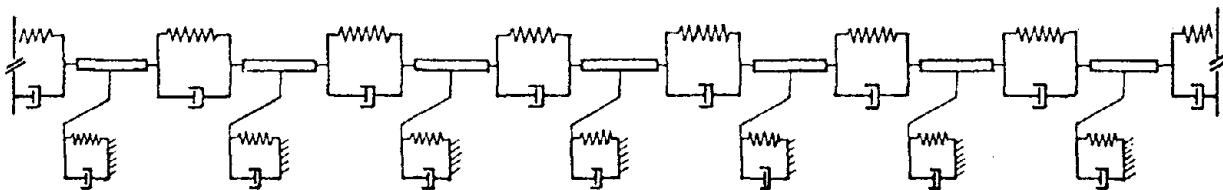
FIG. 1 LONG JOINTED PIPE SUPPORTED BY SPRINGS
AND DASHPOTS (AXIAL MOTION ONLY CONSIDERED)
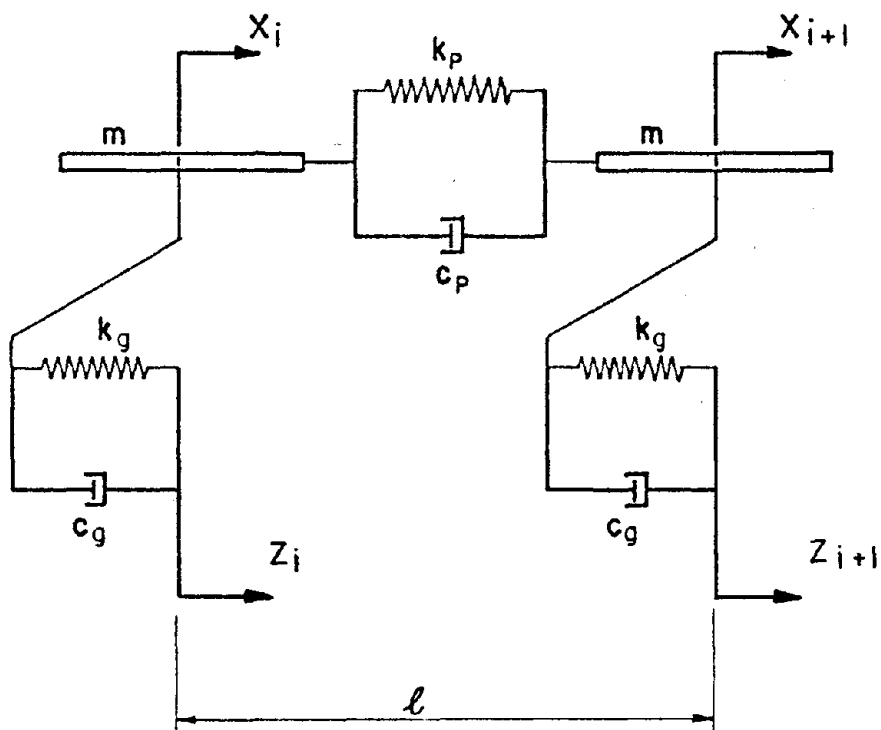
FIG. 2 TWO UNDERGROUND PIPE SEGMENTS
CONNECTED BY JOINT
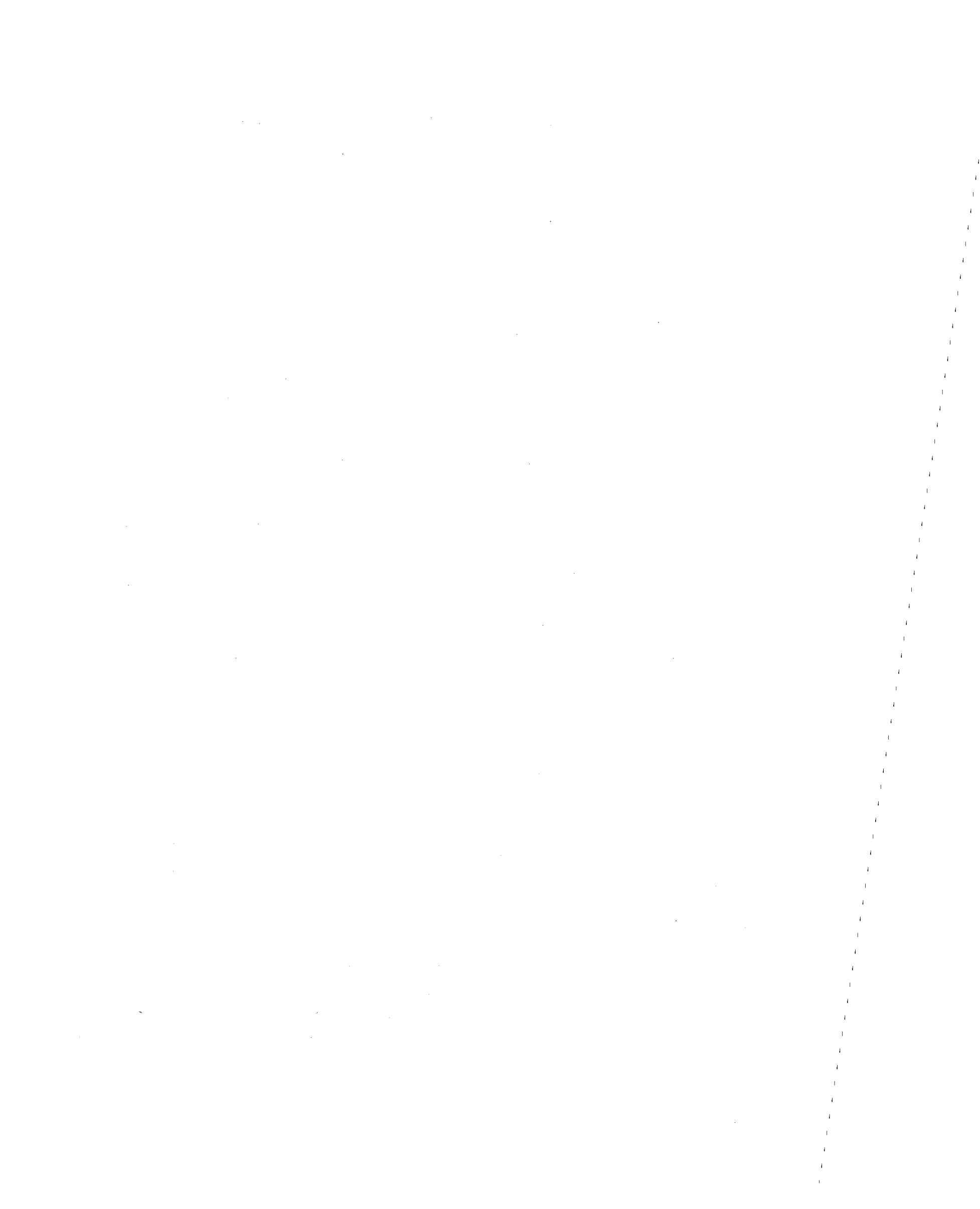
of the undamped system are given by

$$\omega_k^2 = \frac{k_g}{m} + \frac{k_p}{m} \lambda_k \qquad (6)$$

where λ_k are the N eigenvalues of [T], i.e.,

$$[T] \ [\phi^k] = \lambda_k [\phi^k] \qquad (7)$$

where $[\phi^k]$ is the eigenvector which corresponds to λ_k. If the eigenvectors (or mode shapes) are assumed in the form

$$\phi_j^k = A \cos j\theta_k + B \sin j\theta_k \qquad (8)$$

then

$$\lambda_k = 2(1 - \cos \theta_k) \qquad (9)$$

where the θ_k are the N roots of the equation

$$\sin (N + 1)\theta_k - 2(1 - {}^k_{B}/k_p) \sin N\theta_k + (1 - {}^k_{B}/k_p)^2 \sin (N - 1)\theta_k = 0 \qquad (10)$$

The ϕ_j^k are normalized for each mode k so that

$$\sum_{j=1}^{N} (\phi_j^k)^2 = 1 \qquad ,k = 1, 2, \ldots, N \qquad (11)$$

We next write the solution to the system, Eq. (3), as the sum of the modal contributions,

$$x_j(t) = \sum_{k=1}^{N} \phi_j^k \ q_k(t) \qquad (12)$$

When the system is premultiplied by the transpose of the vector $[\phi^k]$, and use is made of the orthogonality condition

$$\sum_{j=1}^{N} \phi_j^k \ \phi_j^\ell = \delta_{k\ell} \qquad (13)$$

($\delta_{k\ell}$ is the Kroneker delta), one obtains the equation for the kth generalized coordinate, $q_k(t)$
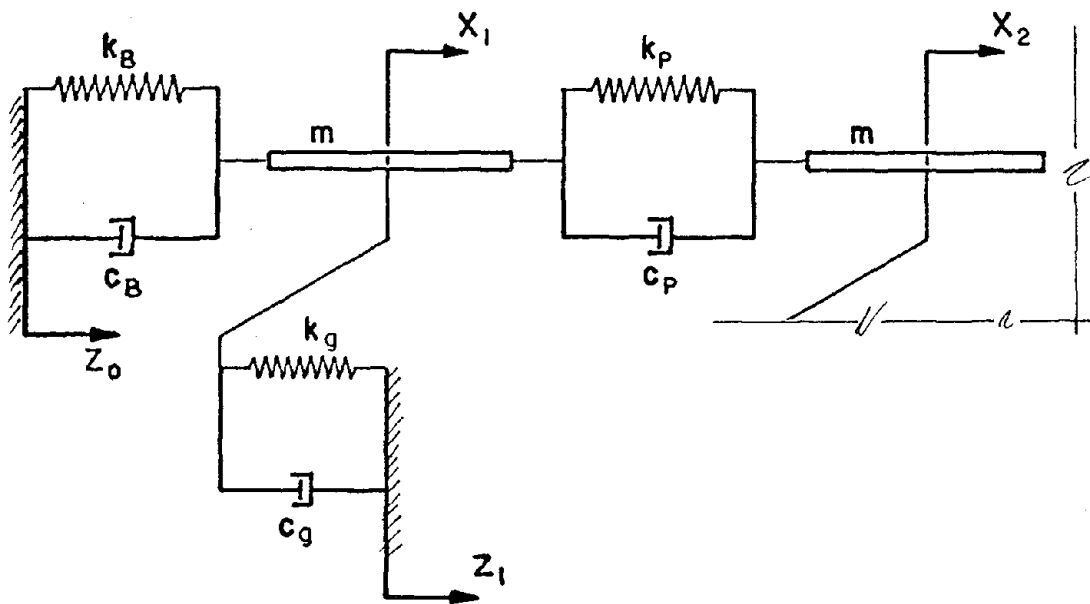
FIG. 3   PIPE   END   CONDITION

$$\ddot{q}_k + (\frac{c_g}{m} + \lambda_k \frac{c_p}{m})\dot{q}_k + (\frac{k_g}{m} + \lambda_k \frac{k_p}{m})q_k = \frac{k_g}{m} \sum_{j=1}^{N} \phi_j^{\ k} z_j$$

$$+ \frac{c_g}{m} \sum_{j=1}^{N} \phi_j^{\ k} \dot{z}_j + \frac{k_B}{m} (\phi_1^{\ k} z_o + \phi_N^{\ k} z_{N+1}) + \frac{c_B}{m} (\phi_1^{\ k} \dot{z}_o + \phi_N^{\ k} \dot{z}_{N+1}) \qquad (14)$$

It is noted that if

$$c_B/c_p = k_B/k_p \qquad (15)$$

then $[T_c]$ is identical to $[T]$ and the modal damping term in Eq. (14) is exact. Otherwise, it is a good approximation.

Up to this point, except for the last comment, no mathematical approximations have been made. To progress further, various special cases must be examined in detail.

A. **Pipe With Very Soft Joints**

The simplest special case is that in which the joints are very soft. Mathematically, this is the limiting case as $k_p/k_g \to 0$ and $c_p/c_g \to 0$. All N natural frequencies then coalesce into a single value[*)]

$$\omega_k = \omega_g = \sqrt{\frac{k_g}{m}} \qquad ,k = 1, 2, \ldots, N \qquad (16)$$

While the expressions for the normal modes, Eq. (8), are still valid, there is no need to use a modal approach. Referring back to the equation of motion of a typical link, Eq. (1), one sees that the equations are completely uncoupled, i.e.,

$$\ddot{x}_i + 2\omega_g \xi_g \dot{x}_i + \omega_g^2 x_i = \omega_g^2 z_i + 2\omega_g \xi_g \dot{z}_i \qquad (17)$$

[*)] This is true provided none of the λ_k are large, see Eq. (6). When $k_B \gg k_p$, two values of λ_k will be large, but Eq. (16) will still apply to the remaining N-2 frequencies.

where

$$\xi_g = \frac{c_g}{2m\omega_g} \tag{18}$$

We may write a similar expression for the adjacent link $i + 1$. Subtracting the two equations, and denoting $x_{i+1} - x_i$ as Δx, and $z_{i+1} - z_i$ as Δz

$$\Delta\ddot{x} + 2\omega_g\xi_g \Delta\dot{x} + \omega_g{}^2 \Delta x = \omega_g{}^2 \Delta z + 2\omega_g\xi_g \Delta\dot{z} \tag{19}$$

Equation (19) relates the relative displacement of two successive links to the incoherent component of the input, $\Delta z(t)$, over the length ℓ of a single link. Letting

$$\Delta y = \Delta x - \Delta z \tag{20}$$

Eq. (19) transforms into

$$\Delta\ddot{y} + 2\omega_g\xi_g \Delta\dot{y} + \omega_g{}^2 \Delta y = - \Delta\ddot{z} \tag{21}$$

The form of Eq. (21) is identical to that for the relative displacement Δy of a single degree of freedom oscillator of circular frequency ω_g, damping ratio ξ_g and input ground acceleration $\Delta\ddot{z}(t)$.

The physical quantity of interest is the maximum difference in absolute displacement of adjacent links, $MAX[\Delta x(t)]$. Since the polarity and direction of propagation of the ground motion generally is unknown a priori, usually one wishes the magnitude of $\Delta x(t)$ without regard to sign, $MAX|\Delta x(t)|$.

By analogy to the standard response spectrum, Weidlinger and Nelson (Refs. [6] and [7]) defined the Interference Response spectrum as

$$\bar{S}_I(\omega, \xi, \ell) \equiv MAX|\Delta x(t)| \tag{22}$$

where $\Delta x(t)$ is the solution to Eq. (19) when the input is $\Delta z(t)$. Rather

than view $\bar{S}_I$ as associated with a particular incoherent motion $\Delta z(t)$, which is generally not available, it will be associated with the total seismic motion $z(t)$ of the earthquake and the interference interval ℓ. In this paper, only incoherent motion caused by a phase delay τ will be considered, so that the Interference Response spectrum may be written as $S_I(\omega, \xi, \tau)$.

Examples of Interference Response spectra, log-log plots of S_I versus period, for several earthquake records are given in Refs. [6] and [7]. The curves are parametric in the phase delay time τ. Methods of estimating S_I, when the standard response spectra are available, are also suggested in Refs. [6] and [7]. It should be noted that for the current case of a pipe with very soft joints, the solution MAX$|\Delta x(t)|$ is immediately available, if S_I is known, by simply evaluating S_I at $\omega = \omega_g$, $\xi = \xi_g$ and the appropriate delay time τ.

B. Pipe Without Intermediate Support Or Bridge

The other extreme is the case where the lifeline is supported only at the ends, such as a bridge. In this case, k_g and c_g are both zero, so that

$$\omega_k^2 = \frac{k_p}{m} \lambda_k \tag{23}$$

and

$$\xi_k = \frac{\lambda_k c_p}{2m\omega_k} \tag{24}$$

The equation of motion for the kth generalized coordinate, Eq. (14), becomes

$$\ddot{q}_k + 2\omega_k \xi_k \dot{q}_k + \omega_k^2 q_k = \frac{k_B}{m} (\phi_1^k z_0 + \phi_N^k z_{N+1})$$
$$+ \frac{c_B}{m} (\phi_1^k \dot{z}_0 + \phi_N^k \dot{z}_{N+1}) \tag{25}$$

Since the structure is symmetric, there will be symmetric and antisymmetric modes. For the symmetric modes, $\phi_1^k = \phi_N^k$, so that the right hand side of Eq. (25) can be written

$$\frac{k_B}{m} \phi_1^{\ k} (z_o + z_{N+1}) + \frac{c_B}{m} \phi_1^{\ k} (\dot{z}_o + \dot{z}_{N+1})$$

$$= \frac{k_B \phi_1^{\ k}}{m} 2\bar{z} + \frac{c_B \phi_1^{\ k}}{m} 2\dot{\bar{z}} \qquad , \text{ k symmetric} \tag{26}$$

where $\bar{z}(t)$ is the coherent component of the input. For the antisymmetric modes, $\phi_1^{\ k} = - \phi_N^{\ k}$, so that the right hand side involves the incoherent motion $\Delta z(t) = z_o(t) - z_{N+1}(t)$, or

$$\ddot{q}_k + 2\omega_k \xi_k \dot{q}_k + \omega_k^{\ 2} q_k = \frac{k_B}{m} \phi_1^{\ k} \Delta z(t)$$

$$+ \frac{c_B}{m} \phi_1^{\ k} \Delta\dot{z}(t) \qquad , \text{ k antisymmetric} \tag{27}$$

We introduce the relative coordinate

$$\eta_k = q_k - \frac{k_B}{m\omega_k^{\ 2}} \phi_1^{\ k} \Delta z \tag{28}$$

so that Eq. (27) becomes

$$\ddot{\eta}_k + 2\omega_k \xi_k \dot{\eta}_k + \omega_k^{\ 2} \eta_k = - \frac{k_B \phi_1^{\ k}}{m\omega_k^{\ 2}} \Delta\ddot{z}$$

$$+ \frac{c_B}{m} (1 - \frac{k_B}{k_p} \frac{c_p}{c_B})\phi_1^{\ k} \Delta\dot{z} \qquad , \text{ k antisymmetric} \tag{29}$$

The expression in the parentheses in the second term on the right hand side of Eq. (29) will vanish under the same condition which was assumed to justify modal damping, namely Eq. (15). Consequently, Eq. (29) may be written

$$\ddot{\eta}_k + 2\omega_k \xi_k \dot{\eta}_k + \omega_k^{\ 2} \eta_k = - P_k \Delta\ddot{z} \qquad , \text{ k antisymmetric} \tag{30}$$

where

$$P_k = \frac{k_B \phi_1^{\ k}}{m\omega_k^{\ 2}} \qquad , \text{ k antisymmetric} \tag{31}$$

is the modal participation factor for the kth mode.

We assume the critical quantity to be the relative displacement Δx across the center joint, or the strain $\Delta x/\ell$ in the center for a continuous system. In order for there to be a joint at exactly the center of the pipe, N must be even. In that case, the contribution to the center joint displacement of the symmetric modes is zero. The contribution to the center joint displacement of the kth antisymmetric mode is

$$\Delta x^{(k)} = x_{\frac{N}{2}}^{(k)} - x_{\frac{N}{2}+1}^{(k)} = (\phi_{\frac{N}{2}}^{(k)} - \phi_{\frac{N}{2}+1}^{(k)})q_k(t)$$

$$= 2\phi_{\frac{N}{2}}^{(k)} q_k(t) \qquad , \text{ k antisymmetric} \tag{32}$$

Finally, the total center joint displacement will be the sum of all the modal contributions

$$\Delta x(t) = x_{\frac{N}{2}} - x_{\frac{N}{2}+1} = \sum_{\substack{k \text{ antisym.}}}^{N} 2\phi_{\frac{N}{2}}^{(k)} q_k(t) \tag{33}$$

In order to use spectral techniques, one observes that when the $\Delta \dot{z}$ term vanishes in Eq. (29), Eq. (27) becomes

$$\ddot{q}_k + 2\omega_k\xi_k \dot{q}_k + \omega_k^2 q_k = \omega_k^2 P_k\Delta z + 2\omega_k\xi_k P_k\Delta\dot{z} \tag{34}$$

which is similar to Eq. (19), except q_k replaces Δx, and the incoherent ground input is multiplied by the modal participation factor P_k. Consequently, the maximum absolute value of the kth generalized coordinate is given by

$$MAX|q_k(t)| = P_k \bar{S}_I(\omega_k, \xi_k, L) \tag{35}$$

where L is the total distance between support points. Recalling Eq. (32), the contribution of the kth (antisymmetric) mode to the center joint displacement is

$$\text{MAX}\left|\Delta x^{(k)}(t)\right| = 2\phi_{\frac{N}{2}}^{k} \; P_k \; \bar{S}_I(\omega_k, \xi_k, L) \tag{36}$$

or, in the case of incoherence due to a phase delay

$$\text{MAX}\left|\Delta x^{(k)}(t)\right| = J_k \; S_I(\omega_k, \xi_k, \tau_L) \tag{37}$$

where the alternate form of the interference spectrum has been used (τ_L is the delay time corresponding to L) and where

$$J_k = 2\phi_{\frac{N}{2}}^{k} \; P_k = \frac{2k_B}{m\omega_k^2} \; \phi_1^{k} \; \phi_{\frac{N}{2}}^{k} \qquad , \text{ k antisymmetric} \tag{38}$$

is a joint modal participation factor.

The final step is to "sum" all the modal contributions. Here, the problem is completely analogous to that faced in the seismic analysis of multi-degree of freedom buildings using the conventional response spectra. If the peak modal responses all occurred simultaneously, then the direct sum would be appropriate. For distinct and widely spaced natural frequencies this is highly unlikely, and most authorities, e.g., Refs. [4], [5] and [10], suggest using the square root of the sum of the squares of the modal contributions. The same approach could be used here.

C. Center Joint Displacement Of Long Continuously Supported Pipe

Returning to the general case, let us consider the quantity of interest to be the relative displacement between two adjacent links near the center of a long continuously supported, either buried or above ground, pipe. This corresponds to the opening up or closing of the center joint. For very long pipes, $N \gg 1$, the end conditions will have a negligible effect on the motion near the center, and thus, the z_o and z_{N+1} terms on the right hand side of Eq. (14) may be dropped. In addition, we introduce the relative generalized coordinate

$$\eta_k = q_k - \frac{\omega_g^2}{\omega_k^2} \sum_{j=1}^{N} \phi_j^{\ k} z_j \tag{39}$$

where ω_g is given by Eq. (16). The fraction of critical damping in the kth mode (with ξ_g given by Eq. (18)) then becomes

$$\xi_k = \xi_g \frac{(1 + \lambda_k\ ^c p/c_g)}{\sqrt{1 + \lambda_k (^k p/k_g)}} \tag{40}$$

Equation (14), in terms of the relative coordinate, and dropping boundary contributions, transforms into

$$\ddot{\eta}_k + 2\omega_k \xi_k \dot{\eta}_k + \omega_k^2 \eta_k = -\frac{\omega_g^2}{\omega_k^2} \sum_{j=1}^{N} \phi_j^{\ k} \ddot{z}_j$$
$$+ 2\omega_g \xi_g \left[1 - \frac{(1 + \lambda_k\ ^c p/c_g)}{(1 + \lambda_k\ ^k p/k_g)} \right] \sum_{j=1}^{N} \phi_j^{\ k} \dot{z}_j \tag{41}$$

In principle, Eq. (41) as is may be solved in the time domain if all the $z_j(t)$ were given. However, it is worthwhile to simplify Eq. (41) further by dropping the second term on the right hand side. There are three instances when this is justified. First, if $^c p/c_g = ^k p/k_g$ the term is identically zero. Second, for an above ground structure, the damping $\xi_g \ll 1$, so that the contribution of the term is small. Finally, for a buried structure, both $^c p/c_g \ll 1$ and $^k p/k_g \ll 1$, while $\lambda_k \leq 4$ typically[*]. Consequently, the expression in the bracket will be small.

The sum of input ground accelerations may be written as

$$\sum_{j=1}^{N} \phi_j^{\ k} \ddot{z}_j \equiv \phi_1^{\ k}(\ddot{z}_1 - \ddot{z}_2) + (\phi_1^{\ k} + \phi_2^{\ k})(\ddot{z}_2 - \ddot{z}_3)$$
$$+ \ldots + (\ddot{z}_m - \ddot{z}_{m+1}) \sum_{j=1}^{m} \phi_j^{\ k} + \ldots + \ddot{z}_N \sum_{j=1}^{N} \phi_j^{\ k} \tag{42}$$

---

[*] By Gerschgorin's theorem, $0 \leq \lambda_k \leq 4$, $k = 1, 2, \ldots, N-2$ while $^k B/k_p \leq \lambda_{N-1}$, $\lambda_N \leq 2 + ^k B/k_p$, for $^k B/k_p > 2$.

Since the structure is symmetric (including the boundary conditions) the normal modes will be either symmetric or antisymmetric.

For large values of N, the response near the center of the pipe should not depend strongly on whether N is odd or even. For convenience, we choose N as even, so that there is a joint at exactly the center of the pipe. In that case, the contribution to the center joint displacement of the symmetric modes is zero. For the antisymmetric modes

$$\sum_{j=1}^{N} \phi_j{}^k \equiv 0 \qquad , \text{ k antisymmetric} \tag{43}$$

Introducing the notation

$$\Delta z_j(t) \equiv z_j(t) - z_{j+1}(t) \tag{44}$$

Eq. (42) becomes

$$\sum_{j=1}^{N} \phi_j{}^k \ddot{z}_j \equiv \sum_{j=1}^{N-1} \Delta \ddot{z}_j \left(\sum_{i=1}^{j} \phi_i{}^k \right) \qquad , \text{ k antisymmetric} \tag{45}$$

which may be inserted into Eq. (41), while a similar expression between the ground displacements may be used in Eq. (39).

Consider $\Delta z_m \neq 0$, while all $\Delta z_j(t) \equiv 0$ for $j \neq m$. Dropping the $\dot{z}$ terms, Eq. (41) becomes

$$\ddot{\eta}_{km} + 2\omega_k \xi_k \dot{\eta}_{km} + \omega_k{}^2 \eta_{km} = - \frac{\omega_g{}^2}{\omega_k{}^2} \Delta \ddot{z}_m \sum_{j=1}^{m} \phi_j{}^k \tag{46}$$

while

$$q_{km} = \eta_{km} + \frac{\omega_g{}^2}{\omega_k{}^2} \Delta z_m \sum_{j=1}^{m} \phi_j{}^k \tag{47}$$

The solution to Eqs. (46) and (47) is

$$q_{km}(t) = \left[\frac{\omega_g{}^2}{\omega_k{}^2} \sum_{j=1}^{m} \phi_j{}^k \right] r_{km}(t) \tag{48}$$

where r_{km} is the solution to

$$\ddot{r}_{km} + 2\omega_k \xi_k \dot{r}_{km} + \omega_k^2 r_{km} = \omega_k^2 \Delta z_m(t) + 2\omega_k \xi_k \Delta \dot{z}_m(t) \tag{49}$$

Equation (49) is of the same form as that used to define the Interference Response spectrum, i.e., Eq. (19), but the input is now Δz_m. The contribution of Δz_m to the kth mode center joint displacement is zero for symmetric modes, and

$$\Delta x_m^{(k)} = x_{\frac{N}{2},m}^{(k)} - x_{\frac{N}{2}+1,m}^{(k)} = 2\phi_{\frac{N}{2}}^k q_{km} \tag{50}$$

for antisymmetric modes. Combining Eqs. (48) and (50)

$$\Delta x_m^{(k)} = \left[2\phi_{\frac{N}{2}}^k \frac{\omega_g^2}{\omega_k^2} \sum_{j=1}^m \phi_j^k \right] r_{km}(t) = D_m^k r_{km}(t) \tag{51}$$

where the quantity D_m^k, defined by the expression within the bracket, is the influence coefficient for center joint displacement, in mode k, for a unit ground relative displacement across joint m. It should be noted that the D_m^k depend only on the geometry and mechanical properties of the system, via the eigenvalues and eigenvectors, and are independent of the input ground motion.

In general, the $\Delta z_m(t)$ are not known. In the case where the incoherent ground displacement across a joint is due solely to a phase delay τ, all Δz_m will be the same, except for a phase delay, i.e.,

$$\Delta z_m(t) = \Delta z(t - (m-1)\tau) \tag{52}$$

where Δz without a subscript is the incoherent ground displacement across the first joint. The resulting $r_{km}(t)$ will also all be related by a similar expression

$$r_{km}(t) = r_k(t - (m-1)\tau) \tag{53}$$

where $r_k(t)$ is the solution to Eq. (49) with input $\Delta z(t)$. Hence, the total k^{th} mode contribution to the center joint displacement is

$$\Delta x^{(k)}(t) = \sum_{m=1}^{N-1} D_m^k \, r_k(t - (m-1)\,\tau) \tag{54}$$

while the total joint displacement is the sum of the modal contributions

$$\Delta x(t) = \sum_{k=1}^{N} \Delta x^{(k)}(t) \qquad , \; k = \text{antisymmetric only} \tag{55}$$

At first, it would appear that spectral techniques could not be used easily. For, in addition to the problem of adding modal contributions which is always present in a multi-degree of freedom system, there is an additional problem represented by Eq. (54). This is the fact that the peak modal response due to the load across each joint will occur at a different time. Consequently, it is uncertain how to combine them. In the limiting case, when the load may be assumed to act simultaneously across the entire [*] pipeline.

$$\text{MAX} \left| \Delta x^{(k)}(t) \right| = S_I(\omega_k, \, \xi_k, \, \tau) \sum_{m=1}^{N-1} D_m^k \tag{56}$$

Finally, if, in addition, the modal frequencies and damping ratios all coalesce to ω and ξ, respectively, then the total response will be

$$\text{MAX} \left| \Delta x(t) \right| = S_I(\omega, \, \xi, \, \tau) \sum_{\substack{k=1 \\ \text{antisym.}}}^{N} \sum_{m=1}^{N-1} D_m^k \tag{57}$$

By Eq. (6), this will only occur when $k_p/k_g \to 0$, i.e., the pipe with very soft joints discussed previously. Nevertheless, it will be shown subsequently that the spectral approach has much wider applicability.

---

[*] It can be shown that Eq. (56) is valid when $N\omega_k\tau \ll \pi$ and $N\Omega\tau \ll \pi$ where Ω is the circular frequency of the highest frequency component in the input Δz. This is done in Appendix C for a single, sinusoidal input.

III NUMERICAL RESULTS FOR LONG SUPPORTED PIPES

Since the application of spectral techniques to the other special cases discussed are straightforward, numerical time domain calculations were restricted to that of the center joint displacement of a long continuously supported pipe.

A. Mode Shapes And Influence Coefficients

The eigenvalues and eigenvectors of the system are particularly simple when $k_B = k_p$, i.e., the end joints are identical to the intermediate ones. In that case, by Eqs. (9) and (10)

$$\lambda_k = 2(1 - \cos \frac{k\pi}{N+1}) \tag{58}$$

and

$$\phi_j^{\ k} = \sqrt{\frac{2}{N+1}} \sin \frac{jk\pi}{N+1} \tag{59}$$

while k = even are the antisymmetric modes. With the $\phi_j^{\ k}$ given above, the inner sum of Eq. (45) may be expressed in closed form (Ref. [11], No. 417),

$$\sum_{i=1}^{j} \phi_i^{\ k} = \sum_{i=1}^{j} \sqrt{\frac{2}{N+1}} \sin \frac{ik\pi}{N+1} = \sqrt{\frac{2}{N+1}} \left[\frac{\sin \frac{jk}{N+1} \frac{\pi}{2} \sin \frac{(j+1)k}{N+1} \frac{\pi}{2}}{\sin \frac{k}{N+1} \frac{\pi}{2}} \right] \tag{60}$$

while

$$D_m^{\ k} = \frac{\frac{4}{N+1} (-1)^{\frac{k}{2} - 1} \sin(\frac{m+1}{N+1} \frac{k\pi}{2}) \sin(\frac{m}{N+1} \frac{k\pi}{2})}{1 + 2(^k p/k_g) (1 - \cos \frac{k\pi}{N+1})} \tag{61}$$

Using No. 469 of Ref. [11], the sum of influence coefficients for a particular mode may be found in closed form

$$\sum_{m=1}^{N-1} D_m^{\ k} = \frac{2(-1)^{\frac{k}{2} - 1} \cos(\frac{k}{N+1} \frac{\pi}{2})}{1 + 2(^k p/k_g) (1 - \cos \frac{k\pi}{N+1})} \tag{62}$$

For vanishingly small values of k_p/k_g, the double sum in Eq. (57) can be shown to equal unity, i.e.,

$$\sum_{k=2,4,6\ldots}^{N} \sum_{m=1}^{N-1} D_m^{\,k} = 1 \qquad\qquad (63)$$

so that, formally, the current modal approach reduces to that of a pipe with very soft joints discussed earlier. It should be mentioned that, numerically, the double sum also equaled unity to the four decimal places that were printed out for $k_p/k_g \neq 0$. This suggests that Eq. (63) may be true in general[*].

The mode shapes and influence coefficients are plotted in Fig. 4 for $N = 20$ and $k_g = 4k_p$. Only the even (antisymmetric) modes are plotted. The values of $D_m^{\,k}$ for the odd modes are, of course, all zero. The tick marks represent the joints. It should be noted that the mode shapes represent the axial displacement of each segment, even though they are plotted transversely. Also shown on the figure are the corresponding values of the circular frequencies. These values are based on $\omega_g = 2\pi/\sec$ (frequency = 1 Hz). Any other value of ω_g would change the ω_k proportionately. The influence coefficients $D_m^{\,k}$ are plotted on the right. Each element of D is constant across a joint. The triangle in the middle marks the center joint. It is observed that the $D_m^{\,k}$ are symmetric. The magnitudes of the $D_m^{\,k}$ generally are small near the ends. Moreover, the largest value in any particular mode decreases as the mode number increases. The sums of the influence coefficients for the various modes are given in Fig. 4. They alternate in sign and decrease in magnitude as

---

[*] It was subsequently shown in Appendix D that Eq. (63) is true in general, at least for $N \to \infty$, see Eq. (D-53).
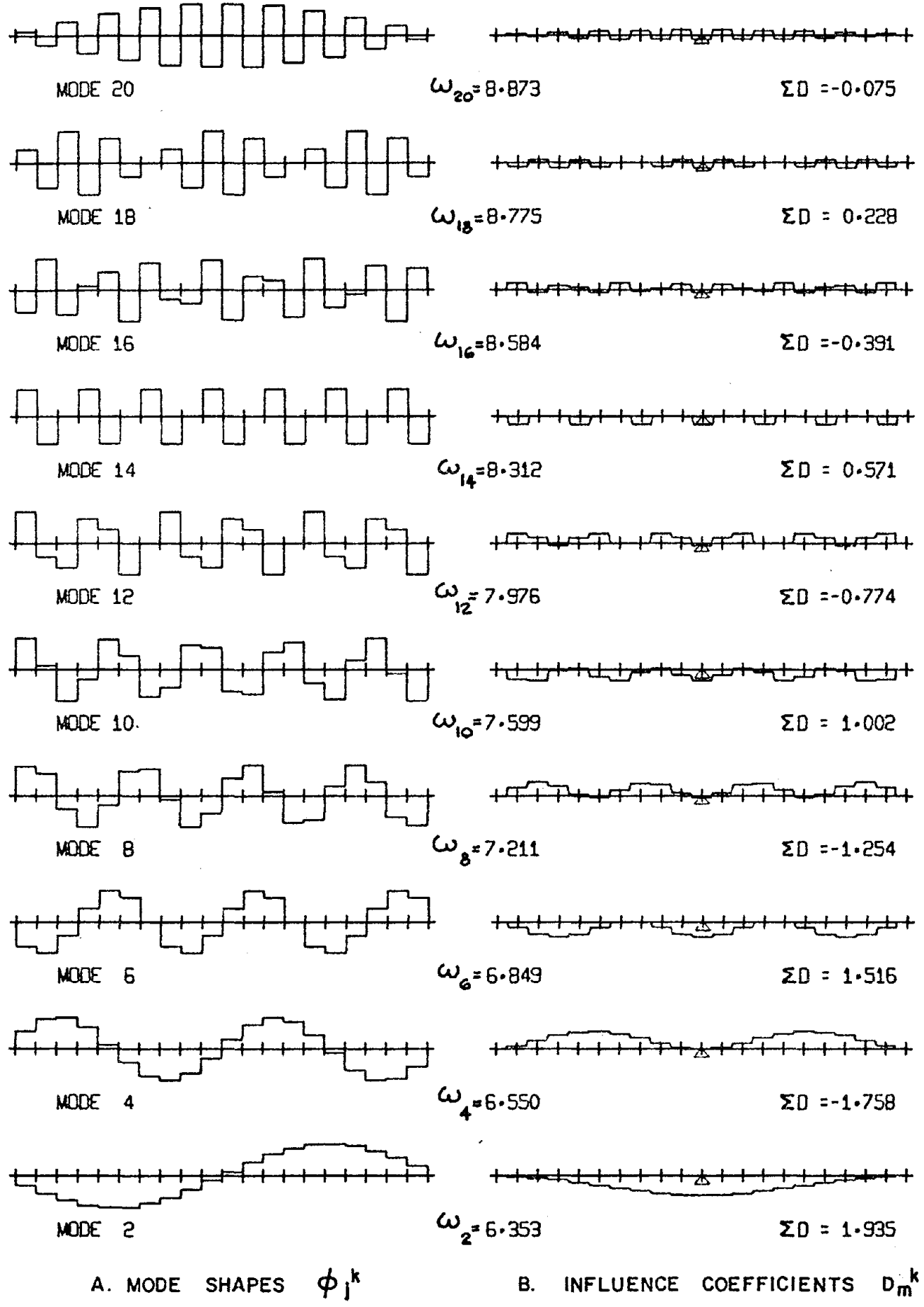
A. MODE SHAPES $\phi_j{}^k$

B. INFLUENCE COEFFICIENTS $D_m{}^k$

FIG. 4 ANTISYMMETRIC (EVEN) AXIAL MODE SHAPES AND INFLUENCE COEFFICIENTS FOR CENTER JOINT RELATIVE DISPLACEMENT FOR 20 SEGMENT PIPE ($k_B = k_p$, $k_g = 4k_p$, $\omega_g = 2\pi/sec$)

MODE 20 $\omega_{20} = 8.873$ $\Sigma D = -0.075$

MODE 18 $\omega_{18} = 8.775$ $\Sigma D = 0.228$

MODE 16 $\omega_{16} = 8.584$ $\Sigma D = -0.391$

MODE 14 $\omega_{14} = 8.312$ $\Sigma D = 0.571$

MODE 12 $\omega_{12} = 7.976$ $\Sigma D = -0.774$

MODE 10 $\omega_{10} = 7.599$ $\Sigma D = 1.002$

MODE 8 $\omega_8 = 7.211$ $\Sigma D = -1.254$

MODE 6 $\omega_6 = 6.849$ $\Sigma D = 1.516$

MODE 4 $\omega_4 = 6.550$ $\Sigma D = -1.758$

MODE 2 $\omega_2 = 6.353$ $\Sigma D = 1.935$
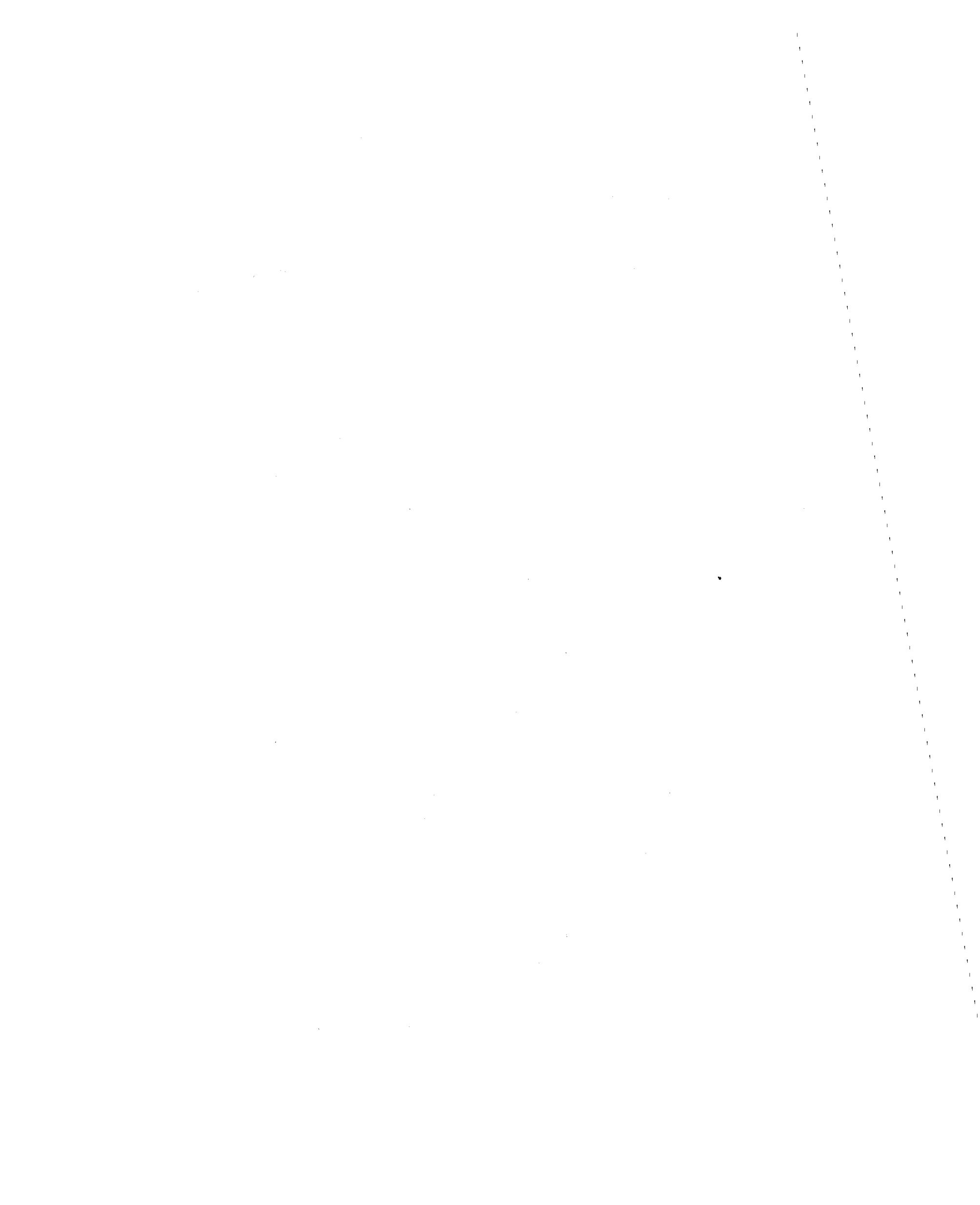
the mode number increases. The mode 2 value is almost 30 times that of mode 20.

All time history calculations were made with $k_B = k_p$. However, this is not an overly restrictive condition. Mode shapes and influence coefficients were computed numerically for other values of k_B/k_p. For example, a case was considered in which $k_B = 10k_p$ and N = 20. There were two very high frequency modes. However, the mode shapes were non-zero only near the boundaries. Moreover, the influence coefficients for center joint displacement were zero. The other 18 modes corresponded almost exactly to the case of $k_B = k_p$, but N = 18. Further details, and other examples, are given in Appendix A.

B. Time Histories

In order to investigate if any further simplifications are justified, time histories were computed for a variety of cases. A computer program, SEGPIPE, was written which computes the total center joint displacement, and the modal contributions to it, due to the identical incoherent ground input $\Delta z(t)$ at every joint, but with a constant time delay τ between successive joints. A total of 29 different calculations were made, only a few of which will be presented. A summary of the various calculations may be found in Appendix B. The first 23 runs used sinusoidal ground motion z(t) with, either a single frequency, or with several in combination. Many aspects of the results were thus more easily understood since analytical approximations (say for small τ) were available. These are described in Appendix C. These analytical results also served as checks on the code. In the undamped case, for $\Omega \neq \omega_k$, beat phenomena were observed in the modal responses where the input frequency Ω was close to a modal frequency. When damping was included, a more complex response occurred, where at early

times, the damped response was similar to but smaller than the undamped result, while at later times a steady state would develop. Except for cases in which $\omega_k \simeq \Omega$, the peak modal responses generally occurred during the transient. It should be mentioned that with 5% of critical damping, it was not possible to excite the highest mode to give the largest response, even when the input frequency Ω was made slightly larger than ω_N.

Among the quantities varied were the number of segments N, the ratio k_g/k_p, the phase delay τ, and the damping as well as the input. Values of N of 20, 22 and 40 were tried. The ratio k_g/k_p controls the spread of the natural frequencies. For $k_B = k_p$, by Gerschgorin's theorem, $0 \leq \lambda_k \leq 4$, so that by Eq. (6)

$$\omega_g = \sqrt{k_g/m} \leq \omega_k \leq \omega_g \sqrt{1 + 4(k_p/k_g)} \tag{64}$$

For buried pipes, large values of k_g/k_p are anticipated. Calculations were made with $k_g/k_p = 2$, 4 and 10. The results presented are all for $k_g/k_p = 4$, so that the modal frequencies (assuming $\omega_g = 2\pi/\text{sec}$) are restricted to

$$1 \text{ Hz} \leq f_k = \omega_k/2\pi \leq \sqrt{2} \text{ Hz} \tag{65}$$

All the results presented are for $\tau = 0.020$ sec. This could represent a 20 ft (6 m) pipe segment and a 1000 ft/sec (300 m/sec) propagation velocity. For small values of τ, the results are linear in τ, see Appendix C.

Also considered was partial loading whereby only the joints near the center were loaded. Leaving off the load near the ends had negligible effect on the center joint response. Loading only the 3 or 5 center joints of a 20 segment pipe actually resulted in slightly higher total responses than loading the entire pipe. However, the individual modal responses varied, with the higher modes contributing more in the partially loaded case. These results suggest that the joint displacement is a local

phenomenon with the situation more than a few segments away having little effect. Thus, the number of links, the end conditions, and even the gradual variation in Δz from point to point would not materially affect the results.

This is not surprising if one examines the sum of influence coefficients, of all modes at each joint, $\sum\limits_{k=2,4,...}^{N} D_m{}^k$. This sum represents the static solution due to a unit input at joint m. It is largest at the center joint, and its value falls off rapidly at either side. Except for the few joints near the center (the actual number depends on k_p/k_g), the sum is essentially zero. The static continuous analog to the current problem, see Appendix D, shows the strain decreasing exponentially from the point of application of the load.

C. Response To Earthquake Input

While Eq. (49) was solved analytically for the various sinusoidal loadings, this was no longer possible once actual earthquake records were used as the input motion. Consequently, the program was revised so that Eq. (49) was solved numerically for each mode, assuming the incoherent ground acceleration $\Delta \ddot{z}$ to be piecewise linear. Then Eq. (53) was used to shift the time scale by the appropriate delay time for each node m.

The total center joint response, and the modal contributions of the lowest five modes, for a 20 segment pipe subjected to the north-south component of the EL CENTRO May 1940 record are shown in Fig. 5. The calculation was continued to a final time of 20 seconds. The damping was assumed to be 5% of critical for each mode[*]. The incoherent ground motion across the center joint is shown in Fig. 5a. It is noted that Δz is zero until the earthquake reaches the center joint. Readers familiar with

---

[*] This assumption is not quite valid, since ξ_k should vary according to Eq. (40).
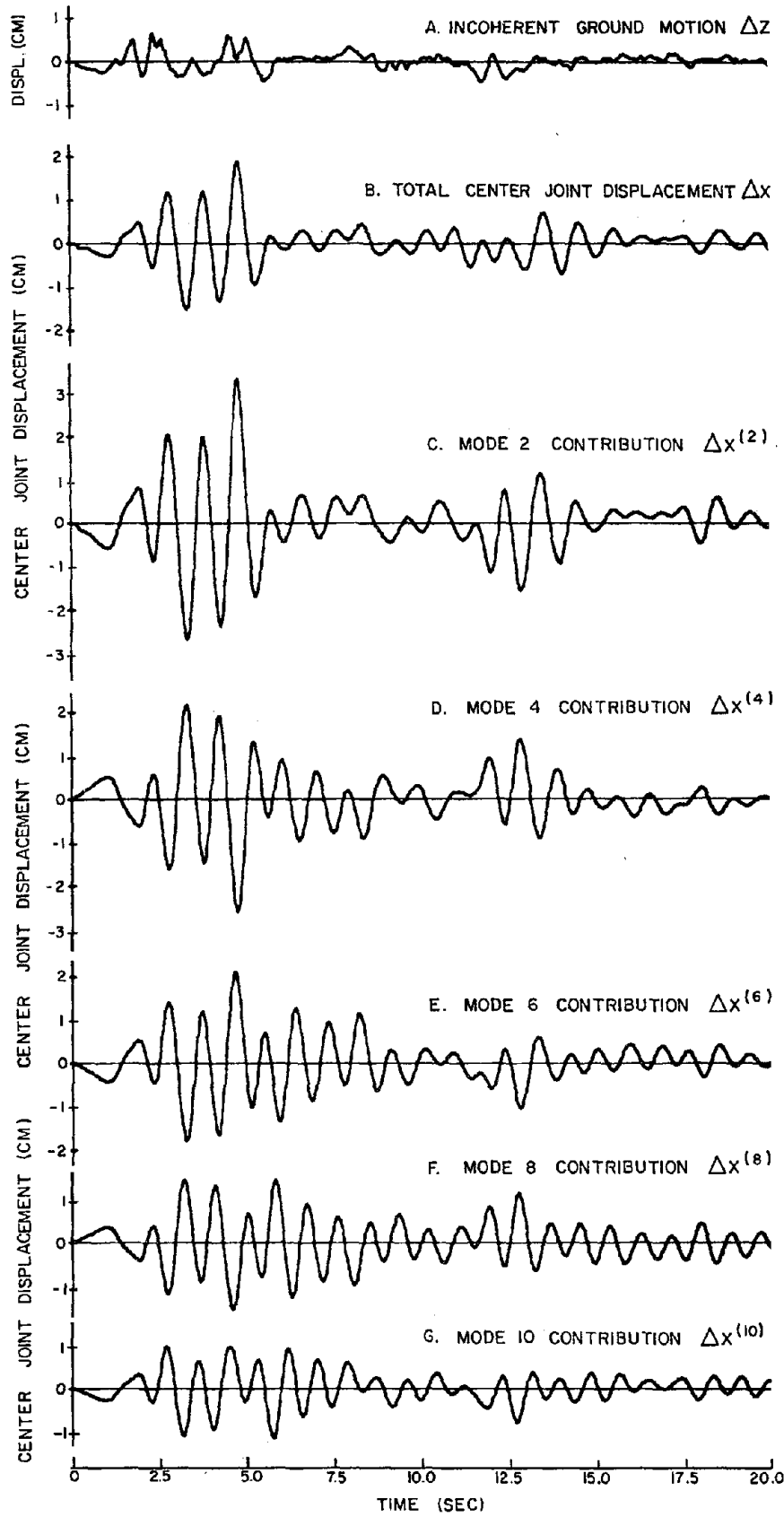
FIG. 5   TOTAL CENTER JOINT RESPONSE AND MODAL
CONTRIBUTIONS FOR A 20 SEGMENT PIPE
SUBJECTED TO THE EL CENTRO MAY 1940 N·S
RECORD (DAMPING RATIO = 5%)

earthquake records will recognize the input as the velocity record times τ [*].
The total joint displacement reaches a maximum value of 1.87 cm, representing
an amplification of 2.85.

The first three modal contributions are larger than the total response.
However, the modes alternate in sign, as do the ΣD (see Fig. 4), so that
all modes are required to reach the total. Nevertheless, the peak modal
responses do decrease as the mode number increases. The peak value of the
lowest mode not shown, mode 12, is 0.80 cm, while that of mode 20 is merely
0.076 cm. Except for a scale factor, the total response is most similar to
the mode 2 contribution, the largest contribution to the total.

The total center joint response of a 40 segment pipe is compared with
that of a 20 segment pipe, both with 5% of critical damping, in Fig. 6. The
corresponding incoherent ground motions across the center joint are shown in
Fig. 6a. The phase delay is the only difference in the two curves [**].
Except for the phase delay, the two total response curves are essentially
the same. Individual modal responses, of course, cannot be compared
directly. It is worth noting, however, that for N = 40, the mode 2 response
is larger than the total response and more than twice any other modal
contribution. Except for the amplitude, the total response is similar to
the mode 2 contribution. The center joint displacement for somewhat larger
damping, 10% of critical, for a 20 segment pipe is shown in Fig. 7. Except

---

[*] For longer delay times this is not necessarily true, see the discussion
in Refs. [6] and [7].

[**] The time scale in each case starts when the traveling ground motion
crosses the center of the first segment.
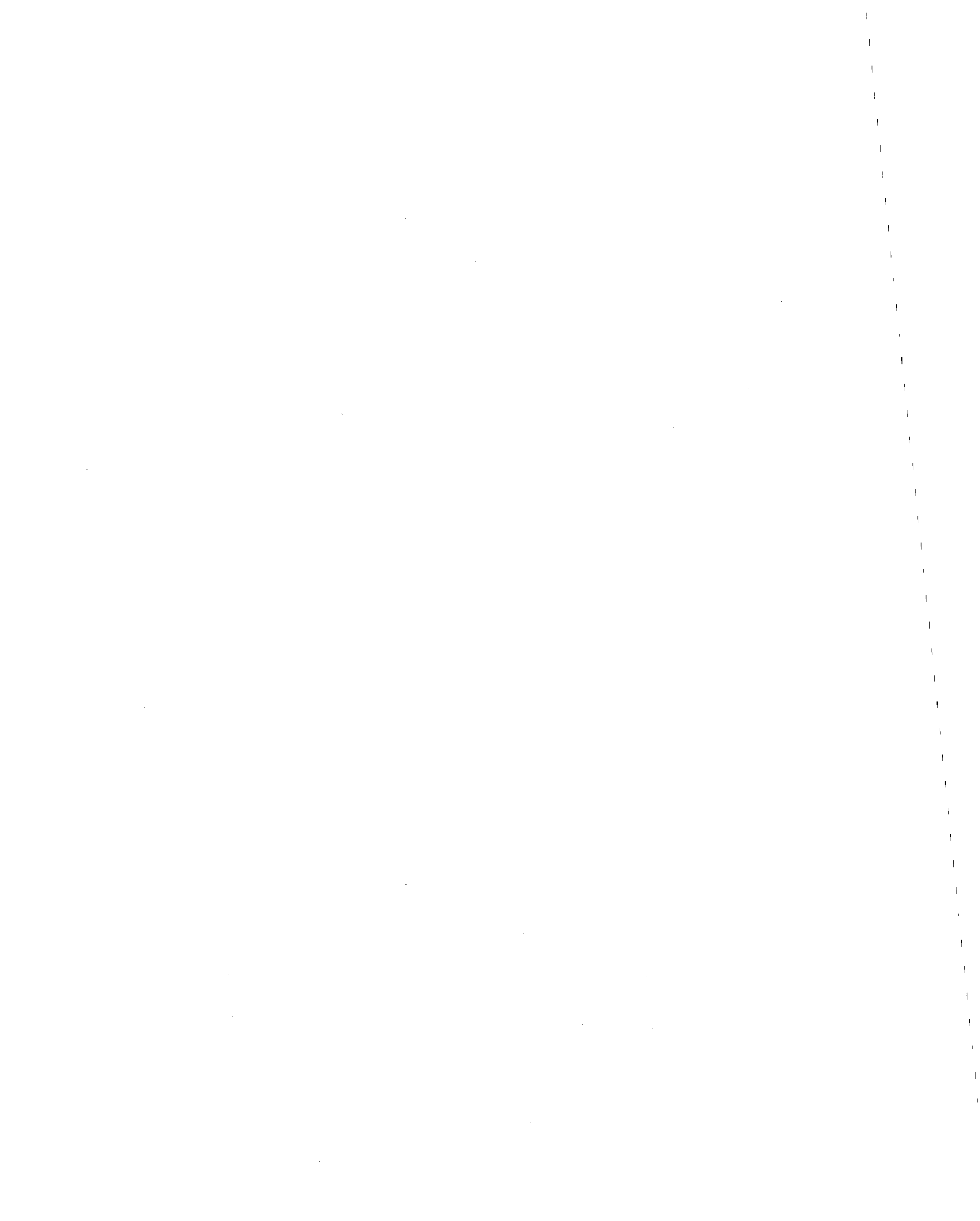
FIG. 6   COMPARISON OF TOTAL CENTER JOINT RESPONSE
FOR 20 AND 40 SEGMENTS
(INPUT GROUND MOTION "EL CENTRO" MAY 1940 N-S)

FIG. 7   TOTAL CENTER JOINT RESPONSE FOR 20 SEGMENT PIPE   FOR 10%
OF CRITICAL DAMPING (INPUT GROUND MOTION EL CENTRO MAY 1940 N·S)

for the obvious decrease in the amplitude of the oscillations, the curve is similar to those in Fig. 6. Here, the amplification is only 2.0.

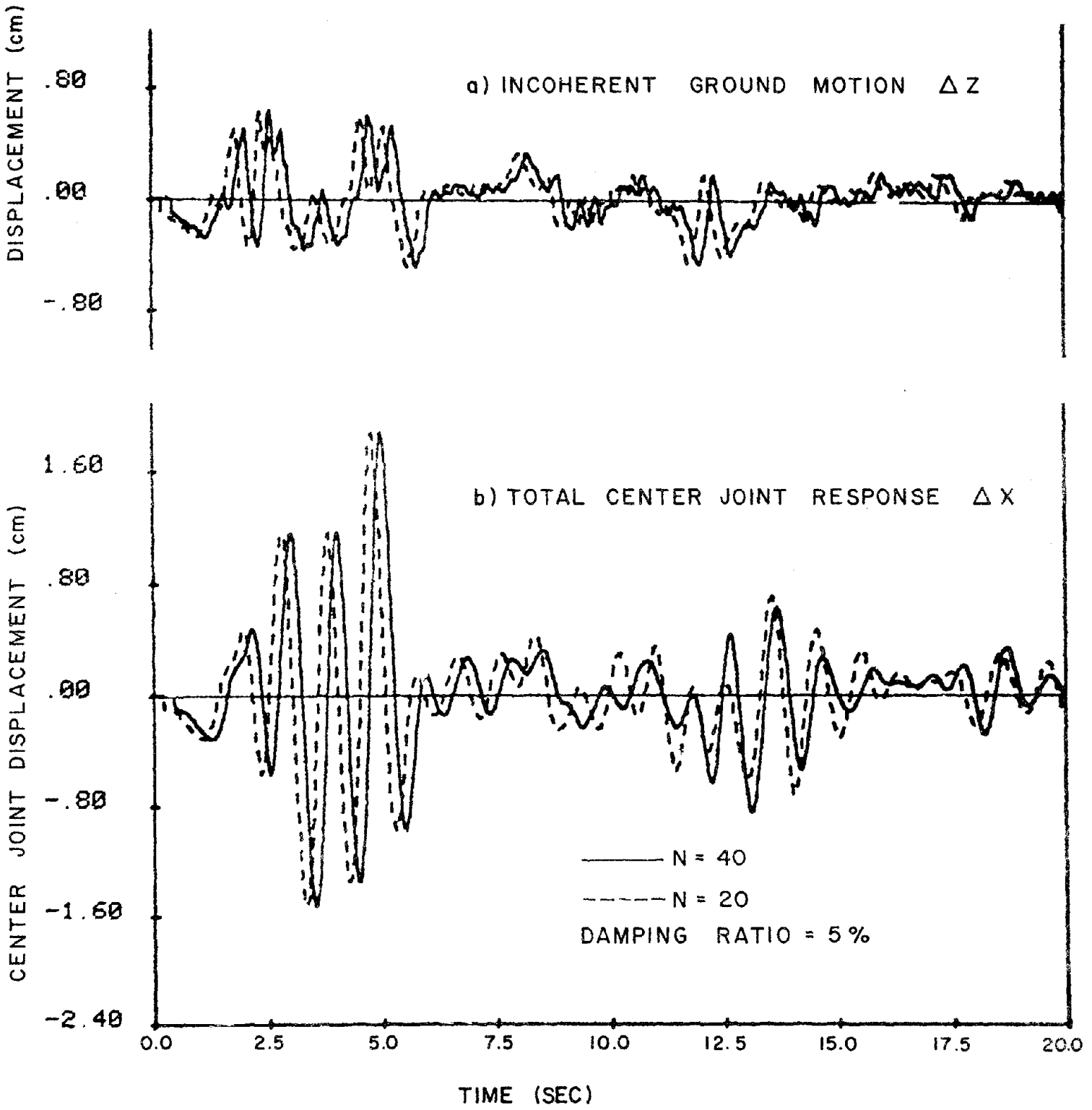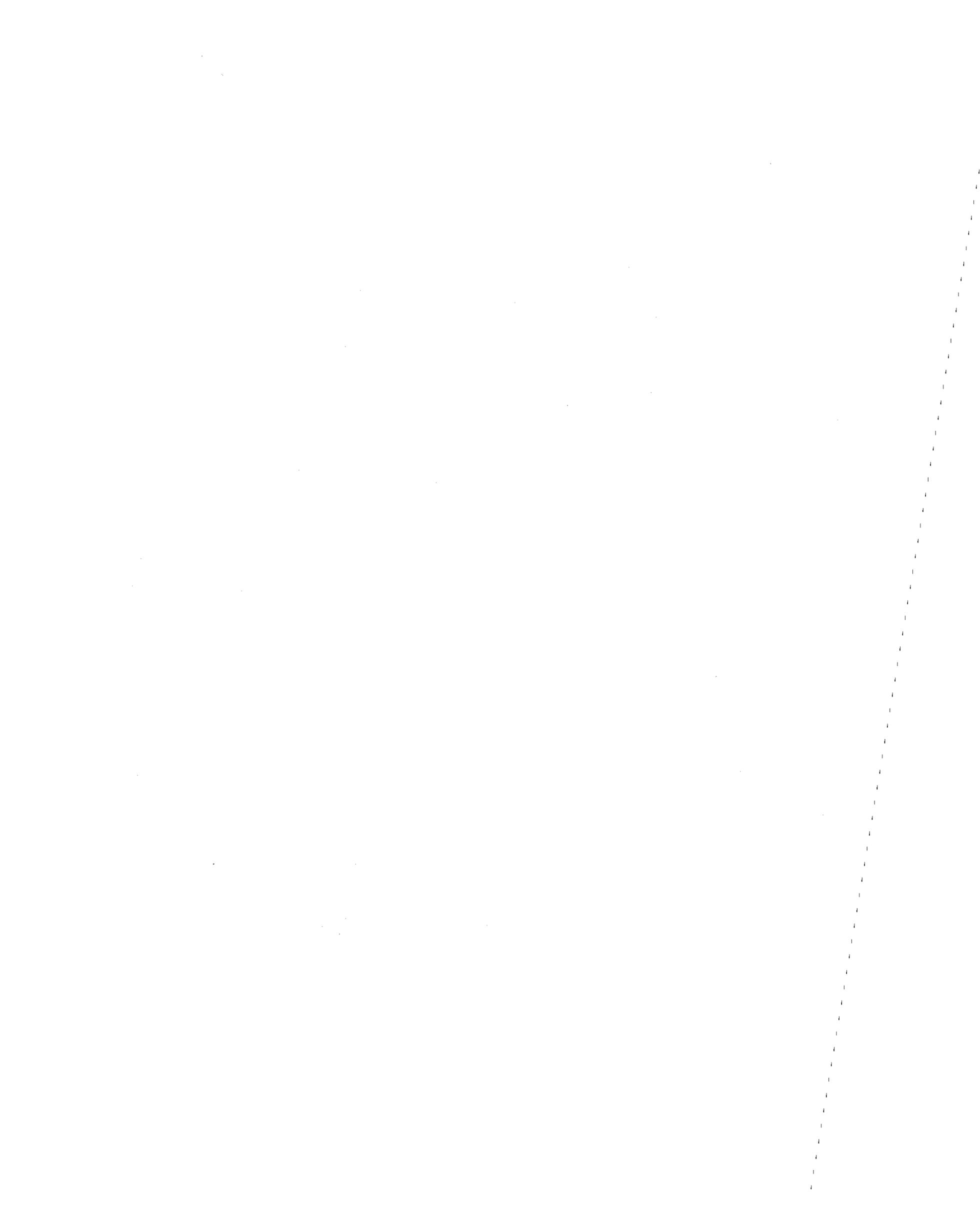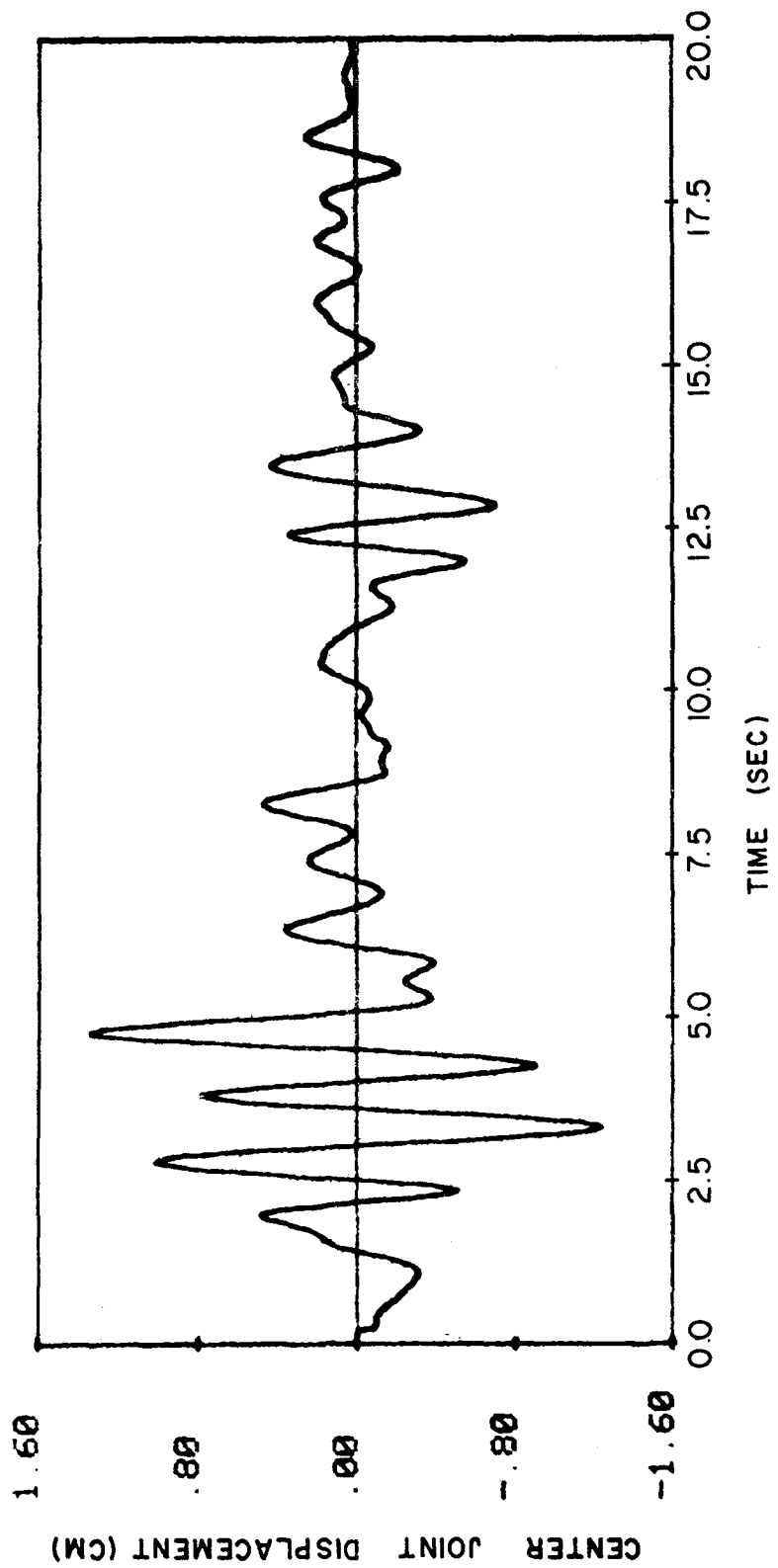The response of 20 and 40 segment lightly damped systems (1% of critical damping) are compared in Fig. 8. For early times, t < 8 sec, the two curves follow one another with the appropriate phase delay. The amplification during this time, and the peak value for N = 40, is 4.05. For N = 40, the mode 2 contribution is again larger than the total response and more than twice any other modal contribution. The peak total response occurs about 2.5 sec after the peak in the input. The situation for N = 20 is different from that in any other case considered. The peak total response is larger than that of any modal contribution, and occurs at later times, long after the peak in the input ground motion. At the time of the peak, eight of the ten modal contributions, the lowest seven plus mode 18, are all moving in the same direction, and thus add to the total response. The largest modal contribution to the peak, mode 8, is only 35% of the total.

If the input were zero for t > 8 sec, each mode would be experiencing free vibrations with a slightly different frequency. If one waited long enough, all the modes would be in phase, and contribute to the total. With any appreciable damping, however, the resulting peak would be much smaller than that observed during forced vibrations. For the longer pipe, N = 40, interference caused by the accumulated phase delay from one end of the pipe to the other leads to smaller responses in the higher modes[*].

---

[*] This statement is more easily understood by referring to Fig. 4b. If there were a phase delay of π radians between the quarter and three-quarter points, the mode 4 response would be zero. Similarly, if the delay were π between modes 3 and 17, the mode 6 response would be only a third of that with no phase delay.
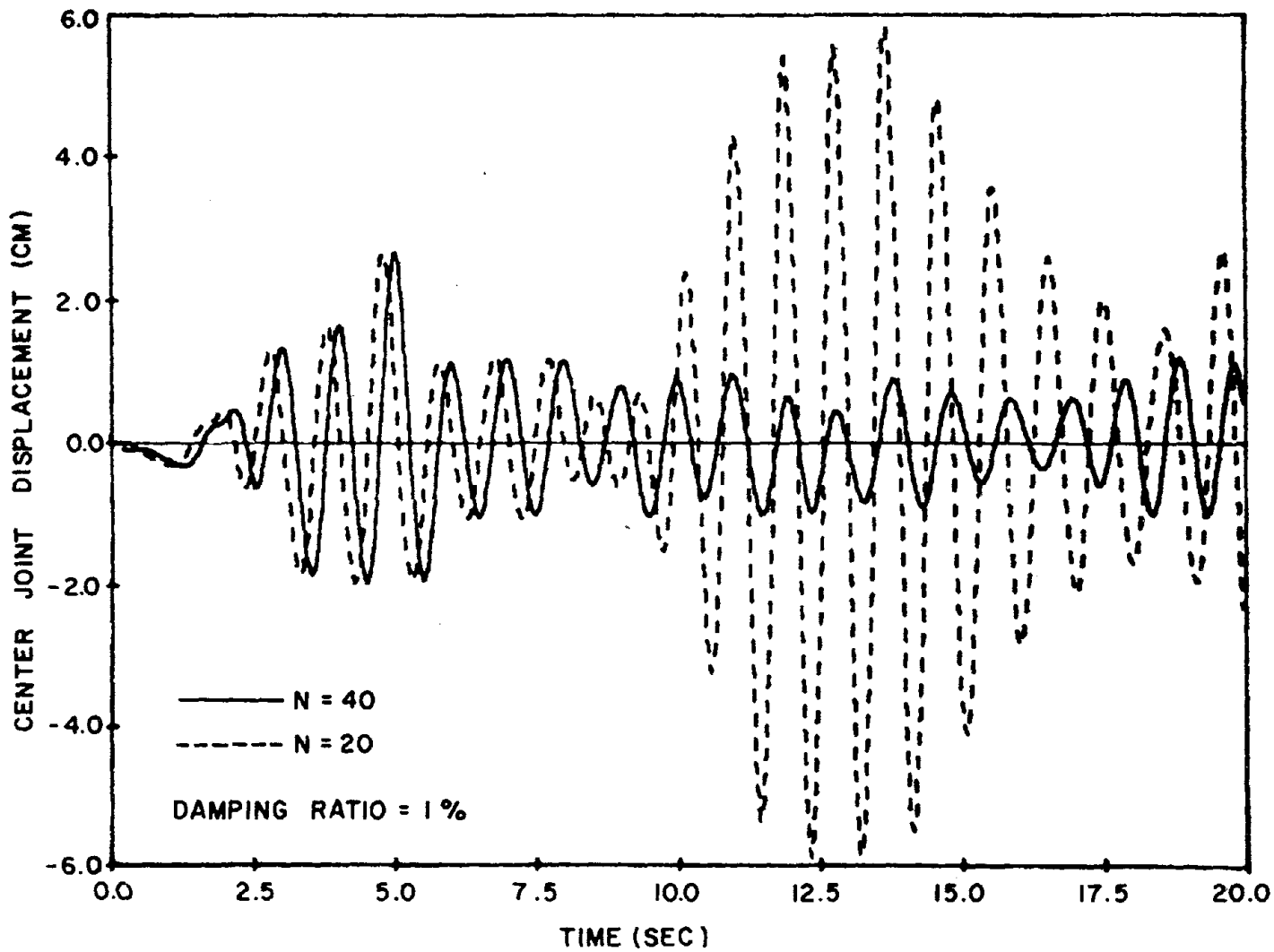
8 COMPARISON OF TOTAL CENTER JOINT RESPONSE FOR 20 AND 40 SEGMENT LIGHTLY DAMPED SYSTEMS (INPUT: EL CENTRO MAY 1940 N-S)
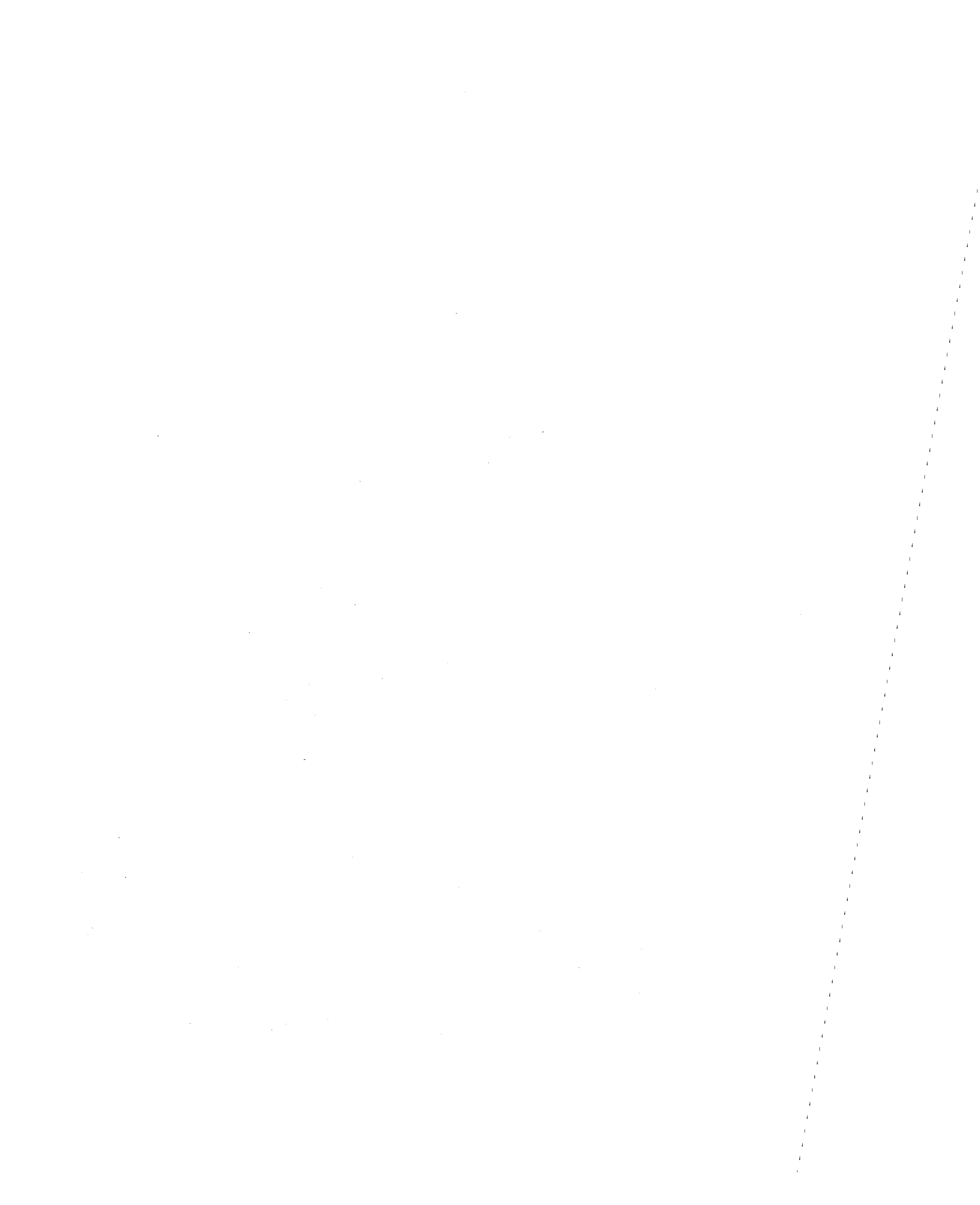
Consequently, even if the various modes were in phase, the resulting total (at least up to 20 sec) is less than that observed during forced vibrations.

D.   Interference Response Spectra

The Interference Response (IR) spectra for the EL CENTRO May 1940 north-south record for $\tau = 0.02$ sec and damping ratios of 1, 5 and 10% are plotted in Fig. 9. The spectra are drawn to a linear scale and only a limited frequency range, 0.7 to 1.5 Hz, is shown. The bounds to the natural frequencies of the system, Eq. (65), are shown in the figure, as are the lowest antisymmetric frequencies for $N = 20$ and 40, $f_2 = 1.011$ Hz and 1.003 Hz, respectively. Horizontal lines are drawn corresponding to the peak values of the center joint relative displacement attained in the various time history calculations. Dots mark the intersection of $MAX|\Delta x(t)|$ and the appropriate f_2. For 5% of critical damping, there were two calculations, both with the same peak response. For 1% damping, the $N = 20$ peak value of 5.90 is off-scale for the reason discussed previously.

In all other cases, the peak response is within 1% of the corresponding IR spectra at the lowest antisymmetric frequency. Moreover, even if the lowest frequency were not known, the spectral value at the lower bound frequency (1 Hz in this case) is an excellent approximation to the peak response of the center joint. One additional earthquake record also was used as input, and the results again agreed with the IR spectrum. Consequently, it appears that the IR spectrum offers a useful technique for evaluating the dynamic response of long segmented pipes.
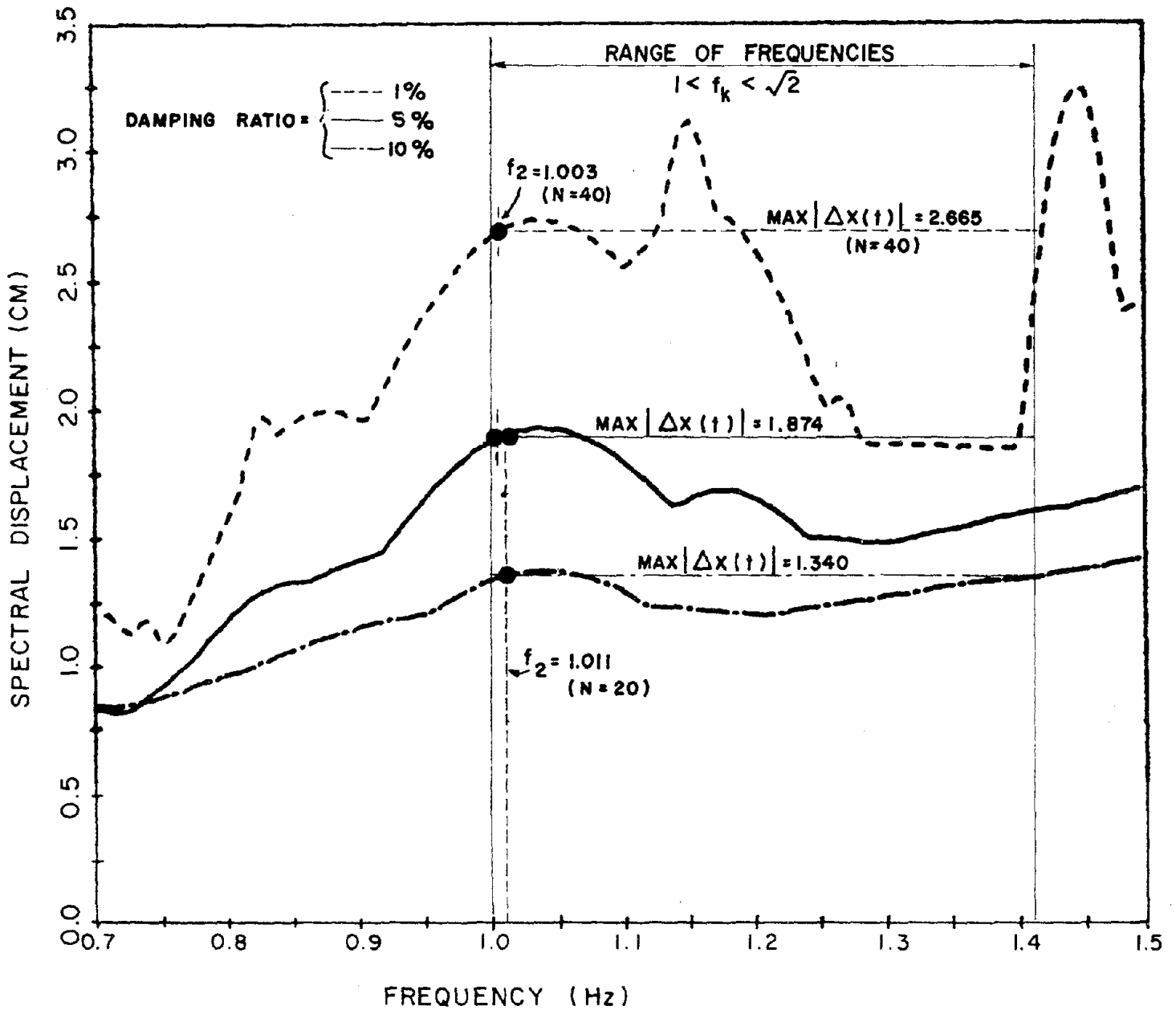
FIG. 9 INTERFERENCE RESPONSE SPECTRA FOR $\tau = 0.02$ sec
FOR EL CENTRO MAY 1940 N-S

IV   SUMMARY AND CONCLUSIONS

The equations which govern the dynamic axial response of a long
segmented pipe subjected to a traveling ground motion were developed. When
the jointed pipe is very soft relative to the ground, $k_p/k_g \ll 1$, the peak
joint response is given directly in terms of the Interference Response (IR)
spectrum.

When there is no intermediate support, modal decomposition can be used.
The natural frequencies will be distinct and separated and a modal
participation factor can be defined. Again, each modal response may be
obtained from the IR spectrum. The problem of combining the modal
contributions is similar to that in multi-degree of freedom buildings, and
the square root of the sum of the squares is probably the best approach.

Finally, the problem of a long supported pipe of non-negligible pipe/
joint stiffness was studied in detail. It was seen that, for reasonable
amounts of damping, the center joint response was predominantly a local
phenomenon, and was not affected by the end conditions, the number of links,
or variations in the ground input near the ends. Amplification ratios with
respect to the difference in ground displacement of from 2 to 4 were
obtained with damping ratios of from 10 to 1% of critical. Actual joint
opening (or closing) of 2 to 3 cm was found for pipes of various parameters
subjected to the EL CENTRO earthquake.

The most important conclusion is that the IR spectrum at the lower
bound frequency can be used directly to predict the response of pipes with
non-negligible values of k_p/k_g. Certainly, for k_p/k_g as large as 1/4,
computed peak responses were within 1% of the IR spectrum at the lowest anti-
symmetric frequency. Thus, the Interference Response spectrum is a useful
tool in the dynamic analysis of lifelines over a broad range of parameters.

REFERENCES

[1] Newmark, N.M., "Problems in Wave Propagation in Soil and Rock", Proceedings of the International Symposium on Wave Propagation and Dynamic Properties of Earth Materials, Albuquerque, New Mexico, 1967, pp. 7-26.

[2] Christian, J.T., "Relative Motion of Two Points During Earthquake", Journal of the Geotechnical Engineering Division, ASCE, Vol. 102, GT 11 Proc. Paper 12513, November, 1976, pp. 1191-1194.

[3] Matsushima, Y., "Spectra of Spatially Variant Ground Motions and Associated Transfer Functions of Soil-Foundation System", Proceedings of the Fourth Japan Earthquake Engineering Synposium-1975, November, 1975, Tokyo, Japan, pp. 351-358.

[4] Newmark, N.M. and Rosenbleuth, E., "Fundamentals of Earthquake Engineering", Prentice-Hall, Inc., Englewood Cliffs, New Jersey, 1971.

[5] Clough, R.W., "Earthquake Response of Structures", Earthquake Engineering, ed. Wiegel, R.L., Prentice-Hall, Inc., Englewood Cliffs, New Jersey, 1970, pp. 307-334.

[6] Weidlinger P. and Nelson, I., "Seismic Analysis of Lifelines with Interference Response Spectra", Grant Report No. 7, prepared for National Science Foundation (RANN), Grant No. ENV P76-9838, Weidlinger Associates, New York, New York, June, 1978.

[7] Weidlinger P. and Nelson, I., "Seismic Analysis of Lifelines with Interference Response Spectra", presented at ASCE Fall Convention, Preprint 3312, October 16-20, 1978, Chicago, Illinois.

[8] Wang, L.R. and O'Rourke, M.J.. "State of the Art of Buried Lifeline
      Earthquake Engineering", _Proceedings of Current State of Knowledge of_
      Lifeline Earthquake Engineering, ASCE, Los Angeles, California,
      August 30-31, 1977, pp. 252-266.

[9] Narita, K., "Study on Pipeline Failure Due to Earthquake", _Proceedings_
      of the U.S.-Japan Seminar on Earthquake Engineering Research with
      Emphasis on Lifeline Systems, November, 1976, Tokyo, Japan, pp. 157-
      176.

[10] Newmark, N.M., "Current Trends in the Seismic Analysis and Design of
      High-Rise Structures", _Earthquake Engineering_, ed. Wiegel, R.L.,
      Prentice-Hall, Inc., Englewood Cliffs, New Jersey, 1970, pp. 403-424.

[11] Jolley, L.B.W., "Summation of Series", 2nd revised ed., Dover
      Publications, New York, New York, 1961.

APPENDIX A

MODE SHAPES AND INFLUENCE COEFFICIENTS

In this appendix examples are given of the variation of the mode shapes $\phi_j{}^k$ and influence coefficients $D_m{}^k$ with the ratio k_B/k_p and the number of links N. The eigenvalues and their associated mode shapes were found numerically. The values of $D_m{}^k$ were obtained via

$$D_m{}^k = \frac{\omega_g{}^2}{\omega_k{}^2} \left(\phi_{\frac{N}{2}}{}^k - \phi_{\frac{N}{2}+1}{}^k \right) \sum_{j=1}^{m} \phi_j{}^k \tag{A-1}$$

where $1 \leq m \leq N - 1$. When N is even and k is restricted to antisymmetric modes, the above reduces to that given by Eq.(51) in the text. For N odd, integer arithmetic (truncation) yields $N/2 \rightarrow (N - 1)/2$ and $N/2 + 1 \rightarrow (N + 1)/2$.

Figure A-1 compares the mode shapes and influence coefficients for N = 12, and for $k_B = k_p$ and $k_B = 0$. In the latter case, the lowest mode corresponds to a rigid body displacement. The influence coefficients of all symmetric (odd) modes are zero. The frequencies for the stiffer system on the left are all slightly higher than the corresponding values for the free end pipe. Also, the magnitude of the sum of the influence coefficients in each mode is larger for the stiffer system. It is noted that the double sum of the influence coefficients is unity, even for the case of $k_B = 0$.

Figure A-2 compares the mode shapes and influence coefficients for N = 20, but with stiff boundary springs ($k_B = 10\ k_p$), with those for N = 18 and $k_B = k_p$. The highest two modes for N = 20 affect only the links near the ends, the left for mode 20 and the right for mode 19. The two frequencies are the same and much larger than all the others. In both modes, the influence coefficients for center joint displacement are all zero. For all other modes, the N = 20 frequencies are just below the corresponding values for N = 18. The mode shapes are also very similar (some are plotted upside down). The influence coefficients

MODE 12 ω_{12}=8·853 ΣD =-0·121
MODE 11 ω_{11}=8·758 ΣD =-0·000
MODE 10 ω_{10}=8·602 ΣD = 0·378
MODE 9 ω_9=8·332 ΣD = 0·000
MODE 8 ω_8=8·137 ΣD =-0·677
MODE 7 ω_7=7·848 ΣD =-0·000
MODE 6 ω_6=7·539 ΣD = 1·040
MODE 5 ω_5=7·226 ΣD = 0·000
MODE 4 ω_4=6·929 ΣD =-1·456
MODE 3 ω_3=6·667 ΣD =-0·000
MODE 2 ω_2=6·461 ΣD = 1·837
MODE 1 ω_1=6·329 ΣD = 0·000

MODE 12 ω_{12}=8·848 ΣD =-0·011
MODE 11 ω_{11}=8·736 ΣD = 0·000
MODE 10 ω_{10}=8·554 ΣD = 0·037
MODE 9 ω_9=8·312 ΣD =-0·000
MODE 8 ω_8=8·020 ΣD =-0·078
MODE 7 ω_7=7·695 ΣD = 0·000
MODE 6 ω_6=7·356 ΣD = 0·158
MODE 5 ω_5=7·025 ΣD = 0·000
MODE 4 ω_4=6·728 ΣD =-0·351
MODE 3 ω_3=6·490 ΣD = 0·000
MODE 2 ω_2=6·336 ΣD = 1·245
MODE 1 ω_1=6·283 ΣD = 0·000

$k_B = k_P$

$k_B = 0$

A. MODE SHAPES ϕ_i^k
B. INFLUENCE COEFFICIENT D_m^k
A. MODE SHAPES ϕ_j^k
B. INFLUENCE COEFFICIENT D_m^k

FIG. A-1 AXIAL MODE SHAPES AND INFLUENCE COEFFICIENTS FOR CENTER JOINT RELATIVE DISPLACEMENT FOR 12 SEGMENT PIPE
($k_g = 4k_p$; $\omega_g = 2\pi$; $k_B = k_p$, 0)

MODE 20 $\omega_{20}=12\cdot212$ $\Sigma D = -0\cdot000$

MODE 19 $\omega_{19}=12\cdot212$ $\Sigma D = -0\cdot000$

MODE 18 $\omega_{18}=8\cdot870$ $\Sigma D = 0\cdot107$ MODE 18 $\omega_{18}=8\cdot871$ $\Sigma D = 0\cdot083$

MODE 17 $\omega_{17}=8\cdot824$ $\Sigma D = 0\cdot000$ MODE 17 $\omega_{17}=8\cdot825$ $\Sigma D = 0\cdot000$

MODE 16 $\omega_{16}=8\cdot747$ $\Sigma D = -0\cdot322$ MODE 16 $\omega_{16}=8\cdot751$ $\Sigma D = -0\cdot253$

MODE 15 $\omega_{15}=8\cdot643$ $\Sigma D = -0\cdot000$ MODE 15 $\omega_{15}=8\cdot648$ $\Sigma D = -0\cdot000$

MODE 14 $\omega_{14}=8\cdot512$ $\Sigma D = 0\cdot539$ MODE 14 $\omega_{14}=8\cdot520$ $\Sigma D = 0\cdot437$

MODE 13 $\omega_{13}=8\cdot357$ $\Sigma D = 0\cdot000$ MODE 13 $\omega_{13}=8\cdot367$ $\Sigma D = 0\cdot000$

MODE 12 $\omega_{12}=8\cdot182$ $\Sigma D = -0\cdot762$ MODE 12 $\omega_{12}=8\cdot194$ $\Sigma D = -0\cdot643$

MODE 11 $\omega_{11}=7\cdot990$ $\Sigma D = -0\cdot000$ MODE 11 $\omega_{11}=8\cdot004$ $\Sigma D = -0\cdot000$

MODE 10 $\omega_{10}=7\cdot786$ $\Sigma D = 0\cdot998$ MODE 10 $\omega_{10}=7\cdot800$ $\Sigma D = 0\cdot879$

MODE 9 $\omega_{9}=7\cdot574$ $\Sigma D = 0\cdot000$ MODE 9 $\omega_{9}=7\cdot589$ $\Sigma D = 0\cdot000$

MODE 8 $\omega_{8}=7\cdot359$ $\Sigma D = -1\cdot249$ MODE 8 $\omega_{8}=7\cdot374$ $\Sigma D = -1\cdot146$

MODE 7 $\omega_{7}=7\cdot149$ $\Sigma D = -0\cdot000$ MODE 7 $\omega_{7}=7\cdot162$ $\Sigma D = -0\cdot000$

MODE 6 $\omega_{6}=6\cdot948$ $\Sigma D = 1\cdot509$ MODE 6 $\omega_{6}=6\cdot959$ $\Sigma D = 1\cdot434$

MODE 5 $\omega_{5}=6\cdot763$ $\Sigma D = 0\cdot000$ MODE 5 $\omega_{5}=6\cdot771$ $\Sigma D = 0\cdot000$

MODE 4 $\omega_{4}=6\cdot600$ $\Sigma D = -1\cdot752$ MODE 4 $\omega_{4}=6\cdot606$ $\Sigma D = -1\cdot711$

MODE 3 $\omega_{3}=6\cdot466$ $\Sigma D = -0\cdot000$ MODE 3 $\omega_{3}=6\cdot470$ $\Sigma D = -0\cdot000$

MODE 2 $\omega_{2}=6\cdot366$ $\Sigma D = 1\cdot932$ MODE 2 $\omega_{2}=6\cdot368$ $\Sigma D = 1\cdot921$

MODE 1 $\omega_{1}=6\cdot304$ $\Sigma D = 0\cdot000$ MODE 1 $\omega_{1}=6\cdot305$ $\Sigma D = -0\cdot000$

N = 20   KG/KP = 4·0   KEND/KP = 10·0   0·9999 = $\Sigma\Sigma D$ N = 18   KG/KP = 4·0   KEND/KP = 1·0   0·9999 = $\Sigma\Sigma D$

A. ϕ_j^k B. D_m^k C. ϕ_j^k D. D_m^k

FIG. A-2   COMPARISON OF MODE SHAPES AND INFLUENCE COEFFICIENTS FOR N = 20 WITH STIFF BOUNDARY SPRINGS AND FOR N = 18 WITH $k_B = k_P$ ($\omega_g = 2\pi$)

for the lower modes, those which contribute the largest shares to the dynamic response, again are very similar. The two ΣD's for mode 2 agree to 0.5%. The relative difference between the two cases, in the ΣD's, grows as the mode number increases, with the maximum difference reaching ~25%, but only 1% of the mode 2 sum. Consequently, one can expect that the dynamic response of the two systems would be virtually identical. Once again, note the double sum of influence coefficients is (essentially) unity in both cases.

The effect of the number of links, including whether N is odd or even, on the mode shapes and influence coefficients is illustrated in Fig. A-3, where those corresponding to N = 18, 19, and 20 are compared. All cases were computed with k_g/k_p = 4 and $k_B = k_p$. For N = 19, the influence coefficients apply to the ninth joint, marked with the triangle. As anticipated, the sum of the influence coefficients in the odd modes are not zero for N = 19. Nevertheless, for the lowest modes, the odd sums are much smaller than the adjacent even ones. For example, the mode 1 value is only 7% of that of mode 2.

For the lowest several modes, there is a general correspondence in frequency, mode shape and influence coefficients for the three cases. For the highest modes, there is also agreement when the mode number is counted from the top, i.e. highest compare to highest, next highest with next highest, etc. It is only in the middle modes, where for N = 19 the adjacent ΣD's are comparable, that it is difficult to relate one case to the others. Nevertheless, based on the lower modes, restricting the discussion in the text to N = even does not appear to be unduly restrictive. Again, the double sums of influence coefficients are all (essentially) unity, even for N odd.
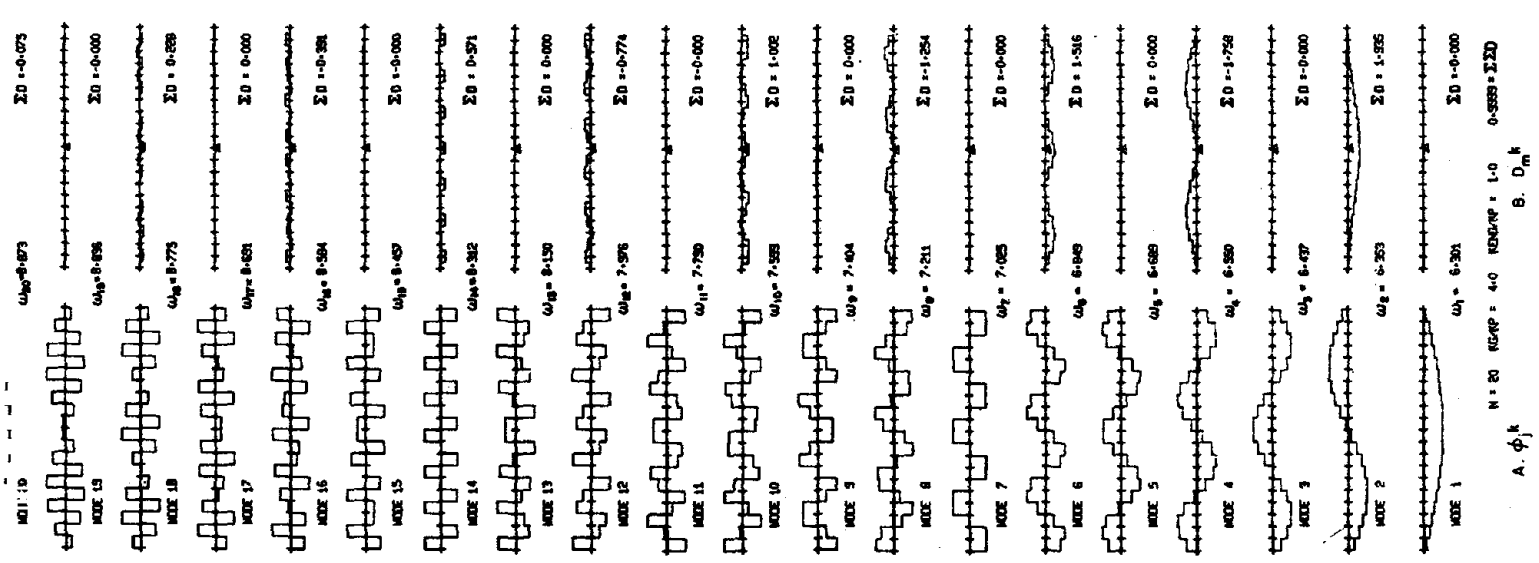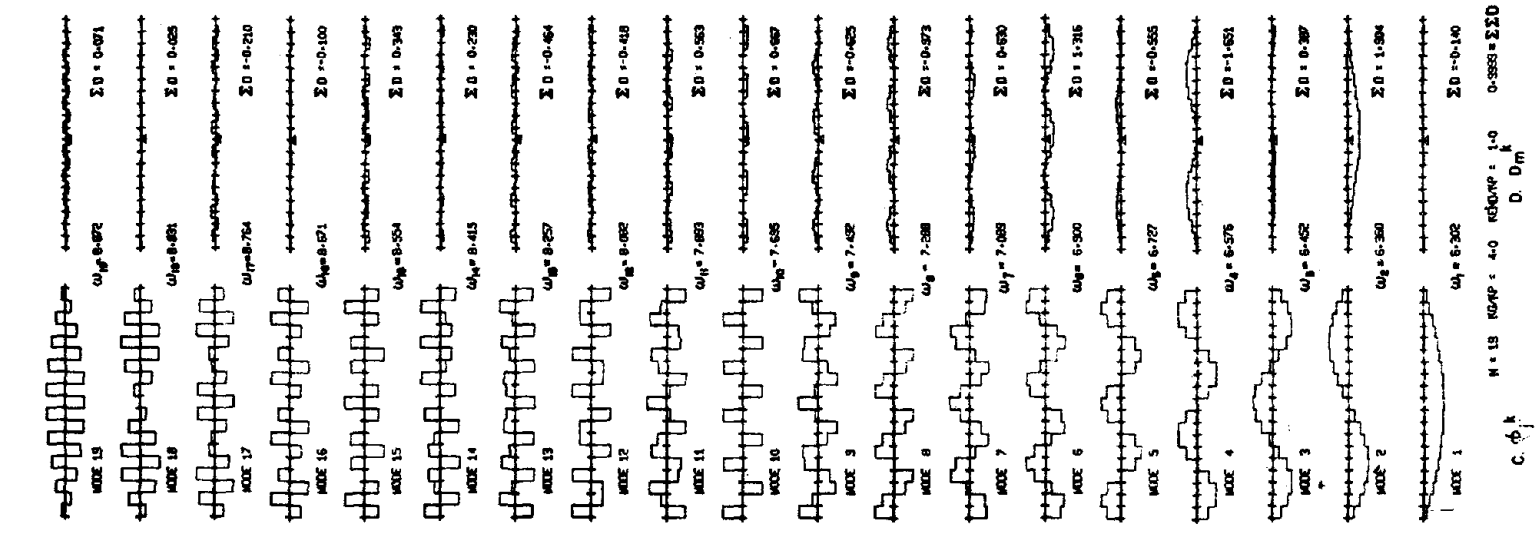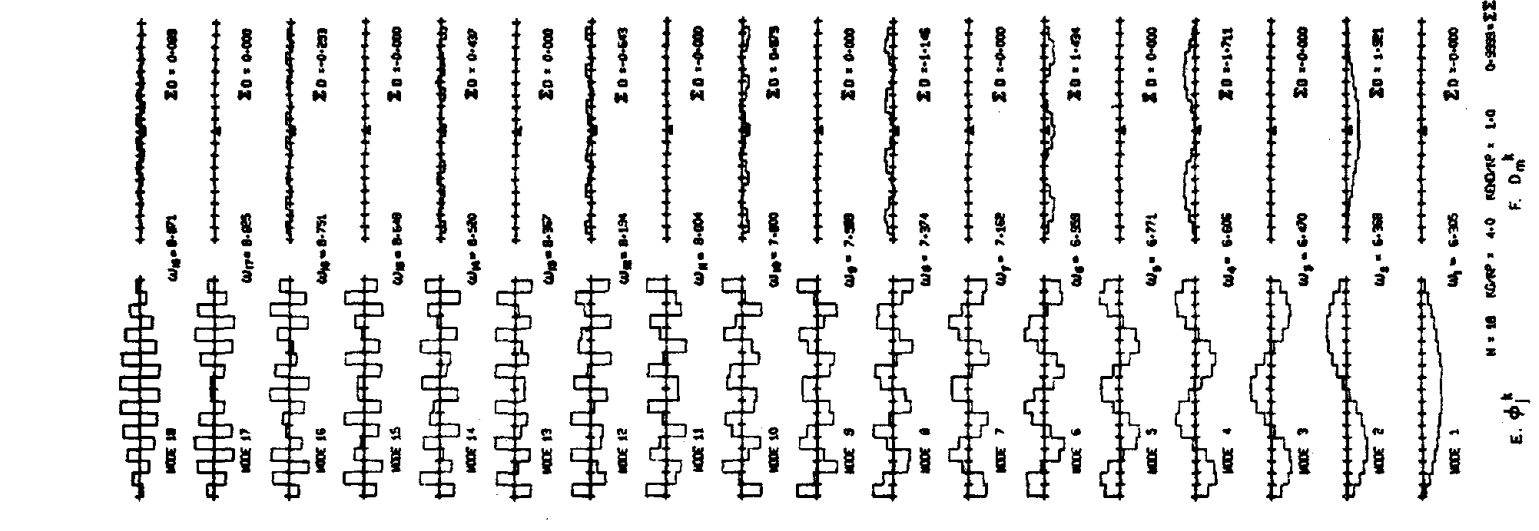
40
Int. Blank

APPENDIX B

SUMMARY OF SEGPIPE CALCULATIONS

APPENDIX B – Summary of SEGPIPE Calculations

Run	File	N Links	k_g/k_p	ω_k	τ	Load	Ω	Damping	T_{final}
1	–	20	10	1.0044→1.1823	0.10	$\sin\Omega t$	1.3	0	2.5
2	–	20	10	1.0044→1.1823	0.10	$\sin\Omega t$	1.3	0	12.5
3	–	20	10	1.0044→1.1823	0.10	$\sin\Omega t$	1.3	0	50
4	–	20	2	0.457→0.7732	0.10	$\sin\Omega t$	1.3	0	50
5	–	20	10	1.0044→1.1823	0.10	$\frac{1}{2}(1-\cos\Omega t)$	1.3	0	20
6	–	20	10	1.0044→1.1823	0.025	$\frac{1}{2}(1-\cos\Omega t)$	1.3	0	20
7	–	20	4	6.3526→8.8734	0.02	$\frac{1}{2}(1-\cos\Omega t)$	5.88	0	8
8	–	20	4	6.3526→8.8734	0.02	$\frac{1}{2}(1-\cos\Omega t)$	5.88	0.05	8
9	–	20	4	6.3526→8.8734	0.02	$\frac{1}{2}(1-\cos\Omega t)$	9.0	0	8
10	–	20	4	6.3526→8.8734	0.02	$\frac{1}{2}(1-\cos\Omega t)$	9.0	0.05	8

Joints Loaded	Purpose	Conclusions	Run
19	First try.	Too short, $\Omega T_{final} < \pi$.	1
19	Try to observe beat developing.	Beat observed. Uncertain if max actually reached.	2
19	Show complete Beat.	Two complete beats mode 2 ($\omega_2 = 1.004$), One complete beat mode 20 ($\omega_{20}^2 = 1.182$).	3
19	Try to spread natural frequencies ω_k.	Total response is only about 1/4 of input Δz.	4
19	More realistic (smooth) input than Run 3.	More complex beating phenomena.	5
19	Test linearized result for "small" τ.	Error 0.65% for k=2, increases to 15% for k=20.	6
19	More realistic numerical input, i.e. $f_k \sim 1$ Hz.	Half beat mode 2, close to resonance. Mode 2 response ~ 20 times input.	7
19	Effect of Damping by comparing to Run 7.	Total response $\sim 1/2$ of undamped $\sim 7 \times \Delta z$. Also true for mode 2, effect on higher modes smaller.	8
19	Attempt to excite higher modes, $\Omega > \omega_n$.	T_{final} too short, since the mode 20 max should occur at $t \approx 25$. Max modal contribution is mode 16; mode 2 next.	9
19	Effect of Damping by comparing to Run 9.	Total response only $\sim$ twice input Δz and occurs during transient. Largest modal contribution is mode 2. Observe steady state developing.	10

SEGPIPE Calculations- Continued

Run	File	N Links	k_g/k_p	ω_k	τ	Load	Ω	Damping	T_{final}
11	SEGPIPE	20	4	6.3526→8.8734	0.02	$\frac{1}{2}(1-\cos\Omega t)$	7.7872	0	16
12	SEGPIPD	20	4	6.3526→8.8734	0.02	$\frac{1}{2}(1-\cos\Omega t)$	7.7872	0.05	16
13	SEGPU40	40	4	6.3016→8.8825	0.02	$\frac{1}{2}(1-\cos\Omega t)$	7.7872	0	16
14	SEGPD40	40	4	6.3016→8.8825	0.02	$\frac{1}{2}(1-\cos\Omega t)$	7.7872	0.05	16
15	(Noplots)	40	4	6.3016→8.8825	0.02	$\frac{1}{2}(1-\cos\Omega t)$	7.7872	0.05	16

Joints Loaded	Purpose	Conclusions	Run
19	Baseline case when input Ω between ω_{10} & ω_{12}.	Total response ~ 48 x input Δz. (Undamped case is unrealistic.) Modes 10 & 12 are in phase at max.	11
19	Effect of Damping by comparing with Run 11.	Total response only ~ 3.6 x Δz. Occurs during transient, but less than 10% larger than the steady state. Modes 10 & 12 response ~ 0.2 of undamped values.	12
39	Effect of Number of links by comparing with Run 11.	Results may be inconclusive since T_{max} of mode 22 = 58 >> 16 = T_{final}. Total response ~ 5.7 x Δz << that for N=20. (However, max occurs near T_f.) Largest modal contribution is mode 2 which is $\sim$ total response. Mode 22 is building up ($\sim \Delta z$)@t=16.	13
39	Effect of Damping by comparing with Run 13. Effect of Number of links for damped system by comparing with Run 12.	Total response ~ 3.1 x input Δz. All beats except 1st are negligible. For higher modes (k>2) steady state response << transient < Δz. Thus, k=2 time history almost identical to that of total response. For different N, cannot compare individual modal responses. Early transient (peak for N=40) same as for N=20. Later transient (peak for N=20) and steady state smaller for N=40. Hence, max total response $\sim .85$ of N=20.	14
7	Effect of partial loading by comparing with Run 14.	Total response $\sim$ same as fully loaded. Mode 2 response smaller, higher modes larger.	15

SEGPIPE Calculations – Continued

Run	File	N Links	k_g/k_p	ω_k	τ	Load	Ω	Damping	T_{f}
16	S5GPD40	40	4	6.3016→8.8825	0.02	$\frac{1}{2}(1-\cos\Omega t)$	7.7872	0.05	16
17	S3GPD40	40	4	6.3016→8.8825	0.02	$\frac{1}{2}(1-\cos\Omega t)$	7.7872	0.05	16
18	S1GPD40	40	4	6.3016→8.8825	0.02	$\frac{1}{2}(1-\cos\Omega t)$	7.7872	0.05	16
19	SF3FD20	20	4	6.3526→8.8734	0.02	$\sum_{i=1}^{3}\frac{1}{6}(1-\cos\Omega_i t)$	5.88, 7.7872, 9.0	0.05	16
20	SN3FD20	20	4	6.3526→8.8734	0.02	$\sum_{i=1}^{3}\frac{1}{6}(1-\cos\Omega_i t)$	5.88, 7.7872, 9.0	0.05	16

Joints Loaded	Purpose	Conclusions	Run
5	Effect of partial loading by comparing with Run 14.	Total response peak and steady state larger than fully loaded Run 14. Peak $\sim 15\%$ > Run 14 Peak. Mode 2 still largest contribution, but only $\sim 40\%$ of fully loaded case. Mode $4 \sim 0$ ($D_j^4 \sim 0$ for $j \sim N/2$). Higher modes generally > those of Run 14. Many modes contribute to total response.	16
3	Effect of partial loading by comparing with Run 14.	Total response peak and steady state both larger than fully loaded Run 14. Peak $\sim 20\%$ > Run 14 Peak; Peak ~ 3.86 x Δz. Order of modal contributions is 18, 14, 10, 2, 6, 22. Many modes contribute to total response.	17
1	Effect of partial loading by comparing with Run 14. Check analytical result for small τ.	Peak total response 75% of Run 14, 2.3 Δz. Both occur during transients. Steady state 83% of peak and essentially same as that of Run 14. Order of modal contributions is 22, 18, 14, 26, 10, 6, 2, 30. Modes divisible by 4 << others. ($D_{N/2}^{4m}$ are small). Mode 2 response increases with number of joints loaded. Mode 4, full load causes large transient; partial load responses are small; mode 8 similar. Error in calculating steady state modal contributions (assuming $\frac{\Omega\tau}{2} << 1$) less than 1%. ($\frac{\Omega\tau}{2} = 0.08 << 1$).	18
19	Effect of more realistic loading. Establish new Baseline.	No steady state since complicated input. Peak total response ~ 3.28 xΔz input peak. Mode 2 waveform largest and similar in shape to total response.	19
17	Effect of not loading end joints ($\sim$ boundary conditions).	Negligible!	20

SËGPIPE Calculations - Continued

Run	File	N Links	k_g/k_p	ω_k	τ	Load	Ω	Damping	T_{final}
21	SF3FD22	22	4	$6.34 \rightarrow 8.88$	0.02	$\sum_{i=1}^{3} \frac{1}{6}(1-\cos\Omega_i t)$	5.88, 7.79, 9.0	0.05	16
22	SF3FD40	40	4	$6.30 \rightarrow 8.88$	0.02	$\sum_{i=1}^{3} \frac{1}{6}(1-\cos\Omega_i t)$	5.88, 7.79, 9.0	0.05	16
23	CHKFILE	40	4	$6.30 \rightarrow 8.88$	0.02	$\sum_{i=1}^{3} \frac{1}{6}(1-\cos\Omega_i t)$	5.88, 7.79, 9.0	0.05	16

Joints Loaded	Purpose	Conclusions	Run
21	Effect of small variation in number of links by comparing with Run 19.	Total response very similar to Run 19. Peak total response ∿15% less than that of Run 19. (Perhaps sensitive to whether or not N is divisible by 4.) Lower modal responses virtually identical.	21
39	Effect of large variation in number of links by comparing with Runs 19 & 21. Effect of more realistic loading by comparing with Run 14.	Except for being ∿15% larger, mode 2 response is the same as the total response. Other modes < ∿40% of total. Total response for N=40 & N=22 almost identical. Total response for N=40 & N=20 similar except N=40 ∿20% smaller. With single input frequency beat developed shape with complicated load different, but peaks of total response within ∿20%. Note, peak response = $S_I(\omega_2, \xi, \tau)$.	22
39	Check revised code, i.e. read ground motion from file.	Total response almost identical. Some modes, where the peak occurs early, differ by 3% or 4% or more.	23

Run	File	N Links	k_g/k_p	ω_k	τ	Input Ground Motion	Comp	Damping	$T_{f\ldots}$
24	SGPLCNT	40	4	$6.30 \rightarrow 8.88$	0.02	EL CENTRO May 1940	S00E	0.05	20
25	SGPVNT7	40	4	$6.30 \rightarrow 8.88$	0.02	14724 Ventura SAN FERNANDO Feb. 1971	N78W	0.05	20
26	SGPLCN2	20	4	$6.35 \rightarrow 8.87$	0.02	EL CENTRO May 1940	S00E	0.05	20
27	SGPLCN3	20	4	$6.35 \rightarrow 8.87$	0.02	EL CENTRO May 1940	S00E	0.01	20
28	SGPLCN4	20	4	$6.35 \rightarrow 8.87$	0.02	EL CENTRO May 1940	S00E	0.10	20
29	SGPLCN5	40	4	$6.30 \rightarrow 8.88$	0.02	EL CENTRO May 1940	S00E	0.01	20

Joints Loaded	Purpose	Conclusions	Run
39	Find response to real earthquake.	Mode 2 > twice any other modal contribution and total response. Peak total response occurs ~ 2.5 sec after input peak. Amplification $= 2.85$. Except for amplitude, total response $\sim$ mode 2. Peak within 0.5% of S_I at ω_2.	24
39	Alternate earthquake record.	Mode 2 > any other modal contribution and total response. Peak total response almost simultaneous with input peak. Amplif. $= 1.80$. Peak total within 0.2% of S_I at ω_2.	25
19	Effect of N for real earthquake by comparing with Run 24.	Except for phase shift, total response almost identical. Amplif. $= 2.85$. Peak $\sim$ within 1% of of S_I at ω_2.	26
19	Effect of small damping by comparing with Run 26.	Total response peak > any modal contribution. Total response peak occurs much later than input peak. Amplif. $= 9.0$! First 7 modes, plus mode 18 contribute to peak. Largest, mode 8, only 35% of total. S_I at ω_2 only 1/2 of peak, but $\simeq$ early time peak.	27
19	Effect of larger damping by comparing with Run 26.	Except for less amplification, similar to Run 26. Amplif. $= 2.0$. Peak within $\sim 1\%$ of S_I at ω_2.	28
19	Effect of N for real earthquake for small damping by comparing with Run 27.	Except for amplification, similar to Run 24, i.e. peak occurs ~ 2.5 sec after input peak. Amplif. $= 4.05$. Mode 2 > twice any other mode and greater than total response. For $t < 8$ sec, total response similar to Run 27. Peak total response within 0.5% of $S_I(\omega_2)$.	29

-52-

Intentionally Blank

APPENDIX C

ANALYTIC SOLUTIONS FOR SINUSOIDAL TYPE INPUT

1. Undamped Case - Sinusoidal Input

Consider the solution $r_k(t)$ to Eq. (49) when

$$\Delta z(t) = \begin{cases} 0 & t \leq 0 \\ A \sin \Omega t & 0 \leq t \leq \tau \\ A[\sin \Omega t - \sin \Omega(t - \tau)] & t \geq \tau \end{cases} \qquad (C-1)$$

Without damping, Eq. (49) reduces to

$$\ddot{r}_k + \omega_k^2 r_k = \omega_k^2 \Delta z(t) \qquad (C-2)$$

Rest initial conditions are assumed

$$\left. \begin{array}{l} r_k(0) = 0 \\[2mm] \dot{r}_k(0) = 0 \end{array} \right\} \qquad (C-3)$$

The solution for the three time domains are

$$r_k(t) \equiv 0 \qquad t \leq 0 \qquad (C-4a)$$

$$r_k(t) = \frac{A}{1 - \Omega^2/\omega_k^2} \left[\sin \Omega t - \frac{\Omega}{\omega_k} \sin \omega_k t \right] \qquad 0 \leq t \leq \tau \qquad (C-4b)$$

$$r_k(t) = \frac{A}{1 - \Omega^2/\omega_k^2} \left\{ \sin \Omega t - \sin \Omega(t - \tau) - \frac{\Omega}{\omega_k} [\sin \omega_k t - \sin \omega_k(t - \tau)] \right\}$$

$$= \frac{2A}{1 - \Omega^2/\omega_k^2} \cdot \left[\sin \frac{\Omega \tau}{2} \cos \Omega(t - \tau/2) - \frac{\Omega}{\omega_k} \sin \frac{\omega_k \tau}{2} \cos \omega_k(t - \tau/2) \right]$$

$$t \geq \tau \qquad (C-4c)$$

Equation (53) may now be used in conjuction with Eqs. (C-4) to obtain $r_{km}(t)$, which is then inserted into Eq. (54) to give the joint modal response $\Delta x^{(k)}(t)$. The values of both r_k and $\dot{r}_k$ at the transition time $t = \tau$

$$r_k(\tau) = \frac{A}{1 - \Omega^2/\omega_k^2} \left[\sin \Omega\tau - \frac{\Omega}{\omega_k} \sin \omega_k\tau \right]$$ (C-5a)

$$\dot{r}_k(\tau) = \frac{A\Omega}{1 - \Omega^2/\omega_k^2} \left[\cos \Omega\tau - \cos \omega_k\tau \right]$$ (C-5b)

are small for small values of τ, i.e.,

$$\Omega\tau \ll \pi/2 \quad \text{and} \quad \omega_k\tau \ll \pi/2$$ (C-6)

Rather than three separate expressions, $r_{km}(t)$ may be written as a single approximate expression for small τ, i.e.,

$$r_{km}(t) = \frac{A\Omega\tau}{1 - \Omega^2/\omega_k^2} H(t') \left[\cos \Omega t' - \cos \omega_k t' \right]$$ (C-7)

where

$$t' = t - (m - 1)\tau - \tau/2$$ (C-8)

is the time after the traveling wave has crossed the mth <u>joint</u>. For $m \neq N/2$, the response at the symmetric point $N - m$ is

$$r_{k(N-m)}(t) = \frac{A\Omega\tau}{1 - \Omega^2/\omega_k^2} H(t'') \left[\cos \Omega t'' - \cos \omega_k t'' \right]$$ (C-9)

where

$$t'' = t - (N - m - 1)\tau - \tau/2$$ (C-10)

is the time after the signal has crossed the $N - m^{th}$ joint. Recalling $D_m^k = D_{N-m}^k$, the contribution of joints m and $N - m$ to $\Delta x^{(k)}$ for $t'' > 0$ is

$$D_m^k [r_{km} + r_{k(N-m)}] = \frac{A\Omega\tau \, D_m^k}{1 - \Omega^2/\omega_k^2} \left[\cos \Omega t' + \cos \Omega t'' - \cos \omega_k t' - \cos \omega_k t'' \right]$$

$$= \frac{2A\Omega\tau \, D_m^k}{1 - \Omega^2/\omega_k^2} \left[\cos \Omega(t - \tau \frac{N-1}{2}) \cos \Omega\tau(\frac{N}{2} - m) \right.$$

$$\left. - \cos \omega_k(t - \tau \frac{N-1}{2}) \cos \omega_k\tau(\frac{N}{2} - m) \right], \quad t > (N - m - \frac{1}{2})\tau$$

(C-11)

The largest arguments of the second cosine factors above occur when m = 1. For N >> 1

$$\cos \Omega\tau(\frac{N}{2} - 1) \simeq 1 \qquad \text{and} \qquad \cos \omega_k\tau(\frac{N}{2} - 1) \simeq 1 \qquad \text{(C-12)}$$

if

$$N\Omega\tau \ll \pi \qquad \text{and} \qquad N\omega_k\tau \ll \pi \qquad \text{(C-13)}$$

Physically, Eqs. (C-13) require that the total transit time from one end of the pipe to the other be much smaller than half a period of any component of the input, or of any natural frequency of the system. They are, of course, much more restrictive conditions than Eqs. (C-6).

Assuming Eqs. (C-13) to be valid, Eq. (C-11) may be written approximately [not quite true for $t_c < (N/2 - m)\tau$] as

$$D_m^k[r_{km} + r_{k(N-m)}] \doteq H(t_c) \frac{4A\Omega\tau \ D_m^k}{1 - \Omega^2/\omega_k^2} \sin \frac{\Omega + \omega_k}{2} t_c \sin \frac{\omega_k - \Omega}{2} t_c \qquad \text{(C-14)}$$

where

$$t_c = t - \tau \frac{N - 1}{2} \qquad \text{(C-15)}$$

is the time after the traveling input wave has crossed the center joint. Finally, the contribution from all joints m may be summed, and recalling the symmetry in D_m^k,

$$\Delta x^{(k)}(t) = \frac{2A\Omega\tau \left(\sum_{m=1}^{N-1} D_m^k \right)}{1 - \Omega^2/\omega_k^2} \left[H(t_c) \sin \frac{\Omega + \omega_k}{2} t_c \sin \frac{\omega_k - \Omega}{2} t_c \right] \qquad \text{(C-16)}$$

Equation (C-16) is sketched in Fig. C-1. The function in the brackets starts at $t = \tau(N - 1)/2$ and then exhibits a beat phenomenon. The apparent frequency is the average of Ω and ω_k, while the enveloping function reaches a peak every $2\pi/(\omega_k - \Omega)$. As the input frequency Ω
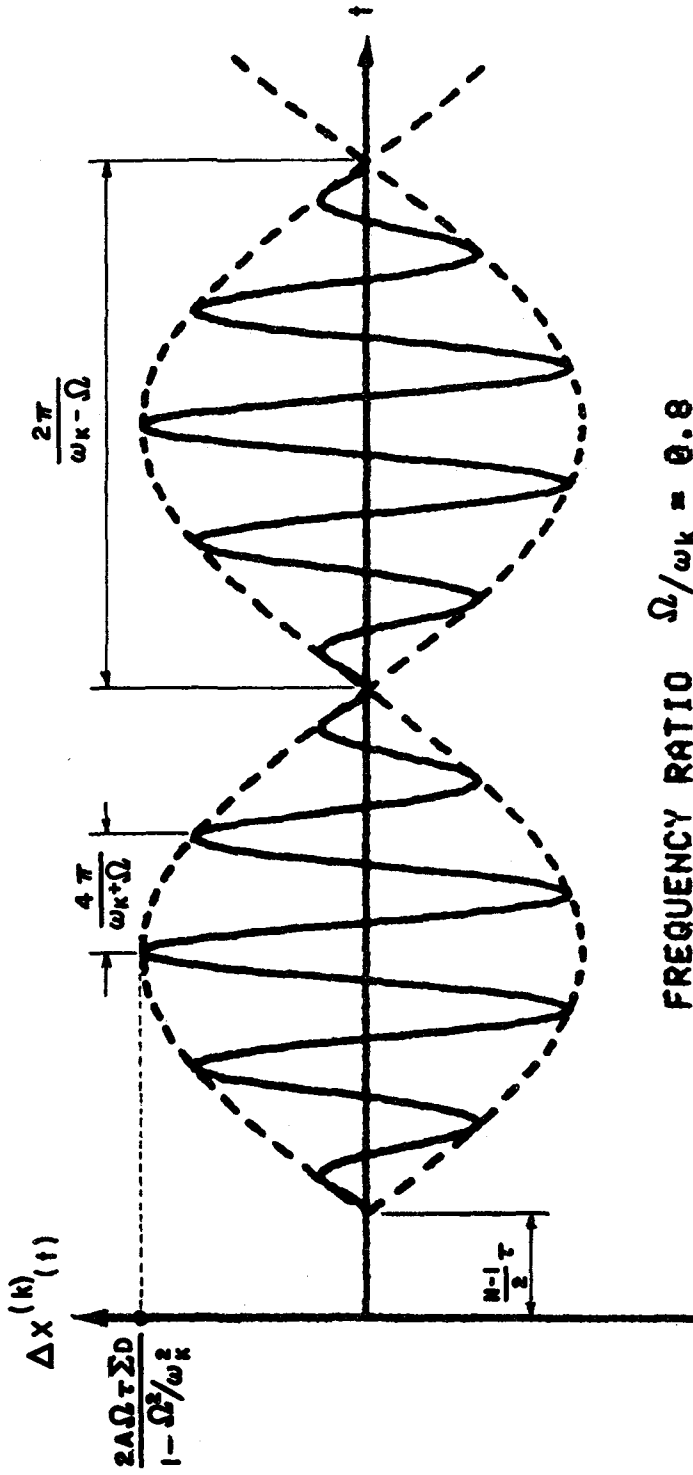
FIG. C-I APPROXIMATE MODAL SOLUTION $\Delta x^{(k)}{}_{(t)}$ FOR SMALL τ AND SINUSOIDAL GROUND MOTION INPUT $Z(t) = A \, SIN \, \Omega t$ UNDAMPED CASE

approaches ω_k, the applitude increase, and also the duration required to reach the peak increases as well. With regard to the last remark, it is worth noting that the strong motion phase of a real earthquake does not last more than several seconds, i.e., a few cycles of the dominant frequency.

2. Undamped Case - Haversine Input

The incoherent input given by Eq. (C-1) corresponds to a ground motion at a point, $z(t) = A H(t) \sin \Omega t$. While this function is initially zero, the corresponding initial velocity is $A\Omega \neq 0$. A discontinuous ground velocity is unrealistic. A function $z(t)$ which is initially zero, and whose first derivative is also initially zero, is the haversine function.

Let the incoherent motion be given by

$$\Delta z(t) = \begin{cases} 0 & t \leq 0 \\ A/2(1 - \cos \Omega t) & 0 \leq t \leq \tau \\ A/2[\cos \Omega(t-\tau) - \cos \Omega t] & t \geq \tau \end{cases} \qquad (C-17)$$

The solution to Eq. (C-2), subject to initial conditions Eq. (C-3), is then

$$r_k(t) \equiv 0 \qquad t \leq 0 \qquad (C-18a)$$

$$r_k(t) = \frac{A}{2} \left\{ 1 - \frac{1}{1 - \Omega^2/\omega_k^2} \left[\cos \Omega t - (\Omega^2/\omega_k^2) \cos \omega_k t \right] \right\} \qquad 0 \leq t \leq \tau \qquad (C-18b)$$

$$r_k(t) = \frac{A}{2(1 - \Omega^2/\omega_k^2)} \left\{ \cos \Omega(t - \tau) - \cos \Omega t - (\Omega^2/\omega_k^2) \left[\cos \omega_k(t - \tau) - \cos \omega_k t \right] \right\} \qquad t \geq \tau \qquad (C-18c)$$

The values of r_k and $\dot{r}_k$ at the transition time $t = \tau$ are smaller than the corresponding values given by Eq. (C-5) for small τ. (They are zero to a higher order in τ.) Again, one may write a single approximate expression for $r_{km}(t)$ for small τ

$$r_{km}(t) = \frac{A\Omega\tau}{2(1 - \Omega^2/\omega_k^2)} H(t') \left[\sin \Omega t' - \frac{\Omega}{\omega_k} \sin \omega_k t' \right] \tag{C-19}$$

and a similar one for $N - m^{th}$ joint

$$r_{k(N-m)}(t) = \frac{A\Omega\tau}{2(1 - \Omega^2/\omega_k^2)} H(t'') \left[\sin \Omega t'' - \frac{\Omega}{\omega_k} \sin \omega_k t'' \right] \tag{C-20}$$

where t' and t'' are given by Eqs. (C-8) and (C-10), respectively. The sum of the two terms, for $t'' > 0$, is

$$r_{km} + r_{k(N-m)} = \frac{A\Omega\tau}{1 - \Omega^2/\omega_k^2} \left[\sin \Omega t_c \cos \Omega\tau(\frac{N}{2} - m) \right.$$
$$\left. - \frac{\Omega}{\omega_k} \sin \omega_k t_c \cos \omega_k \tau(\frac{N}{2} - m) \right]$$
$$t'' > 0 \tag{C-21}$$

which may be simplified if Eqs. (C-13) hold to

$$r_{km} + r_{k(N-m)} = \frac{A\Omega\tau}{1 - \Omega^2/\omega_k^2} H(t_c) \, M \cos(\frac{\Omega + \omega_k}{2} t_c - \theta) \tag{C-22}$$

where the enveloping function $M(t)$ is given by

$$M(t) = \left[1 + \Omega^2/\omega_k^2 - 2\Omega/\omega_k \cos(\Omega - \omega_k)t_c \right]^{1/2} \tag{C-23}$$

and where the variable phase angle is given by

$$\theta(t) = \tan^{-1} \left[\frac{(1 - \Omega/\omega_k) \cos \frac{\Omega - \omega_k}{2} t_c}{(1 + \Omega/\omega_k) \sin \frac{\Omega - \omega_k}{2} t_c} \right] \tag{C-24}$$

In the above, t_c is the time after the traveling input wave has crossed the center joint, given by Eq. (C-15). Finally, recalling the symmetry in D_m^k, Eq. (54) may be written as

$$\Delta x^{(k)}(t) = \sum_{m=1}^{N-1} D_m^k r_{km}(t) = \frac{1}{2} \sum_{m=1}^{N-1} D_m^k [r_{km} + r_{k(N-m)}] \qquad (C-25)$$

or, since Eq. (C-22) is independent of m,

$$\Delta x^{(k)}(t) = \frac{A\Omega\tau \left(\sum\limits_{m=1}^{N-1} D_m^k\right)}{2(1 - \Omega^2/\omega_k^2)} \left\{ H(t_c)\, M(t)\, \cos\left[\frac{\Omega + \omega_k}{2} t_c - \theta(t)\right]\right\} \qquad (C-26)$$

Equation (C-26) is plotted in Fig. C-2 for $\Omega/\omega_k = 0.8$. The enveloping functions $\pm M(t)$, given by Eq. (C-23), are shown as dashed lines. While not a sine curve, the function is periodic with a beat period of $2\pi/(\omega_k - \Omega)$, the same as in the previous figure. The maximum and minimum values of M are $1 \pm \Omega/\omega_k$, respectively. Consequently, the peak modal response is bounded by

$$\text{MAX}\left|\Delta x^{(k)}(t)\right| \leq \frac{A\Omega\tau \left|\sum\limits_{m=1}^{N-1} D_m^k\right|}{2(1 - \Omega/\omega_k)} \qquad (C-27)$$

The period of the actual response function is only approximately $4\pi/(\omega_k + \Omega)$, since the phase angle changes by π within a beat.

3. Haversine Input – Damping Included

When (small) damping is included, the solution for small τ to Eq. (49) with the incoherent ground motion given by Eq. (C-17), and subject to rest initial conditions, Eq. (C-3), is

$$r_{km}(t) = \frac{A\Omega\tau/2 \ H(t')}{\left[\left(1 - \frac{\Omega^2}{\omega_k^2}\right)^2 + \left(2\xi_k \frac{\Omega}{\omega_k}\right)^2\right]}$$

$$\left\{ (\frac{\Omega}{\omega_k}) \ e^{-\omega_k \ \xi_k t'} \left[\frac{(-1 + \frac{\Omega^2}{\omega_k^2} - 2\xi_k^2 \frac{\Omega^2}{\omega_k^2})}{\sqrt{1 - \xi_k^2}} \sin \omega_k \sqrt{1 - \xi_k^2} \ t' \right. \right.$$

$$\left. + 2\xi_k(\frac{\Omega}{\omega_k})^2 \cos \omega_k \sqrt{1 - \xi_k^2} \ t' \right]$$

$$\left. + \left[1 - \frac{\Omega^2}{\omega_k^2} + (2\xi_k \frac{\Omega}{\omega_k})^2 \right] \sin \Omega t' - 2\xi_k(\frac{\Omega}{\omega_k})^3 \cos \Omega t' \right\} \cdot \quad \text{(C-28)}$$

where t' is given by Eq. (C-8). The terms involving $\sin \Omega t'$ and $\cos \Omega t'$ constitute the steady state solution, while those multiplied by the decaying exponential term contribute to the transient solution only. It is observed that setting $\xi_k = 0$ in Eq. (C-28) results in the equation reducing to Eq. (C-19), derived assuming no damping. Also, when $\Omega = \omega_k$, but $\xi_k \neq 0$, Eq. (C-28) becomes

$$r_{km}(t) = \frac{A\Omega\tau}{2} H(t') \left\{ e^{-\Omega\xi_k t'} \left[\frac{-1}{2\sqrt{1 - \xi_k^2}} \sin \Omega \sqrt{1 - \xi_k^2} \ t' \right. \right.$$

$$\left. + \frac{1}{2\xi_k} \cos \Omega \sqrt{1 - \xi_k^2} \ t' \right] + \sin \Omega t' - \frac{1}{2\xi_k} \cos \Omega t' \right\}$$

$$, \ \Omega = \omega_k \quad \text{(C-29)}$$

The peak amplification during the steady state response in that case is

$$\text{Amp. Ratio} = \sqrt{1 + \frac{1}{4\xi_k^2}} \simeq \frac{1}{2\xi_k} \quad \text{(C-30)}$$

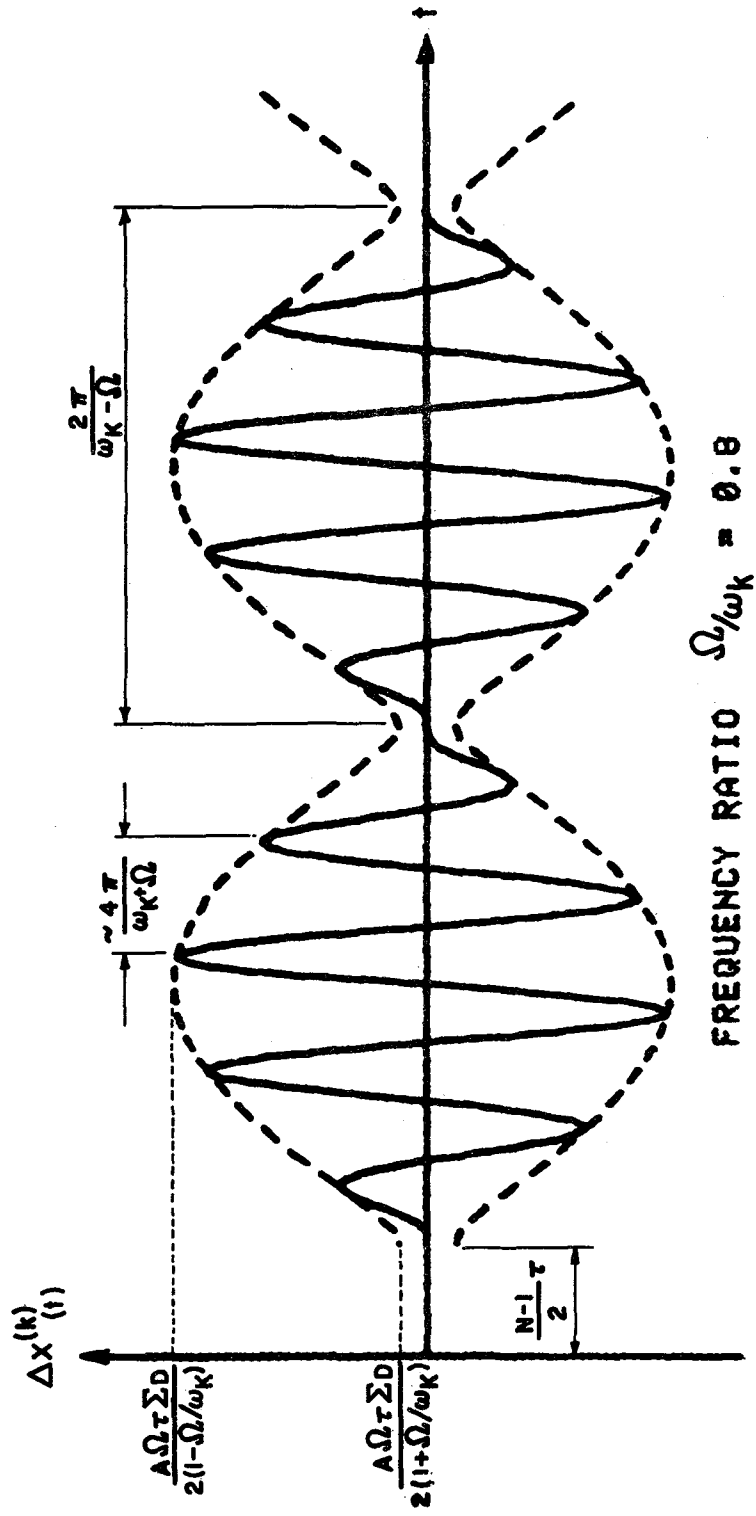where the approximation holds for small damping ξ_k.

FIG. C-2 APPROXIMATE MODAL SOLUTION $\Delta x^{(k)}_{(t)}$ FOR SMALL τ AND GROUND MOTION $Z(t) = \frac{A}{2}(1 - \cos \Omega t)$, UNDAMPED CASE

For the general case, the amplification ratio for the steady state solution to Eq. (C-28) is[*]

$$\text{Amp. Ratio} = \frac{\text{MAX}\left|r_{km}(t)\right|_{\substack{\text{steady}\\\text{state}}}}{\text{MAX}\left|\Delta z(t)\right|} = \sqrt{\frac{1 + (2\xi_k\,\Omega/\omega_k)^2}{(1 - \Omega^2/\omega_k^2)^2 + (2\xi_k\,\Omega/\omega_k)^2}} \qquad \text{(C-31)}$$

At early times, for small damping, Eq. (C-28) involves terms with closely spaced frequencies Ω and $\omega_k\sqrt{1 - \xi_k^2}$, and whose coefficients are comparable. For example, for $t' \simeq 0$, the coefficients of the two cosines terms differ only in sign. Thus, at early times, beat phenomena, similar to those illustrated in Figs. C-1 and C-2, mark the response of a damped system. The "mean" value of the envelope is given by the steady state value, i.e., Eq. (C-31). As time progresses and the transient portion decays, the difference between the envelope maximum and minimum values decreases, until only the steady state portion remains. Finally, if conditions Eq. (C-13) hold, Eq. (C-28) may be converted to the contribution of the kth mode to the center joint displacement, $\Delta x^{(k)}(t)$, by replacing t' with t_c, and multiplying the result by $\sum\limits_{m=1}^{N-1} D_m^{\,k}$.

The effect of damping on the modal contributions is illustrated in Figs. C-3 to C-5. The curves in the figures are the results of actual SEGPIPE numerical calculations, in which conditions Eq. (C-13) are not satisfied. Consequently, the magnitudes of the curves are somewhat

---

[*] Equation (C-31) differs from the amplification ratio for steady state damped vibrations found in textbooks on vibrations. The second term in the numerator does not appear in textbooks. However, most texts have a single sinusoidal input term, while Eq. (49) includes a second term, $2\xi_k\,\Omega/\omega_k$ times the first, and $\pi/2$ radians out of phase with it.

lower, although the trends follow the equations developed in this appendix. In the three figures, the solid line corresponds to $\Delta x^{(k)}$ in the undamped case and the dot-dash line to the response $\Delta x^{(k)}$ in the damped case. The dashed line represents $\Delta z(t)$, the incoherent ground motion across the center joint, i.e., Eq. (C-17). The mode 8 response curves in Fig. C-3 are from SEGPIPE Runs 9 and 10, i.e., $N = 20$, $\tau = 0.02$, $\Omega = 9.0$, $\omega_8 = 7.2115$, $\sum_{m=1}^{19} D_m^8 = -1.2544$ and $\xi_k = 0$ and 0.05, respectively (see Appendix B). It is noted that while conditions Eq. (C-6) are satisfied ($\Omega\tau = 0.18$, $\omega_8\tau = 0.144$, both $<< \pi/2$), conditions Eqs. (C-12) and (C-13) are not, i.e.,

$$\left.\begin{aligned} \cos[\Omega\tau \,(\frac{N}{2} - 1)] &= \cos(1.62) = -0.049 \neq 1 \\ \cos[\omega_8\tau(\frac{N}{2} - 1)] &= \cos(1.30) = 0.269 \neq 1 \end{aligned}\right\} \tag{C-32}$$

Consequently, while the solid curve is very similar to that shown in Fig. C-2 since $\omega_8/\Omega = 0.80$, the peak amplitude of 0.271 cm is considerably less than the 0.455 cm computed via Eq. (C-27). Following Fig. C-2, the response would start at $(N - 1)\tau/2 = 0.19$ sec, and the envelope would peak at $t = 1.947$ and 5.460 sec, while minima would occur at $t = 3.703$ and 7.216 sec. The solid curve agrees with these values. The damped response starts by following very closely the undamped response. However, by the second beat, the amplitude of the beat is considerably reduced.

The trends are perhaps more clearly illustrated in Fig. C-4, where the mode 6 responses with and without damping are shown for $\Omega = 7.7872$ and $\omega_6 = 6.8491$, corresponding to SEGPIPE Runs 11 and 12. Here the ratio $\omega_6/\Omega = 0.88$ is closer to unity so that there are more cycles per beat, and greater amplification. The envelope in the undamped case, Eq. (C-23), reaches its maxima at $t = 3.539$ and 10.237 sec. The Run 11 response maxima (actually minima) occur at $t = 3.64$ and 10.08 sec. The magnitude of the computed value,
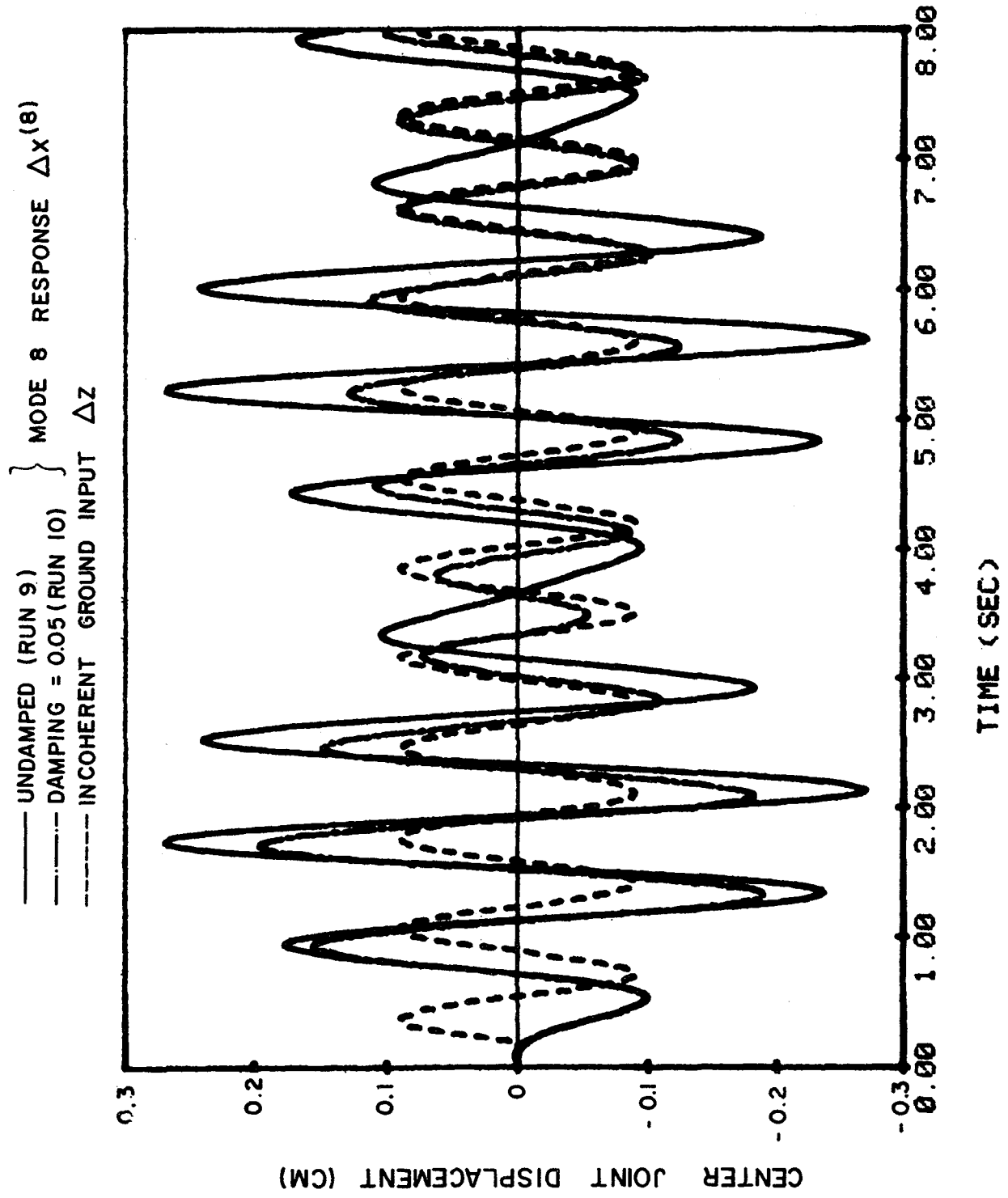
FIG. C-3 COMPUTED. MODE 8 RESPONSE FOR HAVERSINE INPUT WITH AND WITHOUT DAMPING ($\omega_8/\Omega = 7.2115 / 9.0 = 0.801$)
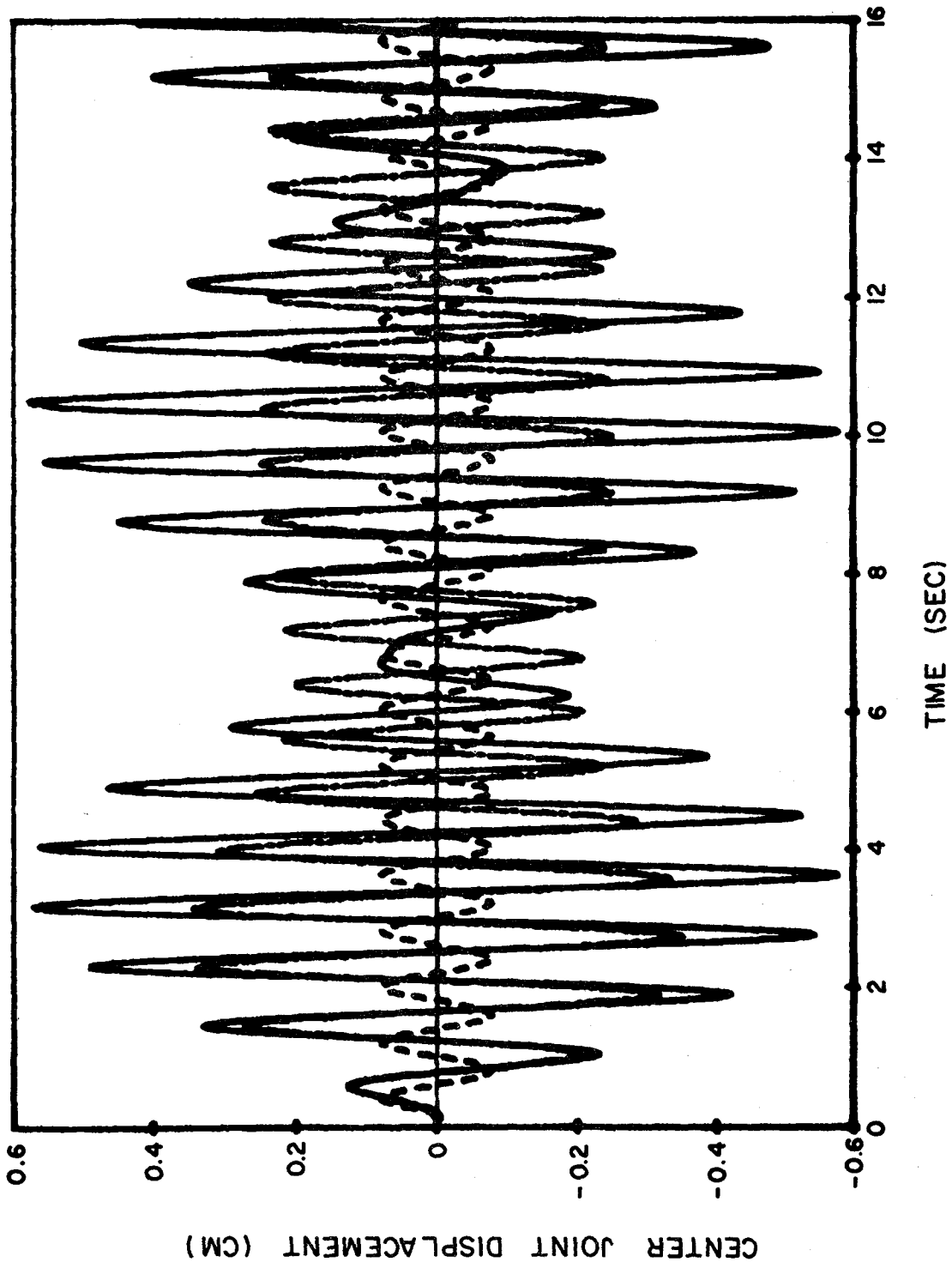
FIG. C-4   COMPUTED MODE 6 RESPONSE FOR HAVERSINE INPUT WITH AND WITHOUT DAMPING (ω_6/Ω = 6.8491/7.7872 = 0.880)

UNDAMPED (RUN II) $\}$ MODE 10 RESPONSE $\Delta x^{(10)}$
DAMPING = 0.05 (RUN I2)
INCOHERENT GROUND INPUT Δz

CENTER JOINT DISPLACEMENT (CM)

TIME (SEC)

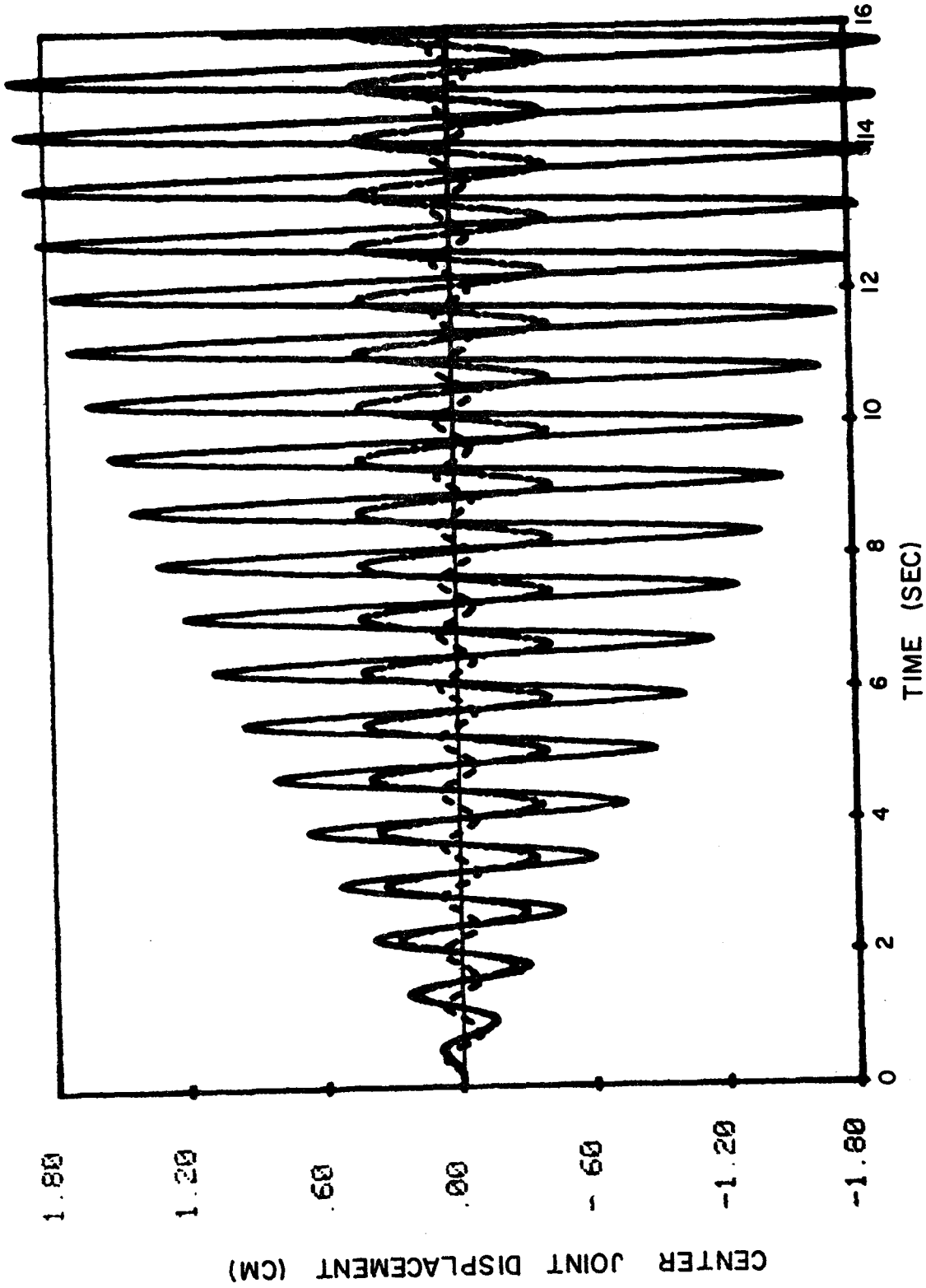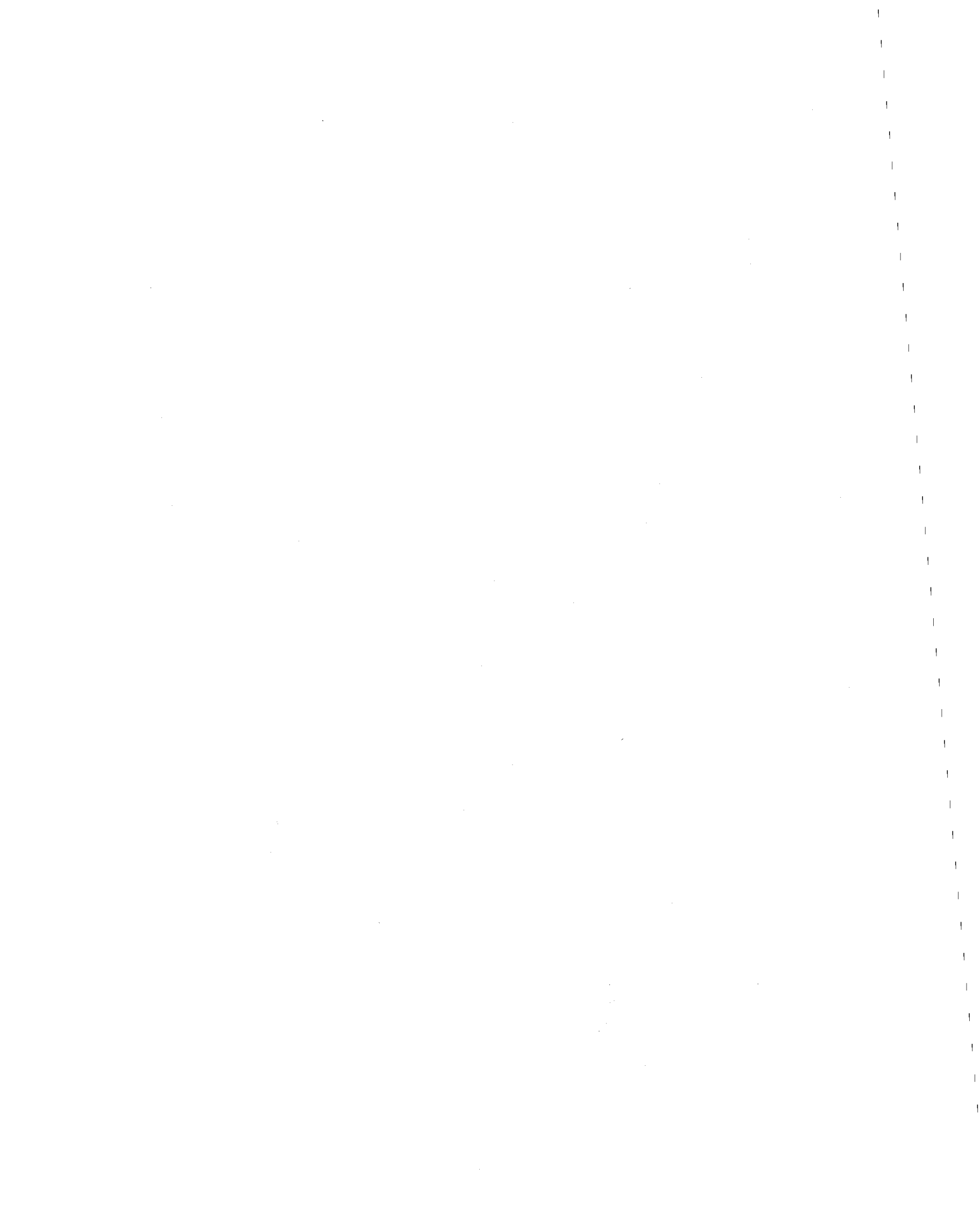FIG. C-5 COMPUTED MODE 10 RESPONSE FOR HAVERSINE INPUT WITH
AND WITHOUT DAMPING ($\omega_{10}/\Omega = 7.5988/7.7872 = 0.9758$)

- 0.5778 cm, is still less than the value $\text{MAX}|\Delta x^{(6)}|$ = 0.8622 cm given by

Eq. (C-27). The damped response again begins by following the undamped

result, but soon deviates from it. By the end of the second beat a steady

state situation is reached. The value of the steady state response is

~ 0.23 cm. The ratio of the steady state response to the undamped peak is

0.40, not far from the 0.437 computed from Eqs. (C-27) and (C-31). The

peak response in the damped case, however, is - 0.3507 cm and occurs

during the transient.

The final example, Fig. C-5, is from the same two calculations, but a

case very close to resonance, mode 10. Here the frequency ratio

ω_{10}/Ω = 0.9758. The peak undamped response based on Eq. (C-27) is 3.1484,

and would occur at t = 16.865 sec, just beyond the end of the calculation.

The computed minimum in Run 11 is - 1.9574 cm and occurs just before the

end of calculation. In this case, the damped response never builds up

beyond the steady state value of 0.4305 cm. The ratio of the computed

steady state response to the undamped maximum is 0.220, very close to the

theoretical value of 0.218 for this case.

-68-

Intentionally Blank

APPENDIX D

CONTINUOUS PIPE SUBJECTED TO A
STATIC DISCONTINUOUS GROUND DISPLACEMENT

A good deal of insight concerning the dynamic response of segmented pipes may be obtained from the simpler static continuous problem. Several aspects of this relation are outlined in this appendix.

1. Physical Interpretation Of D_m^k

The equation governing the static response of the system may be obtained by dropping the $[\ddot{x}]$ and $[\dot{x}]$ terms in Eq. (3), i.e.,

$$\{k_g[I] + k_p[T]\}[x] = k_g[z] + k_B[z_B] \qquad (D-1)$$

Let us introduce the transformation

$$[x] = \sum_{k=1}^{N} A_k[\phi^k] \qquad (D-2)$$

where the constants A_k will be shown to be related to the modal participation factors, and the $[\phi^k]$ are the eigenvectors of $[T]$. Premultiplying Eq. (D-1) by the transpose of $[\phi^k]$, and using the orthogonality condition of the mode shapes, Eq. (13), the equation of equilibrium Eq. (D-1) becomes

$$(k_g + k_p\lambda_k)A_k = k_g[\phi^k]^T[z] + k_B[\phi^k]^T[z_B] \qquad (D-3)$$

When there is no intermediate ground support, $k_g = 0$, so that

$$A_k = \frac{k_B}{k_p\lambda_k}[\phi^k]^T[z_B] = \frac{k_B}{k_p\lambda_k}(\phi_1^k z_0 + \phi_N^k z_{N+1}) \qquad (D-4)$$

For antisymmetric modes

$$A_k = \frac{k_B \phi_1^k}{k_p\lambda_k}(z_0 - z_{N+1}) = P_k \Delta z \qquad (D-5)$$

where P_k is given by Eq. (31)

Returning to the general case, for long pipes we may neglect the boundary contribution. Using Eqs. (6) and (16), the constant A_k becomes

$$A_k = \frac{k_g}{k_g + k_p \lambda_k} [\phi^k]^T [z] = \frac{\omega_g^2}{\omega_k^2} \sum_{j=1}^{N} \phi_j^k z_j \tag{D-6}$$

Considering antisymmetric modes only, and using an identity relating displacements similar to Eq. (45), one obtains

$$A_k = \frac{\omega_g^2}{\omega_k^2} \sum_{j=1}^{N-1} \Delta z_j \left(\sum_{i=1}^{j} \phi_i^k \right) \qquad , k \text{ antisymmetric} \tag{D-7}$$

Taking all $\Delta z_j = 0$, except for $\Delta z_m = 1$, Eq. (D-7) becomes

$$A_{km} = \frac{\omega_g^2}{\omega_k^2} \sum_{i=1}^{m} \phi_i^k \qquad , k \text{ antisymmetric} \tag{D-8}$$

which is the static response in mode k due to a unit discontinuous ground displacement across joint m. The corresponding center joint displacement is the sum of all modal contributions, i.e.,

$$\Delta x_m = x_{\frac{N}{2},m} - x_{\frac{N}{2}+1,m} = \sum_{k=1}^{N} (\phi_{\frac{N}{2}}^k - \phi_{\frac{N}{2}+1}^k) A_{km} = \sum_{k=2,4,.}^{N} 2\phi_{\frac{N}{2}}^k A_{km} \tag{D-9}$$

where (at this point) the antisymmetric modes have been assumed to be even.

Substituting Eq. (D-8) into Eq. (D-9)

$$\Delta x_m = \sum_{k=2,4,.}^{N} 2\phi_{\frac{N}{2}}^k \frac{\omega_g^2}{\omega_k^2} \sum_{j=1}^{m} \phi_j^k \equiv \sum_{k=2,4,.}^{N} D_m^k \tag{D-10}$$

where D_m^k is defined by Eq. (51) in the text.

Equation (D-10) shows that the sum over all antisymmetric modes of the influence coefficients D_m^k at a particular joint m is the static response (center joint displacement) due to a unit ground displacement

across joint m. It was observed that the sums Eq. (D-10) dropped off

extremely rapidly away from the center and appeared to be independent of

N. For example, for $k_B = k_p$ and $k_g = 4k_p$, the values of the sums at the

center and adjacent joints were (to four decimal places)

$$0.7071, \ 0.1213, \ 0.0208, \ 0.0036, \ 0.0006, \ 0.0001 \text{ and } 0.0000 \tag{D-11}$$

for both $N = 20$ and $N = 40$.

For the special case of $k_p/k_g = 0$ (and $k_B = k_p$), the sum may be found

analytically. Using $D_m^{\ k}$ given by Eq. (61),

$$\sum_{k=2,4,.}^{N} D_m^{\ k} = \sum_{k=2,4,.}^{N} \frac{4}{N+1} (-1)^{\frac{k}{2}-1} \sin(\frac{m+1}{N+1} \frac{k\pi}{2}) \ \sin(\frac{m}{N+1} \frac{k\pi}{2})$$

$$= \frac{2}{N+1} \sum_{\frac{k}{2}=1,2,.}^{N/2} (-1)^{\frac{k}{2}-1} [\cos \frac{k\pi}{(N+1)2} - \cos \frac{(2m+1)}{(N+1)} \frac{k\pi}{2}] \tag{D-12}$$

Using No. 429 of Ref. [11],

$$\sum_{k=2,4,.}^{N} D_m^{\ k} = \frac{2}{N+1} (-1)^{N/2} \left\{ - \frac{\cos \pi/2}{2\cos \frac{\pi}{2(N+1)}} + \frac{\cos(2m+1) \frac{\pi}{2}}{2\cos(\frac{2m+1}{N+1}) \frac{\pi}{2}} \right\} \tag{D-13}$$
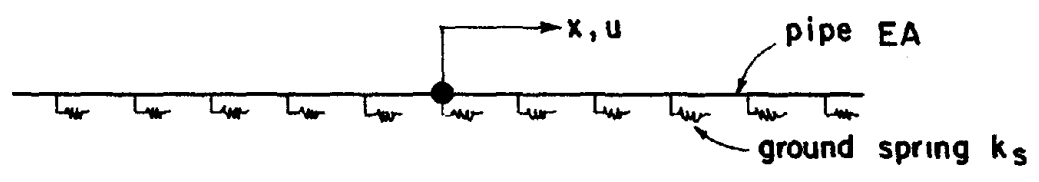
The first term in Eq. (D-13) is always zero; the second term is also

zero provided $2m + 1 \neq N + 1$, or $m \neq N/2$. When $m = N/2$, recalling N is

even and, taking the limit

$$\lim_{\theta \to \pi/2} \left[\frac{\cos(N+1)\theta}{2\cos \theta} \right] = \frac{N+1}{2} \left[\frac{\sin(N+1)\pi/2}{\sin \pi/2} \right] = \frac{N+1}{2}(-1)^{N/2} \tag{D-14}$$

so that

$$\sum_{k=2,4,.}^{N} D_m^{\ k} = \left\{ \begin{array}{l} 1 \text{ for } m = \frac{N}{2} \\[2em] 0 \text{ for } m \neq \frac{N}{2} \end{array} \right\} \quad \text{for } k_p = 0 \tag{D-15}$$

A. GEOMETRY
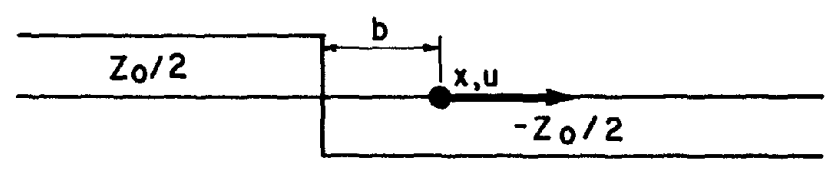
B. INPUT GROUND DISPLACEMENT

FIG. D-I   GEOMETRY AND INPUT DISPLACEMENT FOR AN
INFINITE CONTINUOUS PIPE

Again, when there is no interaction between links, the static joint
displacement follows exactly the corresponding incoherent free field ground
displacement across the joint.

Unfortunately, it was not possible to obtain an analytical expression
for $\sum\limits_{k=2,4,\ldots}^{N} D_m^{\ k}$ when $k_p \neq 0$. However, the observed numerical behavior,
e.g., Eq. (D-11) did provide the motivation for the remainder of this
Appendix.

2.   Static Solution For An Infinite Continuous Pipe

The geometry of the problem is shown in Fig. D-1a. The uniform pipe is
continuously attached to the ground. There is a continuous ground spring so
that the frictional force per unit length is $-k_s(u - z)$, where u is the pipe
(axial) displacement and z is the free field ground displacement. This
frictional force is balanced by the change in the axial force EA du/dx in
the pipe. Consequently, the equation of equilibrium is

$$EA \frac{d^2u}{dx^2} - k_s u = - k_s z \tag{D-16}$$

The ground motion is taken to correspond to Fig. D-1b, i.e.,

$$z(x) = \begin{cases} + z_o/2 & - \infty \leq x < - b \\ - z_o/2 & - b < x \leq \infty \end{cases} \tag{D-17}$$

The location x = 0 is assumed to correspond to the center of the pipe, so
that b is a measure of the distance from the discontinuity to the response
point, the center. Let $u_1(x)$ represent the solution in the region $x \leq - b$,
and $u_2(x)$ that in $x \geq - b$. The boundary conditions are that the displacement
remain finite at either end, i.e.,

$$\left. \begin{array}{l} u_1(- \infty) = \text{finite} \\ \\ u_2(+ \infty) = \text{finite} \end{array} \right\}$$

and that the displacement and pipe force are continuous at $x = -b$, i.e.,

$$\left.\begin{aligned}
u_1(-b) &= u_2(-b) \\
\frac{du_1}{dx}(-b) &= \frac{du_2}{dx}(-b)
\end{aligned}\right\} \tag{D-19}$$

The general solution in both regions are

$$\left.\begin{aligned}
u_1(x) &= C_1 e^{\beta x} + C_2 e^{-\beta x} + z_0/2 & x &\leq -b \\
u_2(x) &= C_3 e^{\beta x} + C_4 e^{-\beta x} - z_0/2 & x &\geq -b
\end{aligned}\right\} \tag{D-20}$$

where

$$\beta = \sqrt{k_s/EA} \tag{D-21}$$

Conditions Eq. (D-18) require C_2 and C_3 both to be zero, while Eqs. (D-19) are satisfied if

$$\left.\begin{aligned}
C_1 e^{-\beta b} + z_0/2 &= C_4 e^{\beta b} - z_0/2 \\
C_1 e^{-\beta b} &= -C_4 e^{\beta b}
\end{aligned}\right\} \tag{D-22}$$

Solving simultaneously for C_1 and C_4, Eqs. (D-20) become

$$\left.\begin{aligned}
u_1(x) &= \frac{z_0}{2}\left[1 - e^{\beta(x+b)}\right] & x &\leq -b \\
u_2(x) &= \frac{z_0}{2}\left[e^{-\beta(x+b)} - 1\right] & x &\geq -b
\end{aligned}\right\} \tag{D-23}$$

The quantity of interest is the strain at $x = 0$

$$\frac{du_2}{dx}(0) = -\frac{\beta z_0}{2} e^{-\beta b} \tag{D-24}$$

Equation (D-24) shows that the strain decreases exponentially with the distance to the discontinuous input, and that as the pipe stiffness to soil stiffness decreases, the rate of decay increases.

3. Static Solution For A Finite Continuous Pipe

The same differential equation applies in the case of a finite pipe as in the previous case, Eq. (D-16), and the same ground motion (except for the limits), Eq. (D-17). The continuity conditions Eqs. (D-19) remain valid, but boundary conditions Eqs. (D-18) are replaced by

$$\left.\begin{array}{l} u_1(-L/2) = z(-L/2) = z_o/2 \\[2mm] u_2(L/2) = z(L/2) = -z_o/2 \end{array}\right\} \tag{D-25}$$

The solution in the two regions are

$$\left.\begin{array}{ll} u_1(x) = C_1 \sinh \beta x + C_2 \cosh \beta x + z_o/2 & -L/2 \le x \le -b \\[2mm] u_2(x) = C_3 \sinh \beta x + C_4 \cosh \beta x - z_o/2 & -b \le x \le L/2 \end{array}\right\} \tag{D-26}$$

where $\beta = \sqrt{k_s/EA}$ [Eq. (D-21)], and where the four constants are unrelated to the previous set. Applying Eqs. (D-25),

$$\left.\begin{array}{ll} u_1(x) = C_1(\sinh \beta x + \tanh \frac{\beta L}{2} \cosh \beta x) + z_o/2 \; , & -L/2 \le x \le -b \\[3mm] u_2(x) = C_3(\sinh \beta x - \tanh \frac{\beta L}{2} \cosh \beta x) - z_o/2 \; , & -b \le x \le L/2 \end{array}\right\} \tag{D-27}$$

Finally, applying Eqs. (D-19)

$$\left.\begin{array}{l} u_1(x) = \dfrac{z_o}{2}\left[1 - \dfrac{\cosh \beta b}{\tanh \frac{\beta L}{2}} (1 + \tanh \frac{\beta L}{2} \tanh \beta b)(\sinh \beta x + \tanh \frac{\beta L}{2} \cosh \beta x)\right] \\[6mm] u_2(x) = -\dfrac{z_o}{2}\left[1 + \dfrac{\cosh \beta b}{\tanh \frac{\beta L}{2}} (1 - \tanh \frac{\beta L}{2} \tanh \beta b)(\sinh \beta x - \tanh \frac{\beta L}{2} \cosh \beta x)\right] \end{array}\right\} \tag{D-28}$$

Here, the displacement and strain at $x = 0$ are

$$u_2(0) = -\frac{z_o}{2}\left[1 - \cosh \beta b + \sinh \beta b \tanh \frac{\beta L}{2}\right] \tag{D-29}$$

and

$$\frac{du_2}{dx}(0) = -\frac{z_o \beta}{2 \tanh \frac{\beta L}{2}}\left[\cosh \beta b - \sinh \beta b \tanh \beta \frac{L}{2}\right] \tag{D-30}$$
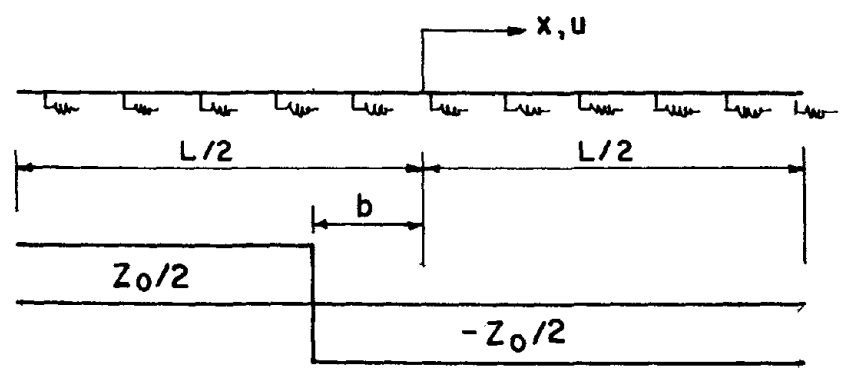
FIG. D-2   GEOMETRY AND INPUT GROUND DISPLACEMENT
FOR CONTINUOUS PIPE

respectively. It is noted that as $L \to \infty$, $\tanh \frac{\beta L}{2} \to 1$ so that Eqs. (D-29) and (D-30) reduce to Eq. (D-23) evaluated at $x = 0$, and Eq. (D-24).

To relate the present solution to the discrete system, one must identify the pipe/joint stiffness as

$$k_p = EA/\ell \qquad (D-31)$$

where ℓ is the finite difference interval, and the discrete ground stiffness as

$$k_g = k_s \ell \qquad (D-32)$$

Consequently, the parameter β, given by Eq. (D-21) is

$$\beta = \sqrt{\frac{k_s}{EA}} = \sqrt{\frac{k_g/\ell}{k_p \ell}} = \frac{1}{\ell} \sqrt{k_g/k_p} \qquad (D-33)$$

For the many calculations in which k_g/k_p was 4, β is $2/\ell$. The distance b from the center joint to the loaded joint may be written as

$$b = j\ell = (\frac{N}{2} - m)\ell \qquad (D-34)$$

while the total length of the pipe is

$$L = N\ell \qquad (D-35)$$

Substituting Eqs. (D-33) to (D-35) into Eq. (D-30), and using the notation of the discrete system,

$$-\ell \frac{du_2}{dx}(0) = \Delta x_{\frac{N}{2} - j} = \frac{z_o \sqrt{k_g/k_p}}{2\tanh(\frac{N}{2}\sqrt{k_g/k_p})} \left[\cosh j \sqrt{k_g/k_p} - \sinh j \sqrt{k_g/k_p} \right.$$
$$\left. \tanh(\frac{N}{2}\sqrt{k_g/k_p}) \right] \qquad (D-36)$$

When $k_g/k_p = 4$ and $z_o = 1$,

$$\Delta x_{\frac{N}{2} - j} = \frac{1}{\tanh N} \left[\cosh 2j - \sinh 2j \tanh N \right] \qquad (D-37)$$
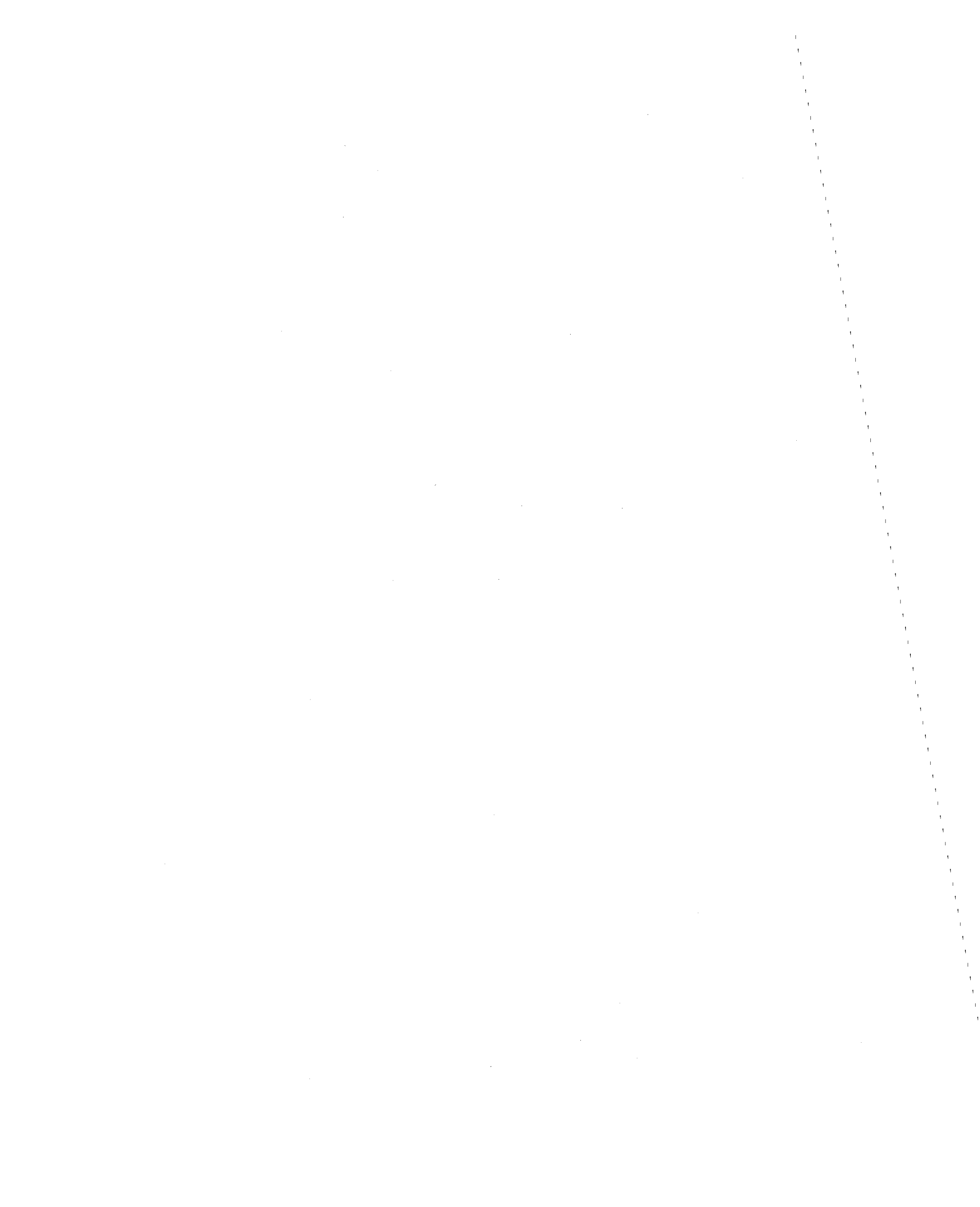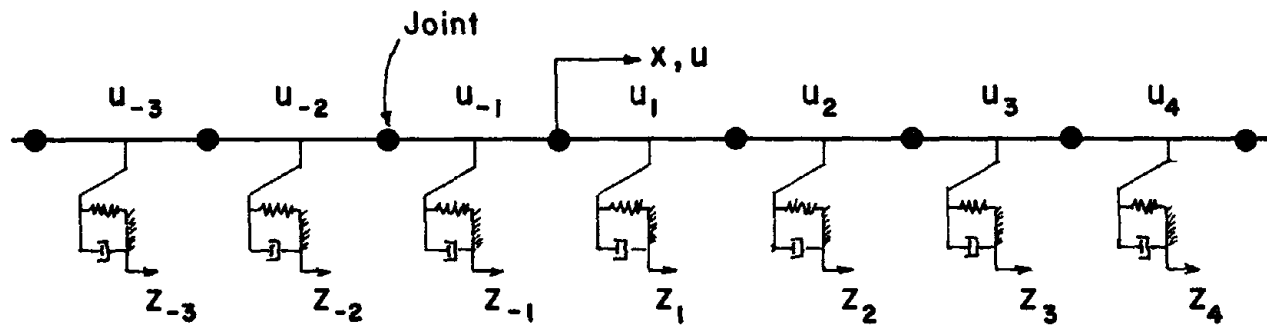
A. NOTATION

B. INPUT GROUND DISPLACEMENT

FIG. D-3   STATIC   FINITE   DIFFERENCE   SOLUTION
FOR   AN   INFINITE   PIPE

The tanh function approaches one very rapidly. For example, $\tanh(5) = 0.999909$ and $\tanh(10) = 1 - 4 \times 10^{-9}$. Thus, for $N > 10$, for all practical purposes the pipe may be considered infinite. Consequently, recalling Eq. (D-10), for $k_g/k_p = 4$

$$\Delta x_m = \sum_{k=2,4,\ldots}^{N} D_m^k \sim e^{-2j} \qquad (D-38)$$

independent of the number of links.

4. Static Finite Difference Solution For An Infinite Pipe

The values given in Eq. (D-11) for the sum of the influence coefficients over all the modes agree only very approximately with those computed according to Eq. (D-38). In order to seek a better understanding of the discrepancy, a closed form solution to the finite difference formulation of the problem in Section 2 of this Appendix was obtained. The notation and the free field ground displacement are shown in Fig. D-3. The pipe and ground displacements are written as u_{+j} and z_{+j} to the right of the discontinuity, and u_{-j} and z_{-j} to the left. The governing differential equation, Eq. (D-16), in finite difference form is

$$u_{j-1} - (2 + \beta^2 \ell^2) u_j + u_{j+1} = -\beta^2 \ell^2 z_j \qquad (D-39)$$

where β is given by Eq. (D-21) and where $z_j = + z_o/2$ for $j < 0$ and $z_j = - z_o/2$ for $j > 0$.

For $j < 0$ we assume a solution in the form

$$u_j = z_o/2 + C_1 \alpha^j \quad , \quad j < 0 \qquad (D-40)$$

where C_1 and α are constants to be determined. We note that for u_j to approach $z_j = z_o/2$ for $j \to -\infty$, $|\alpha|$ must be greater than one. When Eq. (D-40) is substituted into Eq. (D-39), the latter becomes

$$C_1 \, \alpha^{j-1} \left[\alpha^2 - (2 + \beta^2 \ell^2)\alpha + 1 \right] = 0 \qquad \text{(D-41)}$$

Letting the constant $C_1 = 0$ results in the trivial solution, $u_j \equiv z_o/2$. Since $\alpha \neq 0$, the only alternative is for the bracket to be zero, yielding two possible solutions for α

$$\alpha_{1,2} = 1 + \frac{\beta^2 \ell^2}{2} \pm \beta\ell \sqrt{1 + (\frac{\beta\ell}{2})^2} \qquad \text{(D-42)}$$

Since $\alpha > 1$, α_1 (the value with the + sign) is the appropriate choice for $j < 0$.

Alternatively, we could assume a solution for $j > 0$

$$u_j = - z_o/2 + C_2 \, \bar{\alpha}^j \qquad , \; j > 0 \qquad \text{(D-43)}$$

Where $|\bar{\alpha}| < 1$ for $u_j \to - z_o/2$ as $j \to + \infty$. This assumption again results in Eq. (D-41), except C_2 and $\bar{\alpha}$ replace C_1 and α. Noting $\bar{\alpha} < 1$, the solution to Eq. (D-42) with the minus sign, α_2, is the appropriate value for $j > 0$.

Equation (D-39) is next applied at $j = - 1$

$$C_1 \, \alpha_1^{-2} - (2 + \beta^2 \ell^2)C_1 \, \alpha_1^{-1} + C_2 \, \alpha_2^{1} = z_o \qquad \text{(D-44)}$$

and at $j = + 1$

$$C_1 \, \alpha_1^{-1} - (2 + \beta^2 \ell^2)C_2 \, \alpha_2^{1} + C_2 \, \alpha_2^{2} = - z_o \qquad \text{(D-45)}$$

Solving Eqs. (D-44) and (D-45) simultaneously, and noting Eq. (D-42), we obtain

$$C_1 = - z_o \frac{\alpha_1}{\alpha_1 + 1} \qquad \text{and} \qquad C_2 = z_o \frac{\alpha_1}{\alpha_1 + 1} \qquad \text{(D-46)}$$

The solution for $j < 0$ is thus

$$u_{-j} = z_o \left[\frac{1}{2} - \frac{1}{(\alpha_1 + 1)\alpha_1^{j-1}} \right]$$

(D-47)

and for $j > 0$

$$u_j = z_o \left[-\frac{1}{2} + \frac{\alpha_1 \alpha_2^{j}}{\alpha_1 + 1} \right] = z_o \left[-\frac{1}{2} + \frac{1}{(\alpha_1 + 1)\alpha_1^{j-1}} \right] = -u_{-j}$$

(D-48)

where use has been made of $\alpha_1 \alpha_2 = 1$. Thus, not unexpectedly, the solution is completely antisymmetric. Denoting the difference between the displacements of two adjacent links as Δx_j, i.e.,

$$\Delta x_j \equiv u_j - u_{j+1} = u_{-j-1} - u_{-j}$$

(D-49)

then

$$\Delta x_j = \left[z_o \frac{\alpha_1 - 1}{\alpha_1 + 1} \right] \frac{1}{\alpha_1^{j}} = \Delta x_o \frac{1}{\alpha_1^{j}}$$

(D-50)

where Eq. (D-50) applies for all values of $j \geq 0$. The Δx_j are, of course, symmetric. When $\beta\ell = 2$, corresponding to $k_g/k_p = 4$ [see Eq. (D-33)], $\alpha_1 = 3 + 2\sqrt{2}$ so that $\Delta x_o = z_o/\sqrt{2} = 0.7071 z_o$. For $z_o = 1$, the values for Δx_j given by Eq. (D-50) match identically the values of the sum of the influence coefficients given in Eq. (D-11).

Thus, Eq. (D-50) may be used to represent the limiting case for large N of the sum of the influence coefficients over all the modes, i.e.,

$$\underset{N \to \infty}{\text{limit}} \sum_{k=2,4,.}^{N} D_{\frac{N}{2}-j}^{k} = \frac{\alpha_1 - 1}{\alpha_1 + 1} \frac{1}{\alpha_1^{j}}$$

(D-51)

where, using Eqs. (D-33) and (D-42),

$$\alpha_1 = 1 + \frac{1}{2} \left(k_g/k_p \right) + \sqrt{\left(k_g/k_p \right) \left[1 + \frac{1}{4} \left(k_g/k_p \right) \right]}$$

(D-52)

Finally, the limiting case of the double sum over all modes and all joints of the influence coefficients may be written

$$\lim_{N \to \infty} \sum_{k=2,4,..}^{N} \sum_{m=1}^{N-1} D_m^{\ k} = \frac{1}{z_o} \left[\Delta x_o + 2 \sum_{j=1}^{\infty} \Delta x_j \right] \cong 1 \qquad \text{(D-53)}$$

where Eq. (D-50) and the sum of a geometric series have been used. Thus, Eq. (63) in the text has been proved in general, at least for $N \to \infty$.

The final step is to show that the finite difference solution approaches the continuous solution as $\ell \to 0$. Writing the strain as

$$\frac{du}{dx} \simeq -\frac{\Delta x_j}{\ell} = -\frac{z_o}{\ell} \left(\frac{\alpha_1 - 1}{\alpha_1 + 1} \right) \frac{1}{\alpha_1^{\ j}} \qquad \text{(D-54)}$$

For small values of $\beta\ell$, $\alpha_1 \simeq 1 + \beta\ell$, so that Eq. (D-54) becomes

$$\frac{du}{dx} \simeq -\frac{z_o}{\ell} \left(\frac{\beta\ell}{2 + \beta\ell} \right) (1 + \beta\ell)^{-j} \qquad \text{(D-55)}$$

Letting $b = j\ell$ and $\xi = 1/(\beta\ell)$, and taking the limit as $\xi \to \infty$ ($\beta\ell \to 0$)

$$\frac{du}{dx} = \lim_{\beta\ell \to 0} \left(\frac{-z_o \beta}{2 + \beta\ell} \right) \left(1 + \beta\ell \right)^{-b/\ell}$$

$$= \lim_{\xi \to \infty} \left(\frac{-z_o \beta}{2 + 1/\xi} \right) \left[(1 + 1/\xi)^{\xi} \right]^{-\beta b} \qquad \text{(D-56)}$$

Recognizing the limit of the bracket as the definition of e,

$$\frac{du}{dx} = -\frac{z_o \beta}{2} e^{-\beta b} \qquad \text{(D-57)}$$

which is identical to Eq. (D-24).

NATIONAL SCIENCE FOUNDATION
DISTRIBUTION MAILING LIST

PAGE   1

PERRY Y. AMIMOTO, ENGINEERING GEOLOGIST
CALIFORNIA DIVISION OF MINES AND GEOLOGY
1416 9TH STREET,   ROOM 118
SACRAMENTO, CA   95814

SUBHASH C. ANAND
DEPARTMENT OF CIVIL ENGINEERING
CLEMSON UNIVERSITY
CLEMSON, SC   20631

H. WALTER ANDERSON, P. E.
ASSISTANT TO CHIEF, DIVISION OF DESIGN
U.S. DEPARTMENT OF THE INTERIOR
ENGINEERING & RESEARCH CENTER
RM 1440,BLDG 67 DENVER FEDERAL CENTER
DENVER, CO   80225

DR. ROBERT ANDERSON
G. A. I. INC.
570 BEATTY ROAD
PITTSBURGH, PA   15146

PROFESSOR ALFREDO ANG
UNIVERSITY OF ILLINOIS
DEPARTMENT OF CIVIL ENGINEERING
SCHOOL OF ENGINEERING
URBANA, IL   61801

MR. WALTER F. ANTON
DIRECTOR OF ENGINEERING
EAST BAY MUNICIPAL UTILITY DISTRICT
2130 ADELINE STREET
P. O. BOX 24055
OAKLAND, CA 94623

PROFESSOR T. ARIMAN
DEPARTMENT OF AEROSPACE AND
MECHANICAL ENGINEERING
UNIVERSITY OF NOTRE DAME
NOTRE DAME, IN 46556

DR. R. STEVEN ATKINS
G. A. I. INC.
570 BEATTY ROAD
PITTSBURGH, PA 15146

MARY AYRES
AYRES AND HAYAKAWA
1180 SOUTH BEVERLY DRIVE
LOS ANGELES, CA 90035

JULIAN BARDOFF
SAN FRANCISCO WATER DEPARTMENT
PUBLIC UTILITIES COMMISSION
425 MAIN STREET
SAN FRANCISCO, CA 94101

DR. M. L. BARON
WEIDLINGER ASSOCIATES
110 EAST 59TH STREET
NEW YORK, NY 10022

(5 COPIES)

KEITH G. BARRETT, CHIEF, DESIGN BRANCH
THE RESOURCES AGENCY, STATE OF CALIF.
DEPARTMENT OF WATER RESOURCES
POST OFFICE BOX 388   1416 NINTH STREET
SACRAMENTO, CA 95814

JAMES E. BEAVERS
UNION CARBIDE CORPORATION
NUCLEAR DIVISION   BUILDING 9733-2
POST OFFICE BOX Y, MS1
OAK RIDGE, TN   37830

LYNN S. BEEDLE
DIRECTOR, FRITZ ENGINEERING LABORATORY
LEHIGH UNIVERSITY
BETHLEHEM, PA 18015

MR. R. BEHNKE
ST. LOUIS COUNTY WATER COMPANY
8390 DELMAN BOULEVARD
ST. LOUIS, MISSOURI 63123

JACK R. BENJAMIN
EDAC   SUITE 301
480 CALIFORNIA AVENUE
PALO ALTO, CA 94306

JOSEPH W. BERG, JR.
DIVISION OF EARTH SCIENCES
NATIONAL ACADEMY OF SCIENCES
2101 CONSTITUTION AVENUE NW
WASHINGTON, DC   20418

R. V. BETTINGER
CHIEF, CIVIL ENGINEER
PACIFIC GAS AND ELECTRIC COMPANY
77 BEALE STREET
SAN FRANCISCO, CA   94106

PROFESSOR J. M. BIGGS
DEPARTMENT OF CIVIL ENGINEERING
MASSACHUSETTS INSTITUTE OF TECHNOLOGY
CAMBRIDGE, MA   02139

JAMES E. BIHR, MANAGING DIRECTOR
INTERNATIONAL CONFERENCE OF
BUILDING OFFICIALS
5360 SOUTH WORKMAN MILL ROAD
WHITTIER, CA   90601

J. F. BLASCH
BETHLEHEM STEEL CORPORATION
BETHLEHEM, PA   18016

JOHN A. BLUME
URS/JOHN A. BLUME & ASSOCIATES
SHERATON-PALACE, 130 JESSIE
SAN FRANCISCO, CA   94105

ELMER E. BOTSAI
BOTSAI, OVERSTREET AND ROSENBERG, AIA
321 WAILUPE CIRCLE
HONOLULU, HI   96821

JAMES T. BRODIE
PASADENA WATER AND POWER DEPARTMENT
CITY HALL
100 NORTH GARFIELD AVENUE
PASADENA, CA   91109

PROFESSOR JAMES M. BRUNE
UNIVERSITY OF CALIFORNIA, SAN DIEGO
IGPP MAIL CODE A-025
LA JOLLA, CA   92093

DR. M. N. BUEHRING
DEPARTMENT OF WATER AND POWER
CITY OF LOS ANGELES
111 NORTH HOPE STREET
P. O. BOX 111
LOS ANGELES, CA   90051

DON W. BUTLER, ASSISTANT CHIEF
ENG.DIV.,MILITARY CONSTRUCTION--DAEN-MCE
OFFICE, CHIEF OF ENGINEERS
DEPARTMENT OF THE ARMY
WASHINGTON, DC   20314

JOSEPH C. CALDWELL
OFFICE OF PIPELINE SAFETY
DEPARTMENT OF TRANSPORTATION
410 7TH STREET SW
WASHINGTON, DC   20590

MARY LU CASEY
LIBRARY
AGABIAN ASSOCIATES
250 NORTH NASH STREET
EL SEGUNDO, CA   90245

WALTER CASTLE
N. O. A. A.
6010 EXECUTIVE BLVD.
ROCKVILLE, MD   20852

JACK E. CERMAK
FLUID MECHANICS PROGRAM
COLORADO STATE UNIVERSITY
FORT COLLINS, CO   80521

CONWAY CHAN
NUCLEAR ANALYSIS AND SAFETY DEPARTMENT
ELECTRIC POWER RESEARCH INSTITUTE
POST OFFICE BOX 10412
PALO ALTO, CA   94303

MR. R. C. CHANEY
FUGRO, INC.
3777 LONG BEACH BLVD.
P. O. BOX 7765
LONG BEACH, CA   90807

A. K. CHOPRA
DEPARTMENT OF CIVIL ENGINEERING
UNIVERSITY OF CALIFORNIA
DAVIS HALL
BERKELEY, CA   94720

JOHN T. CHRISTIAN
STONE AND WEBSTER ENGINEERING CORP.
P. O. BOX 2325
BOSTON, MA   02107

RAY W. CLOUGH
DEPARTMENT OF CIVIL ENGINEERING
UNIVERSITY OF CALIFORNIA
BERKELEY, CA   94720

GARY COBB
ASSISTANT DIRECTOR
U. S. WATER RESOURCES COUNCIL
2120 L STREET NW
WASHINGTON, DC   20037

C. L. COGSWELL
LEV ZETLIN ASSOCIATES, INC.
1629 K STREET NW
WASHINGTON, DC   20006

JAMES D. COOPER
STRUCTURAL AND APPLIED
MECHANICS DIVISION
DEPARTMENT OF TRANSPORTATION
WASHINGTON, DC   20590

HOLLY A. CORNELL, PRESIDENT
CH2M HILL ENGINEERS, PLANNERS
ECONOMISTS & SCIENTISTS
1600 S. W. WESTERN BLVD.
P. O. BOX 428
CORVALLIS, OR   97330

MR. COSTELLO
NUCLEAR REG. COM.
OFFICE OF STDS. DEVELOPMENT
U.S.N.R.C.
WASHINGTON, DC   20555

LEROY CRANDALL
CONSULTING - GEOTECHNICAL ENGINEERS
711 NORTH ALVARADO STREET
LOS ANGELES, CA   90026

BOB CRIST
STRUCTURES SECTION
NATIONAL BUREAU OF STANDARDS
BUILDING 226
WASHINGTON, DC   20234

JANET M. CULLEN
DEPARTMENT OF URBAN PLANNING
410 GOULD HALL, JO-40
UNIVERSITY OF WASHINGTON
SEATTLE, WA   98195

CHARLES CULVER
ROOM B-244, BUILDING 226
NATIONAL BUREAU OF STANDARDS
WASHINGTON, DC   20234

MR. HAROLD R. DENTON
DIVISION OF TECHNICAL REVIEW
NUCLEAR REGULATORY COMMISSION
WASHINGTON, DC   20555

ASH DHINGRA
JMM, CONSULTING ENGINEERS
555 EAST WALNUT STREET
PASADENA, CA   91101

J. R. DINEEN, DIRECTOR
WESTCHESTER COUNTY WATER AGENCY
532 COUNTY OFFICE BUILDING
WHITE PLAINS, NY   10601

JOHN DRESSEL
DEPARTMENT OF HOUSING AND
URBAN DEVELOPMENT
451 7TH STREET SW
WASHINGTON, DC   20410

MR. M. W. DOWD
METROPOLITAN WATER DISTRICT,NORTHERN
111 SUNSET BOULEVARD   CALIF.
BOX 54153
LOS ANGELES, CA 90054

PROFESSOR C. MARTIN DUKE
ROOM 3173 ENGINEERING I
UNIVERSITY OF CALIFORNIA, L. A.
LOS ANGELES, CA 90024

JOHN EBERHARD
THE A.I.A. RESEARCH CORPORATION
1735 NEW YORK AVENUE NW
WASHINGTON, DC 20006

MR. DALE EMERSON
SEATTLE WATER DEPARTMENT
1015 THIRD AVENUE
SEATTLE, WA 98104

PROFESSOR L. J. FEESER
RENSSELAER POLYTECHNIC INSTITUTE
DEPARTMENT OF CIVIL ENGINEERING
TROY, NY 12181

W. H. FELL
PUBLIC SERVICE DEPARTMENT
119 NORTH GLENDALE AVENUE
GLENDALE, CA 91206

PROFESSOR STEVEN J. FENVES
DEPARTMENT OF CIVIL ENGINEERING
CARNEGIE-MELLON UNIVERSITY
PITTSBURGH, PA   15213

GREER FERVER, PRESIDENT
FERVER ENGINEERING COMPANY
3487 KURTZ STREET
SAN DIEGO, CA   92110

JOSEPH A. FISHER
PARTNER, DAMES & MOORE
6 COMMERCE DRIVE
CRANFORD, NJ   07016

DUANE B. FORD
2421 WITTKOP WAY
SACRAMENTO, CA   95825

PROFESSOR RAYMOND R. FOX
SCHOOL OF ENGINEERING & APPLIED SCIENCE
GEORGE WASHINGTON UNIVERSITY
WASHINGTON, DC   20052

DR. ELLIOT P. FRAMAN
MANAGER PUBLIC SAFETY SYSTEMS
JET PROPULSION LABORATORY   BUILDING 169
4800 OAK GROVE DRIVE
PASADENA, CA   91103

PAGE   12

J. G. FULLER
WASHINGTON WATER POWER COMPANY
BOX 3727
SPOKANE, WA   99220

DR. MICHAEL P. GAUS
NATIONAL SCIENCE FOUNDATION
1800 G STREET   NW
WASHINGTON, DC   20550

SAFDAR A. GILL
SOIL TESTING SERVICES INC.
111 PFINGSTEN ROAD
NORTHBROOK, IL   60062

JOHN T. GORMLEY
D'APPOLONIA CONSULTING ENGINEERS
10 DUFF ROAD
PITTSBURGH, PA   15235

WILLIAM N. GREEN
GEOLOGICAL SURVEY
NATIONAL CENTER
RESTON, VA   22092

NELSON T. GRISAMORE
NATIONAL ACADEMY OF ENGINEERS
2101 CONSTITUTION AVENUE NW
WASHINGTON, DC   20418

RICARDO A. GUZMAN
CONSULTING ENGINEER
4269 COUNTRY CLUB DRIVE
LONG BEACH, CA   90807

MR. W. J. HALL
UNIVERSITY OF ILLINOIS
DEPARTMENT OF CIVIL ENGINEERING
URBANA, IL   61801

THOMAS C. HANKS
U. S. GEOLOGICAL SURVEY
345 MIDDLEFIELD ROAD
MENLO PARK, CA   94025

R. D. HANSON
DEPARTMENT OF CIVIL ENGINEERING
UNIVERSITY OF MICHIGAN
319 WEST ENGINEERING BUILDING
ANN ARBOR, MI   48104

JERRY HARBOR
DIVISION   RRD
ATOMIC ENERGY COMMISSION
WASHINGTON, DC   20545

GARY C. HART
ENGINEERING SCHOOL
UNIVERSITY OF CALIFORNIA, L. A.
6731 BOELTER HALL
LOS ANGELES, CA   90024

WALTER W. HAYS, ASSOCIATE CHIEF
BRANCH OF EARTHQUAKE HAZARDS
U. S. GEOLOGICAL SURVEY, STOP 966
BOX 25046 DENVER FEDERAL CENTER
DENVER, CO   80225

MICHAEL J. HIGGINS
C. I. P. R. A.
EXECUTIVE PLAZA WEST   SUITE 509
1301 WEST 22ND STREET
OAK BROOK, IL   60521

GEORGE W. HOUSNER
CALIFORNIA INSTITUTE OF TECHNOLOGY
DEPARTMENT OF CIVIL ENGINEERING
1201 EAST CALIFORNIA BLVD.
PASADENA, CA   91109

GEORGE HOWARD
APPLIED NUCLEONICS COMPANY, INC.
POST OFFICE BOX 24313   VILLAGE STATION
LOS ANGELES, CA   90024

PROFESSOR BENJAMIN F. HOWELL, JR.
439 DEIKEW
PENNSYLVANIA STATE UNIVERSITY
UNIVERSITY PARK, PA   16802

PAGE   15

DR. J. ISENBERG
WEIDLINGER ASSOCIATES
3000 SAND HILL ROAD
BUILDING 4, SUITE 245
MENLO PARK, CA   94025

(25 COPIES)

W. D. IWAN
CALIFORNIA INSTITUTE OF TECHNOLOGY
DEPARTMENT OF CIVIL ENGINEERING
1201 EAST CALIFORNIA BLVD.
PASADENA, CA   91109

I. M. IDRISS, PRINCIPAL
WOODWARD-CLYDE CONSULTANTS
THREE EMBARCADERO CENTER
SUITE 700
SAN FRANCISCO, CA   94111

ERNEST C. JAMES
CHIEF,CIVIL DESIGN SECTION DESIGN BRANCH
DEPARTMENT OF WATER RESOURCES
1416 9TH STREET
SACRAMENTO, CA   95814

MR. ROBERT JANSEN
CHIEF, DESIGN AND CONSTRUCTION
U. S. BUREAU OF RECLAMATION
DENVER FEDERAL CENTER
DENVER, CO 80225

PAUL C. JENNINGS
CALIFORNIA INSTITUTE OF TECHNOLOGY
DEPARTMENT OF CIVIL ENGINEERING
1201 EAST CALIFORNIA BLVD.
PASADENA, CA   91109

JEFFREY A. JOHNSON
DAMES & MOORE
1100 GLENDON AVENUE
SUITE 1000
LOS ANGELES, CA   90024

WARREN T. LAVERY, SUPERINTENDENT
LATHAM WATER DISTRICT
MEMORIAL TOWN HALL
NEWTONVILLE, NY   12128

DAVID J. LEEDS, EDITOR
EERI NEWSLETTER
11972 CHALON ROAD
LOS ANGELES, CA   90049

JAMES LEFTER
DIRECTOR, CIVIL ENGINEERING SERVICES
OFFICE OF CONSTRUCTION
810 VERMONT AVENUE, N. W.
WASHINGTON, DC   20420

H. S. LEW
BUILDING 226, ROOM B-168
NATIONAL BUREAU OF STANDARDS
WASHINGTON, DC   20234

PAGE   17

NHRAIC LIBRARIAN
IBS BUILDING NO. 6
UNIVERSITY OF COLORADO
BOULDER, CO   80309

JACK LINVILLE, JR.
AMERICAN INSTITUTE OF PLANNERS
1776 MASSACHUSETTS AVENUE NW
WASHINGTON, DC   20036

DR. S. C. LIU
NATIONAL SCIENCE FOUNDATION
1800 G STREET   NW
WASHINGTON, DC   20550

                                                      (10 COPIES)

WALTER B. LUM, PRESIDENT
WALTER LUM ASSOCIATES, INC.
SOIL & FOUNDATION ENGINEERS
3030 WAIALAE AVENUE
HONOLULU, HI   96816

MR. LE VAL LUND
DEPARTMENT OF WATER AND POWER
111 NORTH HOPE STREET
P. O. BOX 111
LOS ANGELES, CA   90051

RONALD MANCINI
GENSERT PELLER ASSOCIATES
ENGINEERING
718 THE ARCADE
CLEVELAND, OH   44114

FRANK MANDA
DEPT. OF HOUSING & URBAN DEVELOPMENT
FEDERAL DISASTER SYSTEM ADMIN.
ROOM B133 MAILROOM
WASHINGTON, DC 20410

JAMES E. MC CARTY
DIRECTOR OF PUBLIC WORKS
CITY HALL
14TH AND WASHINGTON STREET
OAKLAND, CA 94612

PROFESSOR H. D. MC NIVEN
E. E. R. C.
UNIVERSITY OF CALIFORNIA
BERKELEY, CA 94720

D. S. MEHTA
P. O. BOX 607
15740 SHADY GROVE ROAD
GAITHERBERG, MD 20760

DALE R. MERRELL
ANCHORAGE WATER UTILITY
3000 ARTIC BOULEVARD
ANCHORAGE, AK 99503

DR. J. L. MERRITT
MERRITT CASES, INC.
710 BROOKSIDE AVENUE
REDLANDS, CA 92373

EUGENE A. MILLER, VICE PRESIDENT
CONVERSE DAVIS DIXON ASSOCIATES
325 PACIFIC AVENUE
SAN FRANCISCO, CA   94111

ROBERT B. MINOGUE
ASSISTANT DIRECTOR FOR STANDARDS
DIVISION OF REACTOR STANDARDS
U. S. ATOMIC ENERGY COMMISSION
WASHINGTON, DC   20545

TAPPAN MUNROE, ASSOCIATE PROFESSOR
DEPARTMENT OF ECONOMICS
UNIVERSITY OF THE PACIFIC
STOCKTON, CA   95211

DONALD F. MORAN
CONSULTING STRUCTURAL ENGINEER
112 GAY DRIVE
VENTURA, CA   93003

MR. NATHAN M. NEWMARK
UNIVERSITY OF ILLINOIS
DEPARTMENT OF CIVIL ENGINEERING
URBANA, IL   61801

MR. MICHAEL O'DONNER
FELLOWS, REED AND WEBER
CONSULTING ENGINEERS
310 MAIN STREET
TOMS RIVER, NJ   08753

MR. ROBERT A. OLSON
STATE OF CALIFORNIA
SEISMIC SAFETY COMMISSION
1400 TENTH STREET
SACRAMENTO, CA   95814

PROFESSOR IRVING J. OPPENHEIM
CARNEGIE-MELLON UNIVERSITY
DEPARTMENT OF CIVIL ENGINEERING
PITTSBURGH, PA   15213

DR. MICHAEL J. O'ROURKE
RENSSELAER POLYTECHNIC INSTITUTE
ROOM 4046, ENGINEERING CENTER
TROY, NY   12181

PROFESSOR T. D. O'ROURKE
2114 CIVIL ENGINEERING BUILDING
UNIVERSITY OF ILLINOIS
URBANA, IL   61801

MR. DENNIS OSTROM
SOUTHERN CALIFORNIA EDISON
POST OFFICE BOX 800
2244 WALNUT GROVE AVENUE
ROSEMEAD, CA   91770

RICHARD PARK
TECHNICAL DIRECTOR
NATIONAL ACADEMY OF SCIENCES
2101 CONSTITUTION AVENUE NW
WASHINGTON, DC   20418

PROFESSOR RICHARD A. PARMELEE
DEPARTMENT OF CIVIL ENGINEERING
NORTHWESTERN UNIVERSITY
EVANSTON, IL   60201

PROFESSOR RAY PARNES
DEPARTMENT OF SOLID MECHANICS,
MATERIALS AND STRUCTURES
SCHOOL OF ENGINEERING
TEL AVIV UNIVERSITY
RAMAT-AVIV, TEL AVIV ISRAEL

ED PFRANG
CENTER FOR BUILDING TECHNOLOGY
NATIONAL BUREAU OF STANDARDS
WASHINGTON, DC   24234

ROBERT V. PHILLIPS
CONSULTING ENGINEER
844 MONTE VERDE DRIVE
ARCADIA, CA   91006

PROFESSOR KARL S. PISTER
DEPARTMENT OF CIVIL ENGINEERING
UNIVERSITY OF CALIFORNIA
BERKELEY, CA   94720

MR. POULSEN
CITY OF SANTA ROSA
POST OFFICE BOX 1678
SANTA ROSA, CA   95403

THOMAS R. RICE
LAS VEGAS VALLEY WATER DISTRICT
POST OFFICE BOX 4427
LAS VEGAS, NV   89106

PROFESSOR JOSE ROESSET
DEPARTMENT OF CIVIL ENGINEERING
MASSACHUSETTS INSTITUTE OF TECHNOLOGY
CAMBRIDGE, MA   02139

ALAN S. RYALL
ADVANCED RESEARCH PROJECTS AGENCY
1400 WILSON BOULEVARD
ARLINGTON, VA   22209

W. W. SANDERS, JR.
ENGINEERING RESEARCH INSTITUTE
IOWA STATE UNIVERSITY
AMES, IO   50010

DR. JOHN B. SCALZI
NATIONAL SCIENCE FOUNDATION
1800 G STREET   NW
WASHINGTON, DC   20550

ANSHEL J. SCHIFF
DEPARTMENT OF MECHNICAL ENGINEERING
PURDUE UNIVERSITY
WEST LAFAYETTE IN   47907

MARLENE SCHWARTZ
CAPITAL SYSTEMS GROUP
6110 EXECUTIVE BLVD
SUITE 250
ROCKVILEE, MARYLAND   20852

S. D. SCHWARZ
SHANNON WILSON, INC.
1105 NORTH 38TH STREET
SEATTLE, WA   98103

PROFESSOR H. C. SHAH
COLLEGE OF ENGINEERING
STANFORD UNIVERSITY
STANFORD, CA   94305

PROFESSOR MASANOBU SHINOZUKA
COLUMBIA UNIVERSITY
DEPARTMENT OF CIVIL ENGINEERING
NEW YORK, NY   10027

SIDNEY SHORE
DEPARTMENT OF CIVIL ENGINEERING
UNIVERSITY OF PENNSYLVANIA
TOWNE BUILDING
PHILADELPHIA, PA   19174

AVINASH SINGHAL
DEPARTMENT OF CIVIL ENGINEERING
ARIZONA STATE UNIVERSITY
TEMPE, ARIZONA   85281

MR. J. L. SMITH
FUGRO, INC.
3777 LONG BEACH BLVD.
P. O. BOX 7765
LONG BEACH, CA   90807

W. HUDSON SMITH
REGIONAL DIRECTOR OF CODES & STANDARDS
AMERICAN IRON AND STEEL INSTITUTE
508 16TH STREET, SUITE 704
OAKLAND, CA   94612

VERNON A. SMOOTS
DAMES AND MOORE
1100 GLENDON AVENUE
LOS ANGELES, CA   90024

RAUL SOSA - SENIOR WORKS ENGINEER
LOS ANGELES DEPARTMENT OF WATER & POWER
111 NORTH HOPE STREET
LOS ANGELES, CA   90012

MR. KARL V. STEINBRUGGE
INSURANCE SERVICES OFFICE
550 CALIFORNIA STREET
SAN FRANCISCO, CA   94104

ROBERT F. SWALLEY
SWALLEY ENGINEERING
1815 STATE STREET, SUITE C
SANTA BARBARA, CA   93101

HAROLD SWANSON
INTERSPACE CORPORATION
135 MARKET STREET
KENILWORTH, NJ   07033

MR. WALTER TACKLE
BOWE, WALSH AND ASSOCIATES
CONSULTING ENGINEERS
1 HUNTINGTON QUADRANGLE
HUNTINGTON, L. I. , NY   11746

JAMES TANOUYE, ENGINEER
DEPARTMENT OF THE ARMY-CORPS OF ENGINEERS
SOUTH PACIFIC DIVISION
630 SANSOME STREET
SAN FRANCISCO, CA   94111

JOESPH TERRELL
COMMAND 0412
NAVAL FACILITIES ENGINEERING
200 STOVALL DRIVE
ALEXANDRIA, VA   22332

MR. DAVID D. TILLSON
EARTHQUAKE ENGINEERING RESEARCH INSTITUTE
2620 TELEGRAPH AVENUE
BERKELEY, CA   94704

A. D. TOLINS
ROOM 9N05
HOFFMAN BUILDING II
200 STOVALL STREET
ALEXANDRIA, VA   22332

PROFESSOR W. K. TSO
CIVIL AND MECHANICAL ENGINEERING DEPT.
MC MASTER   UNIVERSITY
HAMILTON, ONTARIO, CANADA   L8S4L7

MR. GEORGE TUPAC
U. S. STEEL
600 GRANT STREET
PITTSBURGH, PA   15230

ALAN L. UNEMORI
301/3/A19
P. O. BOX 3965
SAN FRANCISCO, CA   94119

PROFESSOR ERIK VANMARCKE
DEPARTMENT OF CIVIL ENGINEERING
MASSACHUSETTS INSTITUTE OF TECHNOLOGY
CAMBRIDGE, MA   02139

DR. ROBERT WALKER
EQSI
1160 ROCKVILLE PIKE
ROCKVILLE, MD   20852

DR. LEON R. L. WANG
RENSSELAER POLYTECHNIC INSTITUTE
ROOM 4042, ENGINEERING CENTER
TROY, NY 12181

MR. P. WEIDLINGER
WEIDLINGER ASSOCIATES
110 EAST 59TH STREET
NEW YORK, NY 10022

MR. FRANK WEISENEG
FELLOWS, REED AND WEBER
CONSULTING ENGINEERS
310 MAIN STREET
TOMS RIVER, NJ 08753

PROFESSOR ROBERT V. WHITMAN
DEPARTMENT OF CIVIL ENGINEERING
MASSACHUSETTS INSTITUTE OF TECHNOLOGY
CAMBRIDGE, MA 02139

DR. JOHN H. WIGGINS, PRESIDENT
JOHN H. WIGGINS COMPANY
1650 SOUTH PACIFIC COAST HIGHWAY
REDONDO BEACH, CA 90277

F. AYRES WILLIAMSON
AMERICAN INSTITUTE OF STEEL
CONSTRUCTION
8136 OLD KEENE MILL ROAD
SPRINGFIELD, VA 22152

WOODWARD-CLYDE CONSULTANTS
LIBRARY SUITE 700
TWO EMBARCADERO CENTER
SAN FRANCISCO, CA   94111

RICHARD N. WRIGHT, DIRECTOR
CENTER FOR BUILDING TECHNOLOGY
U. S. DEPARTMENT OF COMMERCE
NATIONAL BUREAU OF STANDARDS
WASHINGTON, DC   20234

JAMES T. YAO
SCHOOL OF ENGINEERING
PURDUE UNIVERSITY
WEST LAFAYETTE, IN   47907

PROFESSOR F. YOUNG
PORTLAND STATE UNIVERSITY
DEPARTMENT OF ENGINEERING +
APPLIED SCIENCE
BOX 75
PORTLAND, OR   97207

(4 COPIES)

DR. JOSEPH ZIONY
USGS DEPUTY FOR GEOLOGY
OFFICE OF EARTHQUAKE STUDIES
12201 SUNRISE VALLEY DRIVE
RESTON, VA   22092

PAGE 29

ROBERT S. HENDERSON
UTILITIES CONTRACTING OFFICER
OFFICE OF CONTRUCTION
WASHINGTON, D.C. 20420

ROBERT P. KENNEDY, VICE PRESIDENT
ENGINEERING DECISION ANALYSIS CO. INC.
2400 MICHAELSON DRIVE
IRVINE, CA 92715

J. F. GORMAN, LIBRARIAN
SERGENT, HAUSKINS AND BECKWITH
3940 W. CLARENDON
PHOENIX, ARIZONA 85019